Astrophysical Observable Properties of Black Holes and Neutron Stars

Bobomurat Ahmedov

Ulugh Beg Astronomical Institute
Uzbekistan Academy of Sciences, Tashkent

01 November 2021, Tashkent, Uzbekistan
6th Maidanak Users Meeting

Content

Under One Sky: The IAU Centenary Symposium
Proceedings IAU Symposium No. 349, 2019
C. Sterken, J. Hearnshaw & D. Valls-Gabaud, eds.

doi:10.1017/S1743921319000437

Relativistic Astrophysics in Uzbekistan

Bobomurat Ahmedov[1,2]

[1]Ulugh Beg Astronomical Institute, Astronomicheskaya 33, Tashkent 100052, Uzbekistan
[2]National University of Uzbekistan, Tashkent 100174, Uzbekistan
email: ahmedov@astrin.uz

Abstract. During the last twenty years, due to the extensive help and assistance of the international scientific community, there has been a great success in the development and establishment of new well-functioning and competitive scientific groups specialized in general relativity and relativistic astrophysics in Uzbekistan (Tashkent), Kazakhstan (Astana and Almaty), Kyrgyzstan (Bishkek) and great achievements have been made on the study in Central Asia in relativistic cosmology and astrophysics of compact gravitational objects.

Keywords. Relativistic astrophysics, Central Asia, black holes, neutron stars.

1. Introduction

The main fields in which the scientific activity on relativistic astrophysics in Uzbekistan

Recent discoveries related to BHs & NSs

- First image of a black hole (M87) by EHT (Apr 2019) – submillimeter
- Detection of close orbital motion around SgrA* by GRAVITY@ESO (Oct 2018) – near infrared (K-band) & multiwavelength
- First test of GR at the SMBH scale by ESO's VLT (Jul 2018) – infrared/near infrared
- Extragalactic HE neutrino pointing to Blazar by IceCube (Jul 2018) – neutrino astronomy
- Extragalactic UHECRs above 10^18 eV by PAO (Argentina, Sept 2017) & TA (2018) – cosmic ray astronomy
- Detection of GWs from BH-NS merger by LIGO/Virgo (Aug 2017) – Multimessenger era!
- First detection of *gravitational waves* by LIGO/Virgo (Feb 2016) – GW astronomy

Credits: IceCube

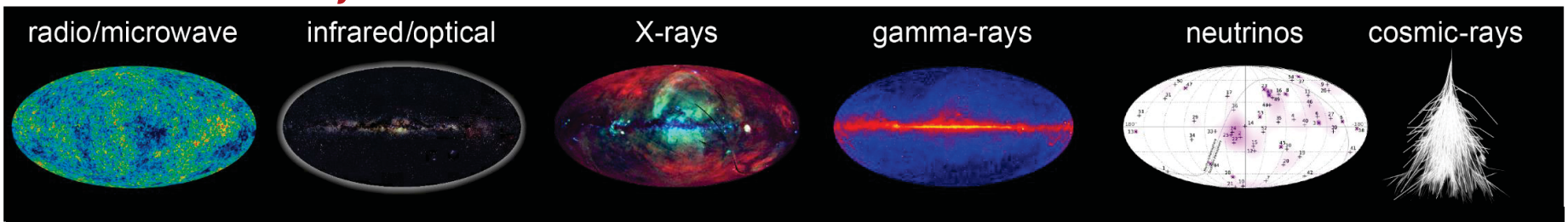

Research in Theoretical Astrophysics Department, UBAI, Tashkent

- Optical Properties of Black Holes: BH Shadow and Gravitational Lensing, X-ray: LMXB (Frankfurt, Opava, Shanghai, Nur-Sultan)
- Exact Analytical Solutions to Field Equations and Black Hole Properties (Pune, Opava, Nur-Sultan, Dhahran, Minsk)
- Energy extraction from Black Holes (Opava, Pune, Frankfurt)
- Electromagnetic/Gravitational Fields and Radiation from Neutron Stars and Compact Objects. Quasinormal Modes of Black Holes. Particles and Fields in Vicinity of Black Holes (Frankfurt, Opava, Pune, Shanghai, Nur-Sultan, Dhahran)
- Numerical Models of Supernova Light Curves (Penn State)
- Ionospheric Studies (Stanford)
- China, Kazakhstan, Belarus, Saudi Arabia, Naples University...

Research in Theoretical Astrophysics Department, UBAI, Tashkent

- Optical Properties of Black Holes: BH Shadow and Gravitational Lensing, X-ray: LMXB (Frankfurt, Opava, Shanghai, Nur-Sultan)
- Exact Analytical Solutions to Field Equations and Black Hole Properties (Pune, Opava, Nur-Sultan, Dhahran, Minsk)
- Energy extraction from Black Holes (Opava, Pune, Frankfurt)
- Electromagnetic/Gravitational Fields and Radiation from Neutron Stars and Compact Objects. Quasinormal Modes of Black Holes. Particles and Fields in Vicinity of Black Holes (Frankfurt, Opava, Pune, Shanghai, Nur-Sultan, Dhahran)
- Numerical Models of Supernova Light Curves (Penn State)
- Ionospheric Studies (Stanford)
- China, Kazakhstan, Belarus, Saudi Arabia, Naples University...

Research in Theoretical Astrophysics Department, UBAI, Tashkent

- Optical Properties of Black Holes: BH Shadow and Gravitational Lensing, X-ray: LMXB (Frankfurt, Opava, Shanghai, Nur-Sultan)
- Exact Analytical Solutions to Field Equations and Black Hole Properties (Pune, Opava, Nur-Sultan, Dhahran, Minsk)
- Energy extraction from Black Holes (Opava, Pune, Frankfurt)
- Electromagnetic/Gravitational Fields and Radiation from Neutron Stars and Compact Objects. Quasinormal Modes of Black Holes. Particles and Fields in Vicinity of Black Holes (Frankfurt, Opava, Pune, Shanghai, Nur-Sultan, Dhahran)
- Numerical Models of Supernova Light Curves (Penn State)
- Ionospheric Studies (Stanford)
- China, Kazakhstan, Belarus, Saudi Arabia, Naples University...

Research in Theoretical Astrophysics Department, UBAI, Tashkent

- Optical Properties of Black Holes: BH Shadow and Gravitational Lensing, X-ray: LMXB (Frankfurt, Opava, Shanghai, Nur-Sultan)
- Exact Analytical Solutions to Field Equations and Black Hole Properties (Pune, Opava, Nur-Sultan, Dhahran, Minsk)
- Energy extraction from Black Holes (Opava, Pune, Frankfurt)
- Electromagnetic/Gravitational Fields and Radiation from Neutron Stars and Compact Objects. Quasinormal Modes of Black Holes. Particles and Fields in Vicinity of Black Holes (Frankfurt, Opava, Pune, Shanghai, Nur-Sultan, Dhahran)
- Numerical Models of Supernova Light Curves (Penn State)
- Ionospheric Studies (Stanford)
- China, Kazakhstan, Belarus, Saudi Arabia, Naples University...

Research in Theoretical Astrophysics Department, UBAI, Tashkent

- Optical Properties of Black Holes: BH Shadow and Gravitational Lensing, X-ray: LMXB (Frankfurt, Opava, Shanghai, Nur-Sultan)
- Exact Analytical Solutions to Field Equations and Black Hole Properties (Pune, Opava, Nur-Sultan, Dhahran, Minsk)
- Energy extraction from Black Holes (Opava, Pune, Frankfurt)
- Electromagnetic/Gravitational Fields and Radiation from Neutron Stars and Compact Objects. Quasinormal Modes of Black Holes. Particles and Fields in Vicinity of Black Holes (Frankfurt, Opava, Pune, Shanghai, Nur-Sultan, Dhahran)
- Numerical Models of Supernova Light Curves (Penn State)
- Ionospheric Studies (Stanford)
- China, Kazakhstan, Belarus, Saudi Arabia, Naples University...

Research in Theoretical Astrophysics Department, UBAI, Tashkent

- Optical Properties of Black Holes: BH Shadow and Gravitational Lensing, X-ray: LMXB (Frankfurt, Opava, Shanghai, Nur-Sultan)
- Exact Analytical Solutions to Field Equations and Black Hole Properties (Pune, Opava, Nur-Sultan, Dhahran, Minsk)
- Energy extraction from Black Holes (Opava, Pune, Frankfurt)
- Electromagnetic/Gravitational Fields and Radiation from Neutron Stars and Compact Objects. Quasinormal Modes of Black Holes. Particles and Fields in Vicinity of Black Holes (Frankfurt, Opava, Pune, Shanghai, Nur-Sultan, Dhahran)
- Numerical Models of Supernova Light Curves (Penn State)
- Ionospheric Studies (Stanford)
- China, Kazakhstan, Belarus, Saudi Arabia, Naples University...

Research in Theoretical Astrophysics Department, UBAI, Tashkent

- Optical Properties of Black Holes: BH Shadow and Gravitational Lensing, X-ray: LMXB (Frankfurt, Opava, Shanghai, Nur-Sultan)
- Exact Analytical Solutions to Field Equations and Black Hole Properties (Pune, Opava, Nur-Sultan, Dhahran, Minsk)
- Energy extraction from Black Holes (Opava, Pune, Frankfurt)
- Electromagnetic/Gravitational Fields and Radiation from Neutron Stars and Compact Objects. Quasinormal Modes of Black Holes. Particles and Fields in Vicinity of Black Holes (Frankfurt, Opava, Pune, Shanghai, Nur-Sultan, Dhahran)
- Numerical Models of Supernova Light Curves (Penn State)
- Ionospheric Studies (Stanford)
- China, Kazakhstan, Belarus, Saudi Arabia, Naples University...

Content

What Is a Black Hole?

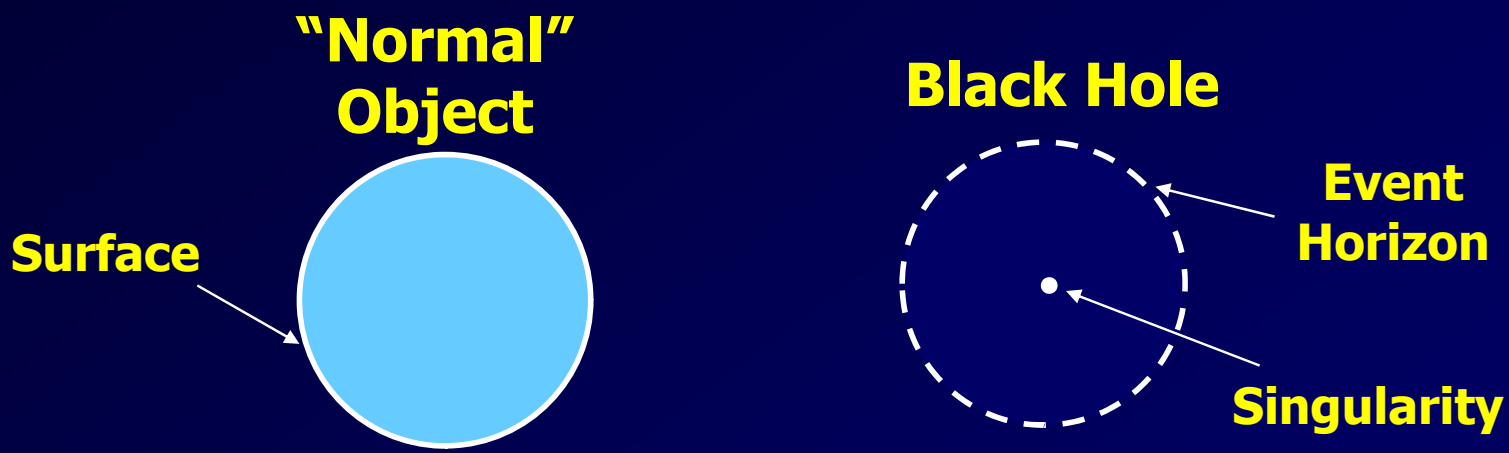

- **Black Hole:** A remarkable prediction of Einstein's General Theory of Relativity – represents the victory of gravity
- Matter is crushed to a **SINGULARITY**
- Surrounding this is an **EVENT HORIZON**

X-ray Binaries

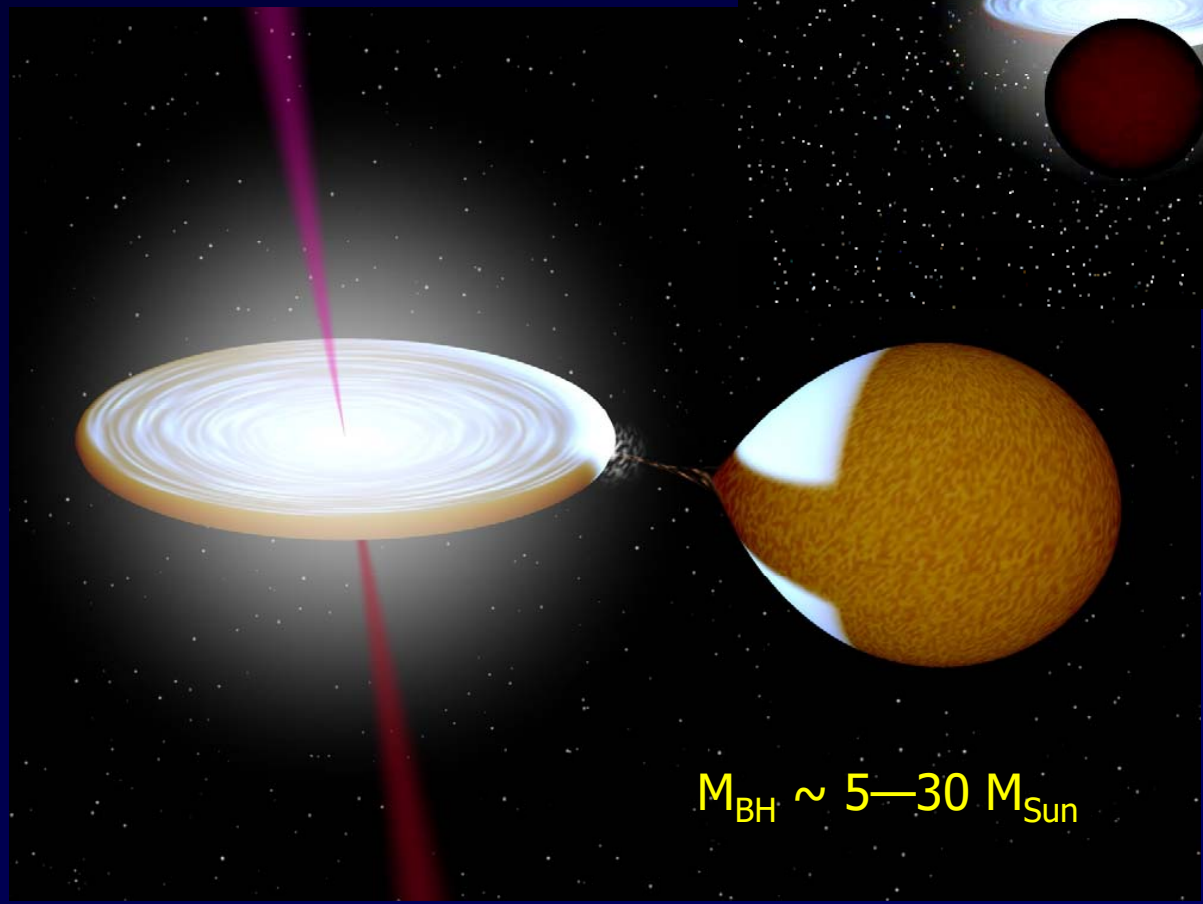

Image credit: Robert Hynes

Galactic Nuclei

Image credit: Lincoln Greenhill, Jim Moran

Accretion in close binaries

Accretion is the most powerful source of energy realized in Nature, which can give a huge energy output.

When matter fall down onto the surface of a neutron star up to 10 % of mc^2 can be released.

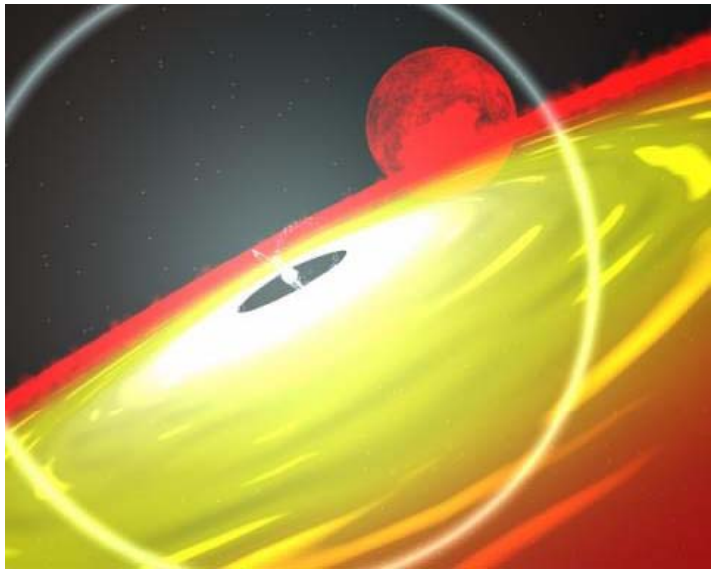

Zel'dovich *Sov. Phys. Dokl.* 9 195 (1964); Salpeter *Astrophys. J.* 140 796 (1964); Shakura & Sunyaev *Astron. Astrophys.* 24 337 (1973)

Black holes have no hair!

- **Schwarzschild**
  $\{M\}$
- **Reissner-Nordstrom**
  $\{M,Q\}$
- **Kerr**
  $\{M,a\}$
- **Kerr-Newman**
  $\{M,a,Q\}$

Wheeler: no-hair theorem

Motivation & Goals

There is a great interest to probe the nature of the black holes, i.e., the mass and spin.

The mass of a black hole can be estimated with the Newtonian orbital motion of the stars surrounding the black hole.

Genzel R., Eisenhauer F., Gillessen S., 2010, Rev. Mod. Phys., 82, 3121;
Ghez A. M. et al., 2008, ApJ, 689, 1044

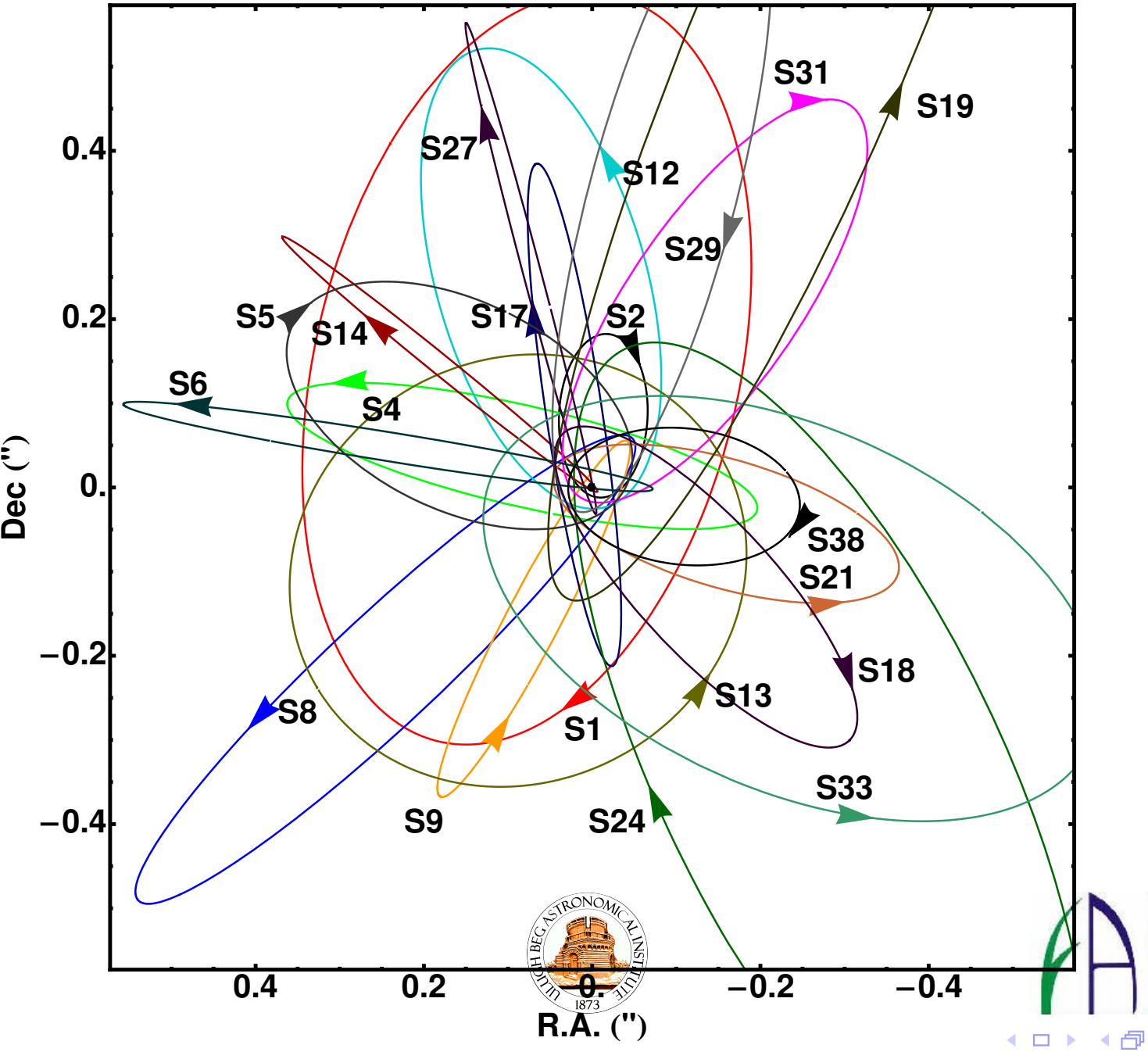
S31
S19
S27
S12
S29
S5
S14
S17
S2
S6
S4
S38
S21
S18
S13
S8
S1
S33
S9
S24
0.4
0.2
0.
−0.2
−0.4
Dec (")
R.A. (")

GRAVITY consortium, Astronomy & Astrophysics, 2018

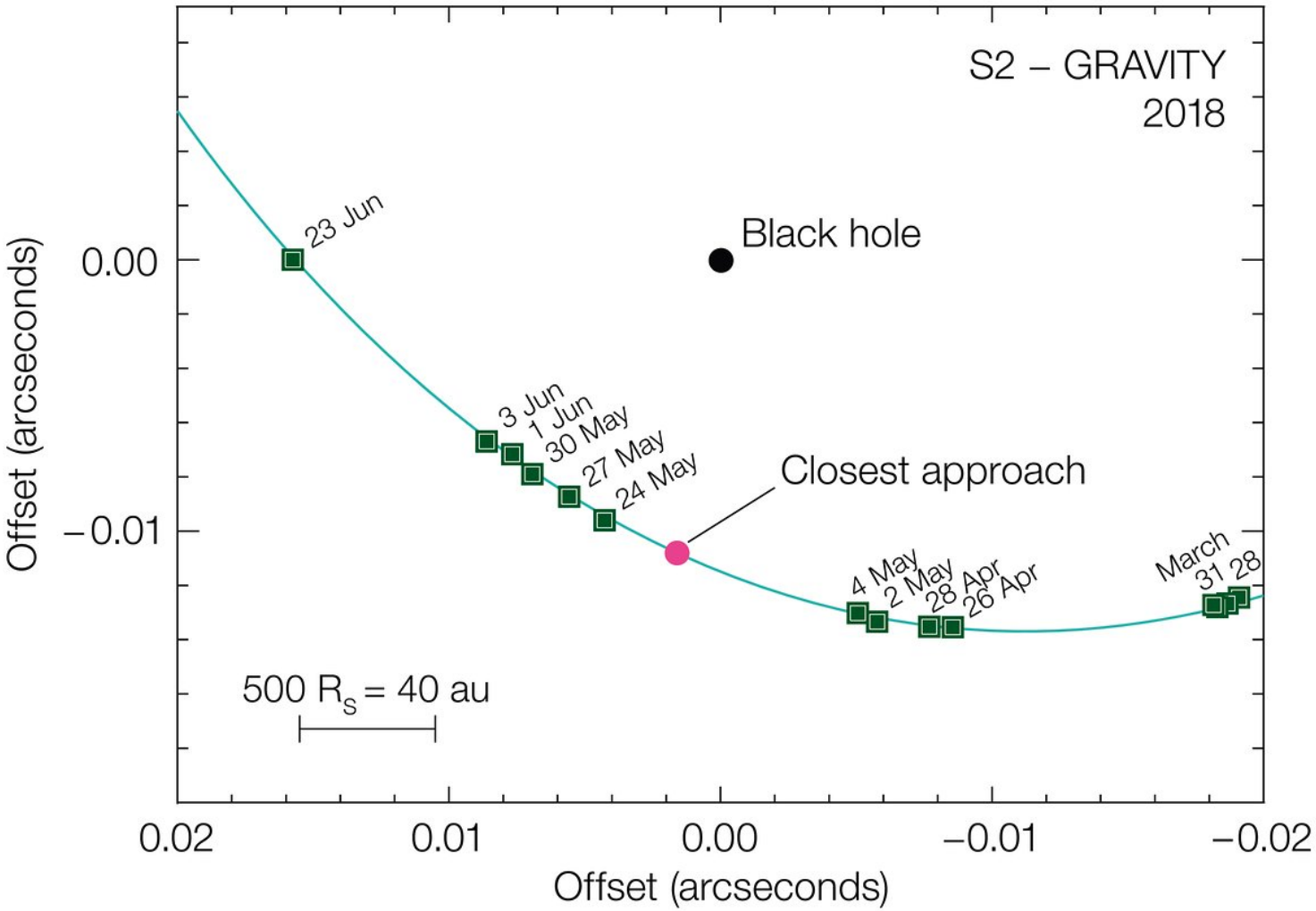
S2 – GRAVITY
2018
Black hole
Closest approach
23 Jun
3 Jun
1 Jun
30 May
27 May
24 May
4 May
2 May
28 Apr
26 Apr
March
31
28
500 R_s = 40 au
Offset (arcseconds)
0.00
−0.01
0.02
0.01
0.00
−0.01
−0.02
Offset (arcseconds)

Motivation & Goals

The black hole spin can be measured with the methods based on the thermal continuum emission of accretion disks and relativistically broadened iron lines. These two techniques using X-ray measurements have been widely applied to different sources.

C.S. Reynolds and M.A. Nowak, Fluorescent iron lines as a probe of astrophysical black hole systems, Phys. Rept. 377 (2003) 389;
Cosimo Bambi, 2013, PRD, 87, 023007; 2017, Rev. Mod. Phys., 89, 025001

J.E. McClintock, R. Narayan and J.F. Steiner, Black Hole Spin via Continuum Fitting and the Role of Spin in Powering Transient Jets, Space Sci. Rev (2013);
J.E. McClintock et al., Measuring the Spins of Accreting Black Holes, Class. Quant. Grav. 28 (2011) 114009

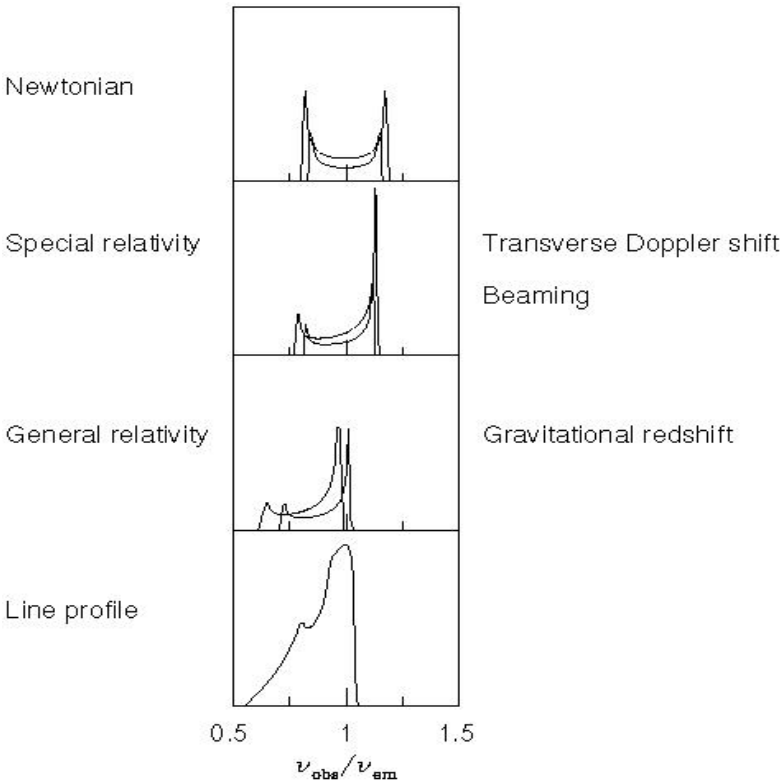

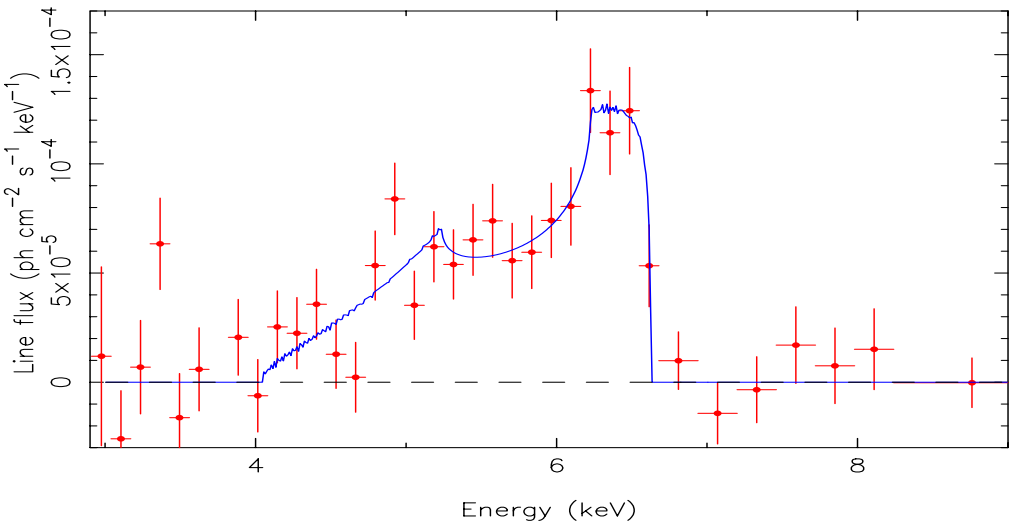

Jovanovich P., **New Astron Rev** 56, 37 (2012).

X-ray reflection spectroscopy → Analysis of reflected component of the Novikov-Thorne disks.

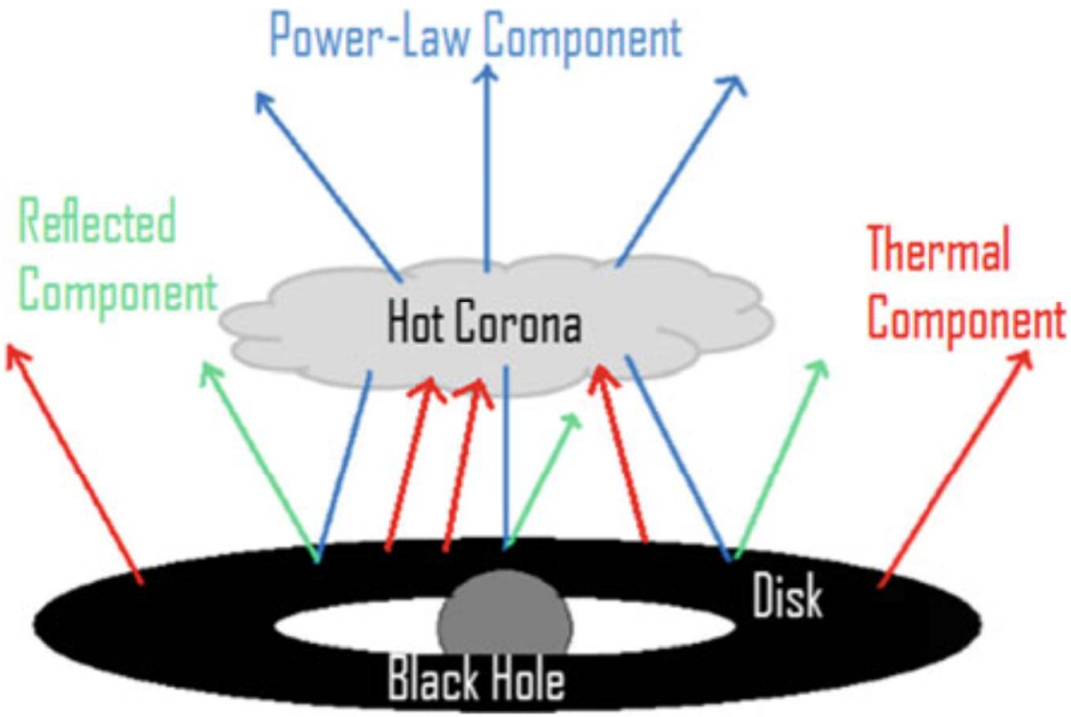

Figures from C. Bambi, Black Holes: A Laboratory for Testing Strong Gravity

RELXILL is currently the most advanced X-ray reflection model to describe the reflection spectrum of thin accretion disks around Kerr black holes.

Garcia & Dauser 2014

RELXILL can be employed to measure black hole spins

RELXILL_NK is the natural extension of RELXIL for non-Kerr spacetimes

RELXILL_NK can be employed to test Kerr black hole hypothesis

In 1H0707–495, Ark 564, GX 339–4, GS 1354– 645, MCG–06–30–15 etc. the Kerr metric is recovered with 99% confidence level

Bambi et al, 2017

Abdikamalov et al, 2019, 202

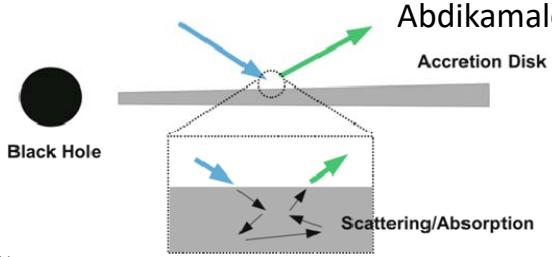

Schwarzschild

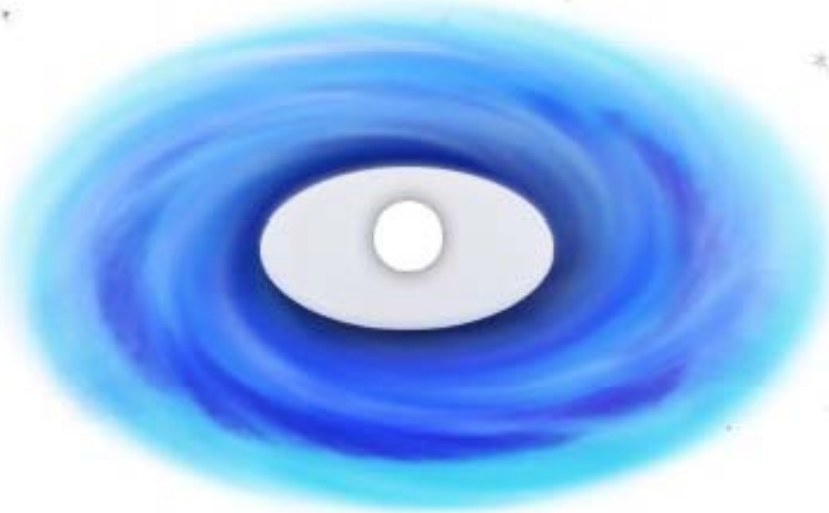

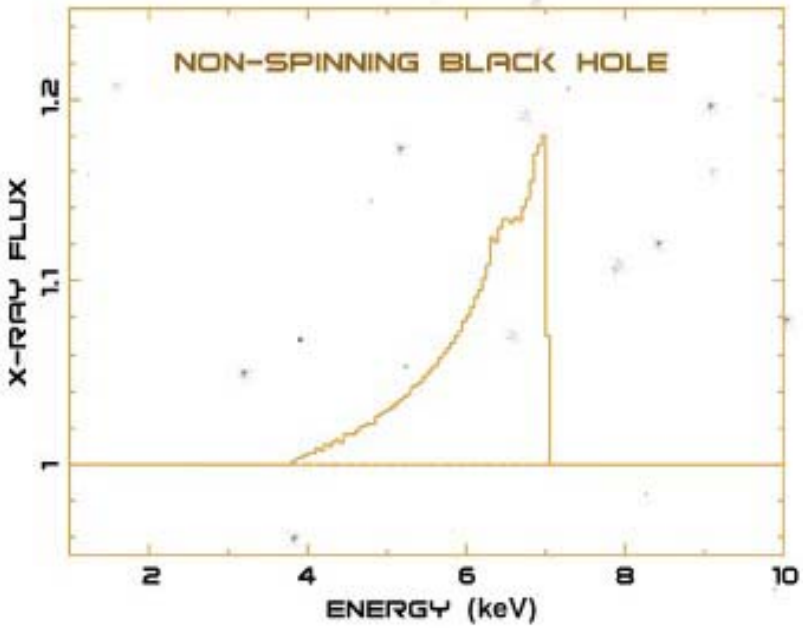

Extreme Kerr

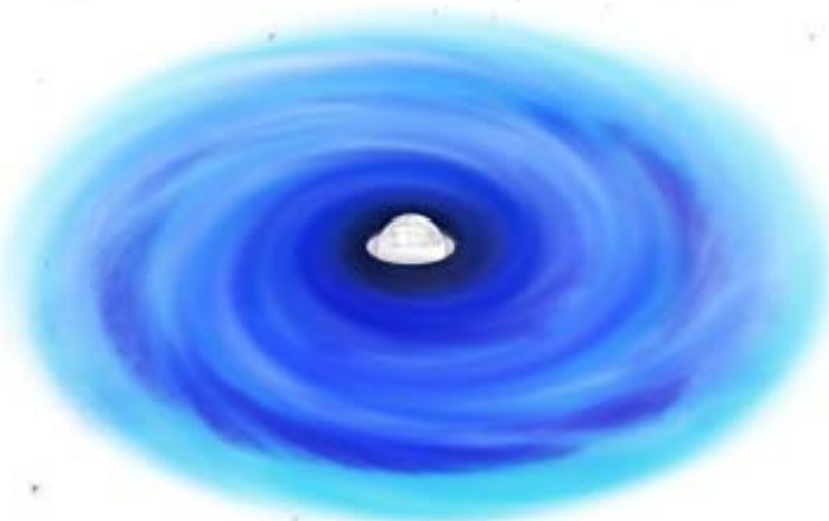

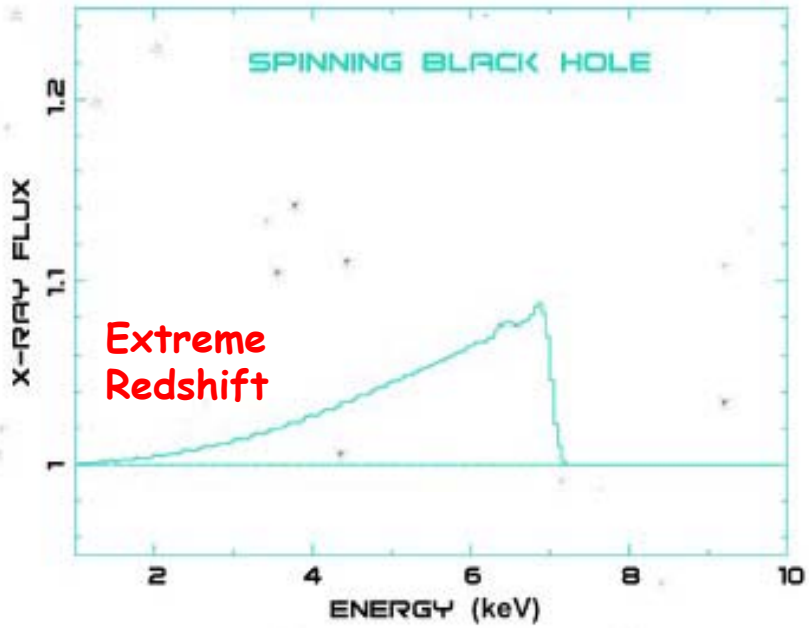

According to the observations ISCO radii are essentially shifted towards the central objects.

BH Masses and Spins

Source Name	BH Mass (M_{Sun})	BH Spin (a)
A0620-00	6.3—6.9	0.12 ± 0.19
LMC X-3	5.9—9.2	~0.25
XTE J1550-564	8.5—9.7	0.34±0.24
GRO J1655-40	6.0—6.6	0.70 ± 0.05
4U1543-47	8.4—10.4	0.80 ± 0.05
M33 X-7	14.2—17.1	0.84 ± 0.05
LMC X-1	9.4—12.4	0.92 ± 0.06
Cyg X-1	13.8—15.8	> 0.97
GRS 1915+105	10—18	> 0.98

Shafee et al. (2006); McClintock et al. (2006); Davis et al. (2006); Liu et al. (2007,2009); Gou et al. (2009,2010, 2011); Steiner et al. (2010)

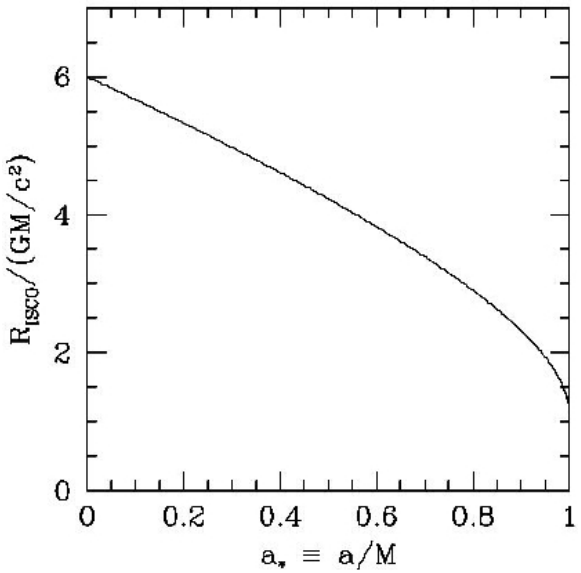

N. K. Dadhich, R. Maartens, P. Papodopoulos, V. Rezania, **PLB** 487, 1 (2000).

Minimal radius of circular orbits

$$r_{\rm mc} > \frac{4Q^*}{3M - \sqrt{9M^2 - 8Q^*}} \,,$$

$$r_{\rm mc} \approx 3M - \frac{2Q^*}{3M} - \frac{4Q^{*2}}{27M^3} + \mathcal{O}\left(\frac{Q^{*3}}{M^5}\right) \,.$$

Stable circular orbits

$$r_{\rm ISCO} = \frac{4Q^*}{3M + \sqrt[3]{A-B} + \sqrt[3]{A+B}} \,,$$

$$A = 8MQ^* - 9M^3 \,,$$
$$B = 4\sqrt{(4MQ^* - 5M^3)(MQ^* - M^3)} \,.$$

$$r_{\rm ISCO} \approx 6M - 1.5\frac{Q^*}{M} + 0.0018\frac{Q^{*2}}{M^3} + \mathcal{O}\left(\frac{Q^{*3}}{M^5}\right) \,.$$

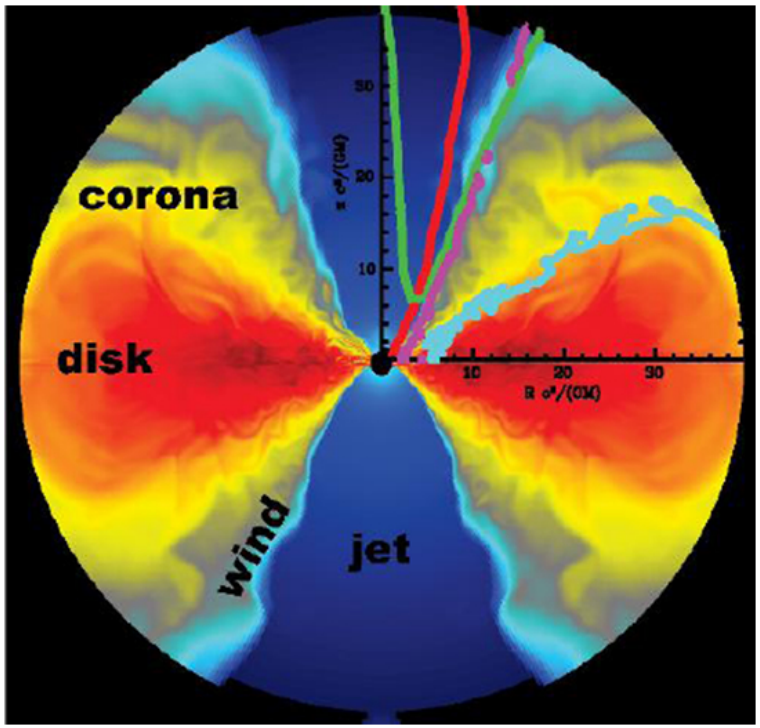

Dependence of the lower limit for radiuses of circular orbits r_{mc} (left graph) and ISCO $r_{\rm ISCO}$ (right graph) from the tidal charge Q^*.

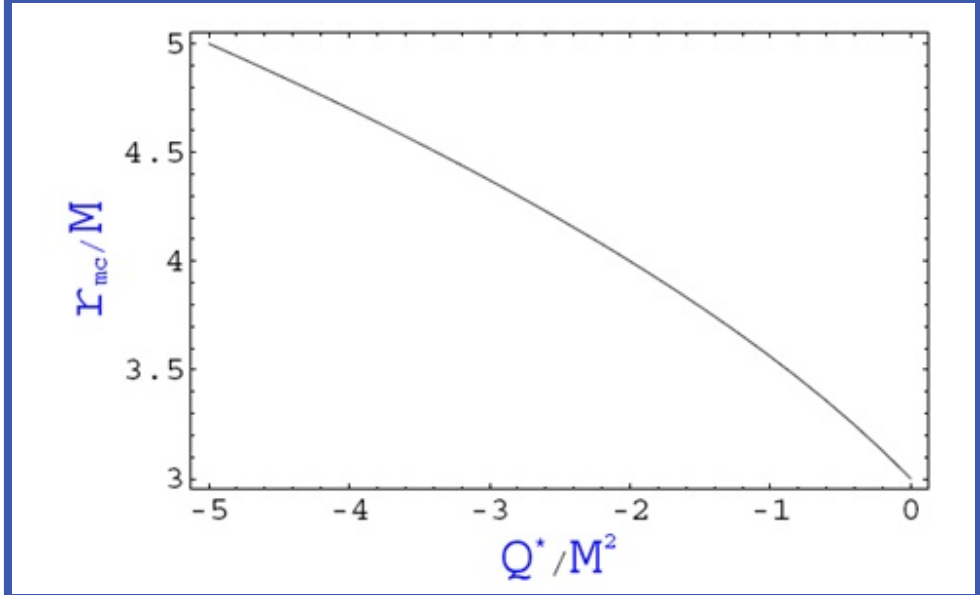

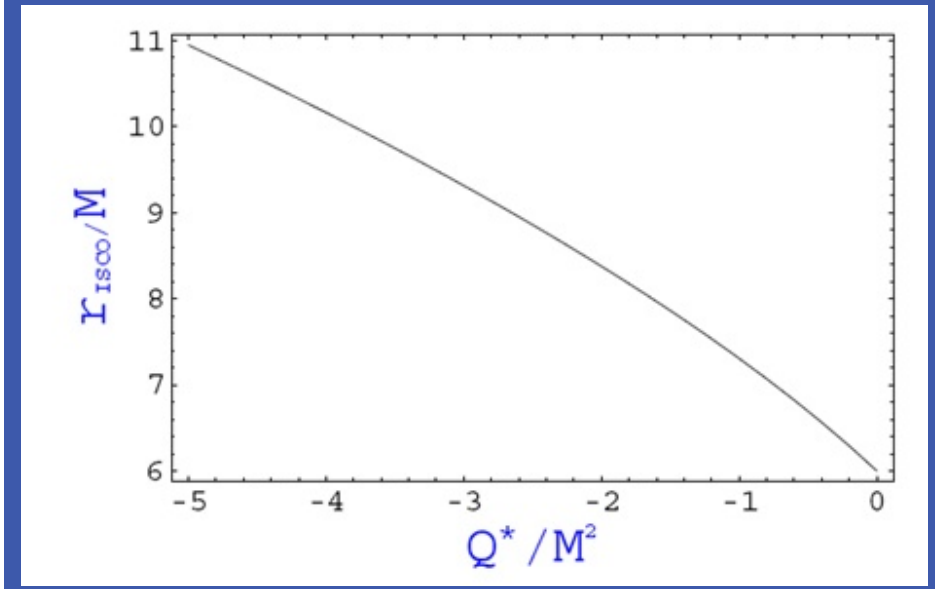

On the base of comparison of observations of ISCO in accretion disks around black holes and ISCO analysis around black hole in braneworld the brane tidal charge has an upper limit $\lesssim 10^9 \mathrm{cm}^2$.

A.A. Abdujabbarov, BA, **Phys. Rev. D**, 2010, V.81, 044022.

Dependence of the radius of the horizon (measured in M) and $r_{\rm ISCO}$ from Kehagias-Sfetsos (KS) parameter $\tilde{\omega}$.

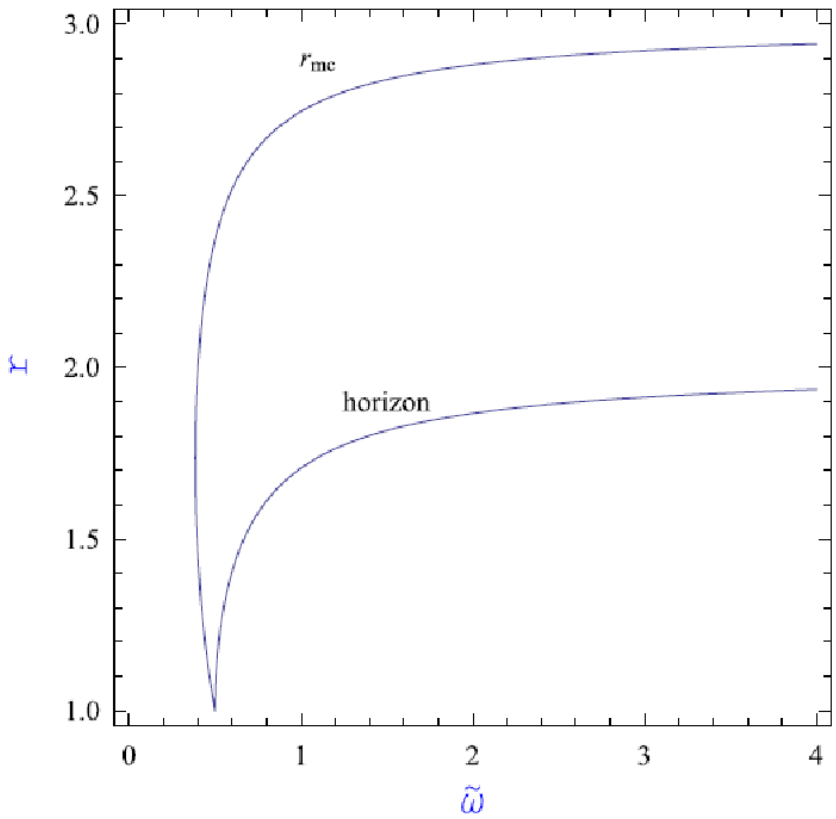

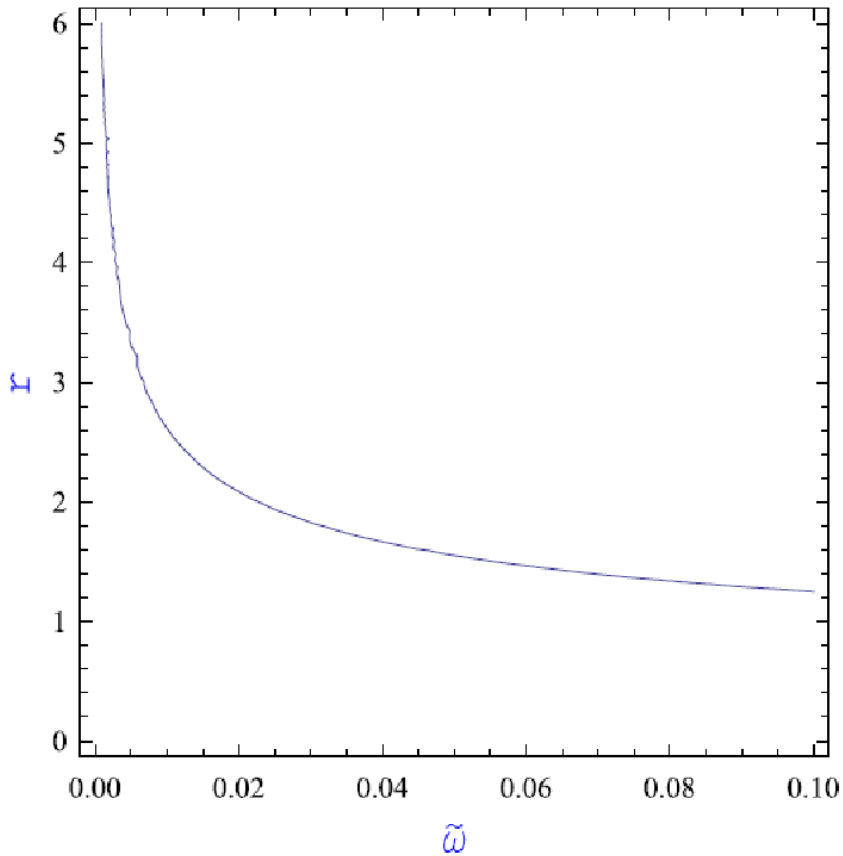

A. Abdujabbarov, BA, A. Hakimov **Phys. Rev. D**, 2011, V.83, 044053.

KS Solution

$$ds^2 = -e^{2\Phi(r)}dt^2 + e^{2\Lambda(r)}dr^2 + r^2 d\theta^2 + r^2 \sin^2\theta d\varphi^2 \ ,$$

where the metric functions Φ and Λ defined as

$$e^{2\Phi(r)} = e^{-2\Lambda(r)} = 1 + \omega r^2 - \sqrt{r(\omega^2 r^3 + 4\omega M)}.$$

The innermost stable circular orbits around black hole and the critic values of the momentum of the particles falling down to the central black hole in Hořava-Lifshitz gravity.

$\tilde{\omega}$	0.5	1	2	4	6	8	10
$r_{\rm ISCO}$	5.23655	5.66395	5.84024	5.92193	5.94834	5.9614	5.96918
$\mathcal{L}^2_{\rm cr}$	14.77	15.454	15.7395	15.8725	15.9156	15.9369	15.9496

Taking typical value for the momentum $a = 0.5M$ of the central black hole, one can obtain the lower value for the parameter as

$$\omega \gtrsim 3.6 \cdot 10^{-24}\mathrm{cm}^{-2}.$$

Motivation & Goals

However, for sources such as Sgr A*, the two techniques are less applicable.

Psaltis D., Wex N., Kramer M., A Quantitative Test of the No-Hair Theorem with Sgr A* using stars, pulsars, and the Event Horizon Telescope, ApJ, 2016

Then an alternate method may be the observation of black hole shadows.

The Event Horizon Telescope Collaboration, "First M87 Event Horizon Telescope results," ApJ Letters, 2019

Yosuke Mizuno et al, The current ability to test theories of gravity with black hole shadows, Nature Astronomy, 2018

Masses, distances, radius of BH

Compact object	Mass/$M_\odot$	Distance, kpc	radius a.u.	Diameter of shadow, μas
Stellar black hole	10^1	1	1.97×10^{-7}	0.001
SgrA*	4.1×10^6	8	7.28×10^{-2}	**45.48**
M31	3.5×10^7	800	6.88×10^{-1}	4.30
NGC4258	3.9×10^7	7200	7.76×10^{-1}	0.53
M87	6.4×10^9	16100	1.26×10^2	**39.08**

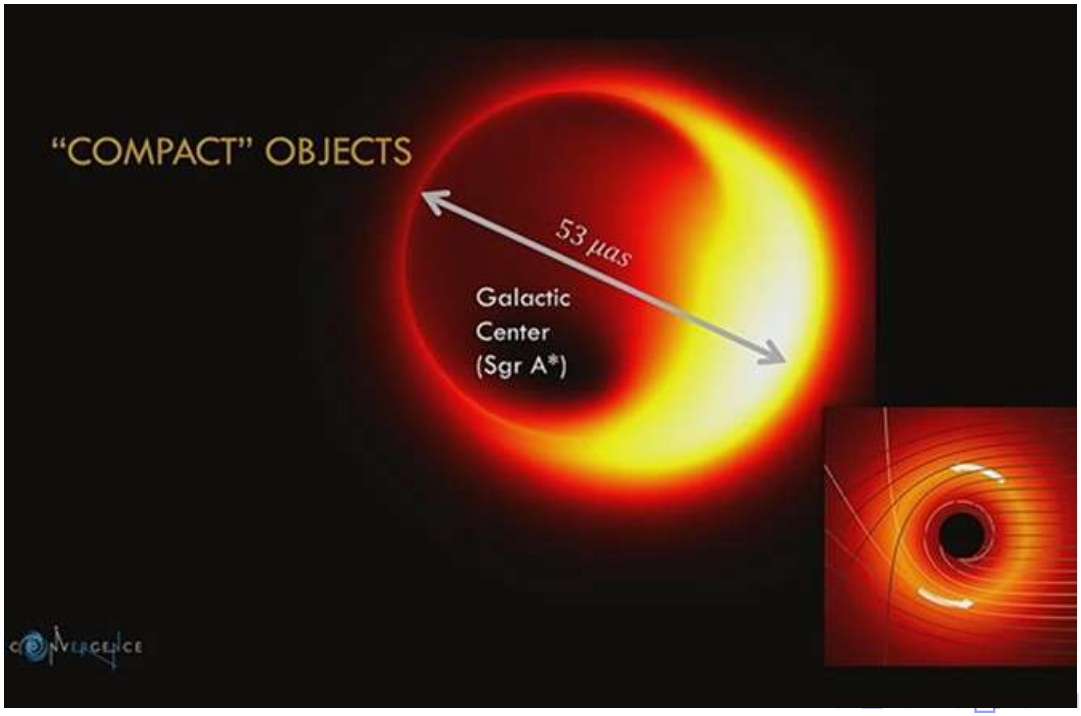

VLBI/EHT

Wavelength should be less than $\lambda < 1\mathrm{mm}$

EHT resolution will reach $2.3 \times 10^{-5} s$ for $\lambda = 1.3\mathrm{mm}$ and frequency $230\mathrm{GHz}$

EHT resolution will reach $1.5 \times 10^{-5} s$ for $\lambda = 0.87\mathrm{mm}$ and frequency $345\mathrm{GHz}$

Doeleman S S et al. **Nature** 455 78 (2008)

Fish V L et al. **Astrophys. J.** 727 L36 (2011)

Doeleman S S et al. **Science** 338 355 (2012)

Johnson M D et al. **Science** 350 1242 (2015)

A.K. Baczko, R. Schulz, M. Kadler, E. Ros et al. **A& A** 593, A47 (2016)

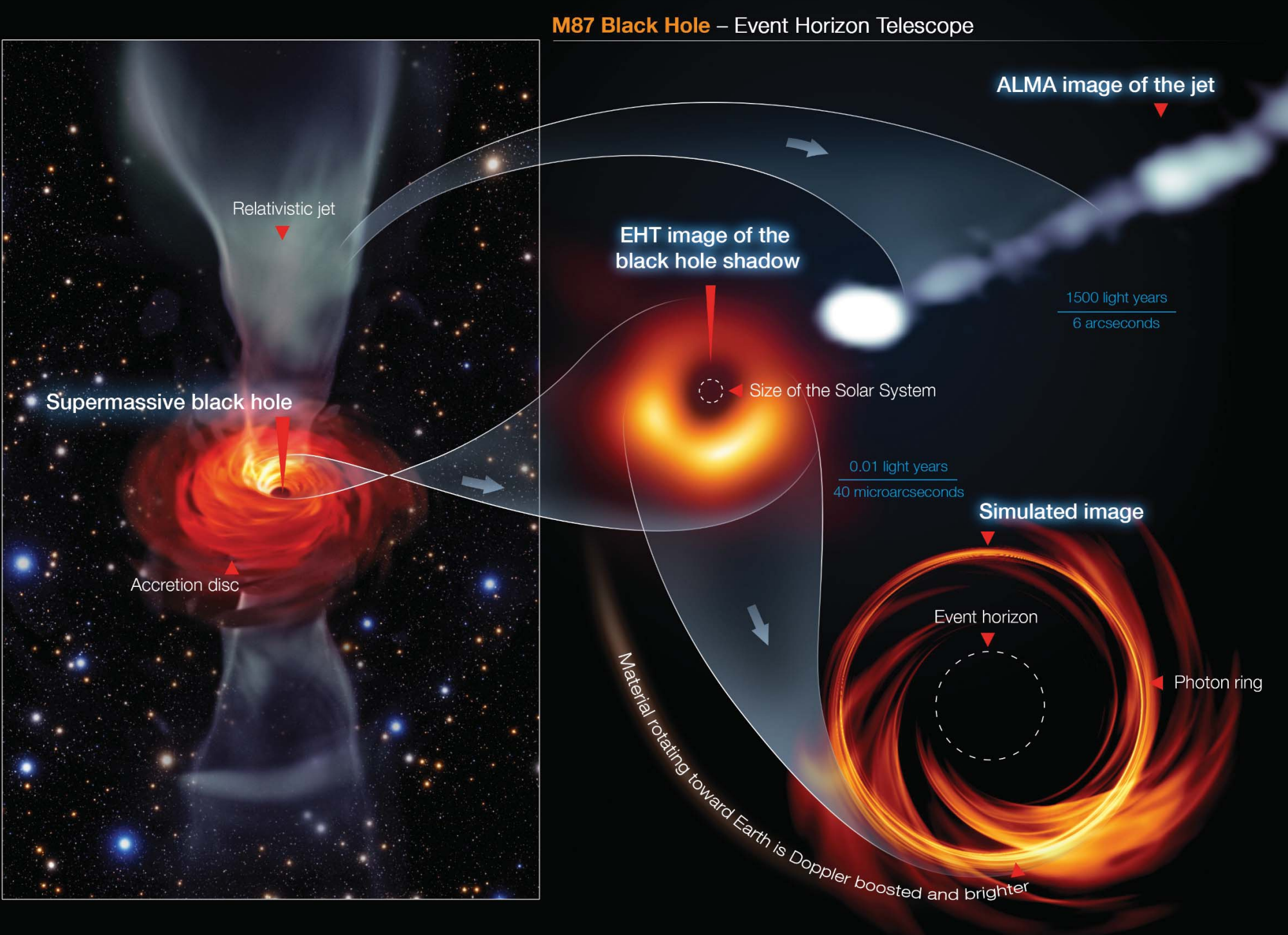
M87 Black Hole – Event Horizon Telescope
ALMA image of the jet
Relativistic jet
EHT image of the black hole shadow
1500 light years
6 arcseconds
Supermassive black hole
Size of the Solar System
0.01 light years
40 microarcseconds
Simulated image
Accretion disc
Event horizon
Photon ring
Material rotating toward Earth is Doppler boosted and brighter

Test case: Kerr a=0.936

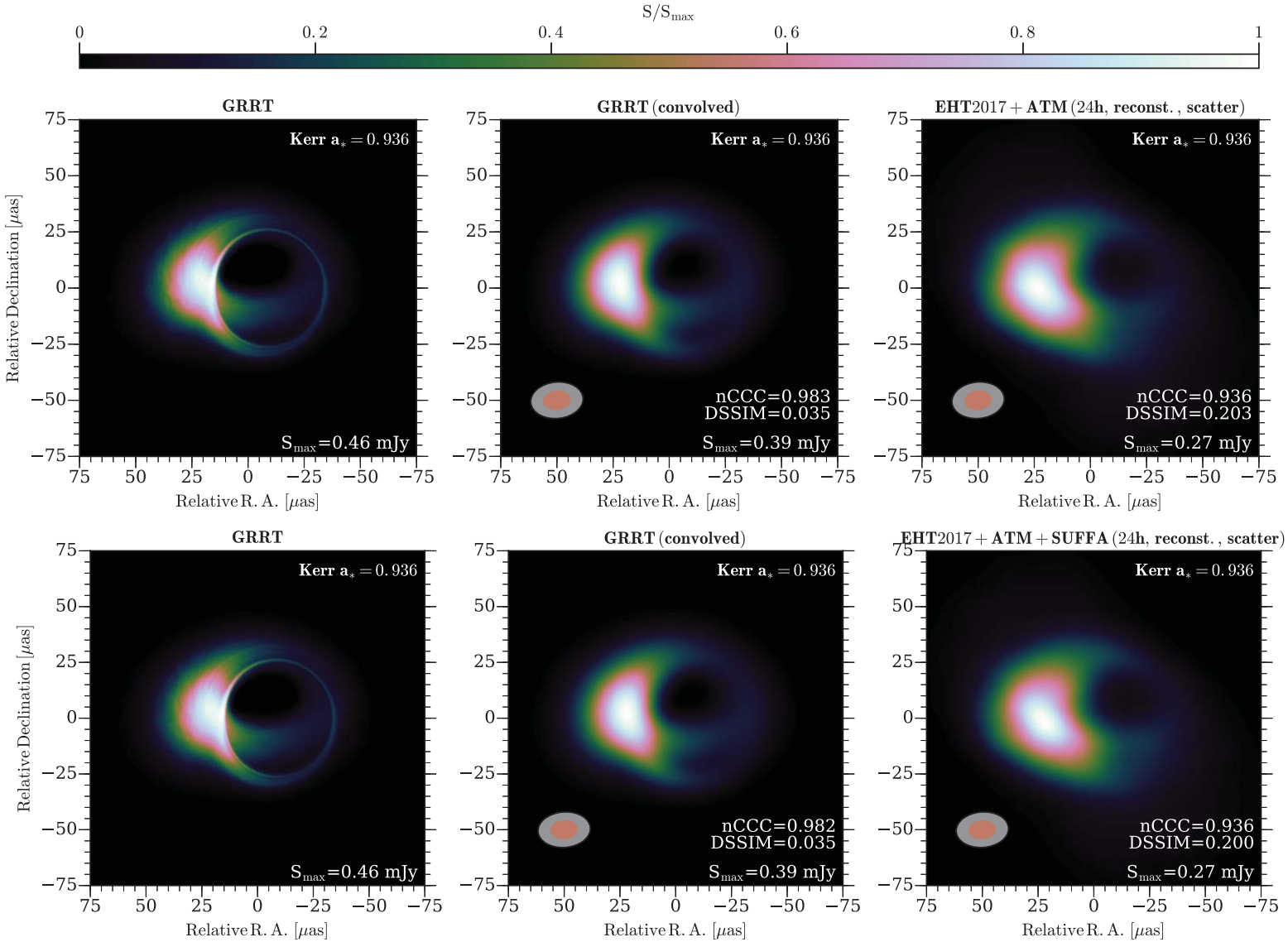

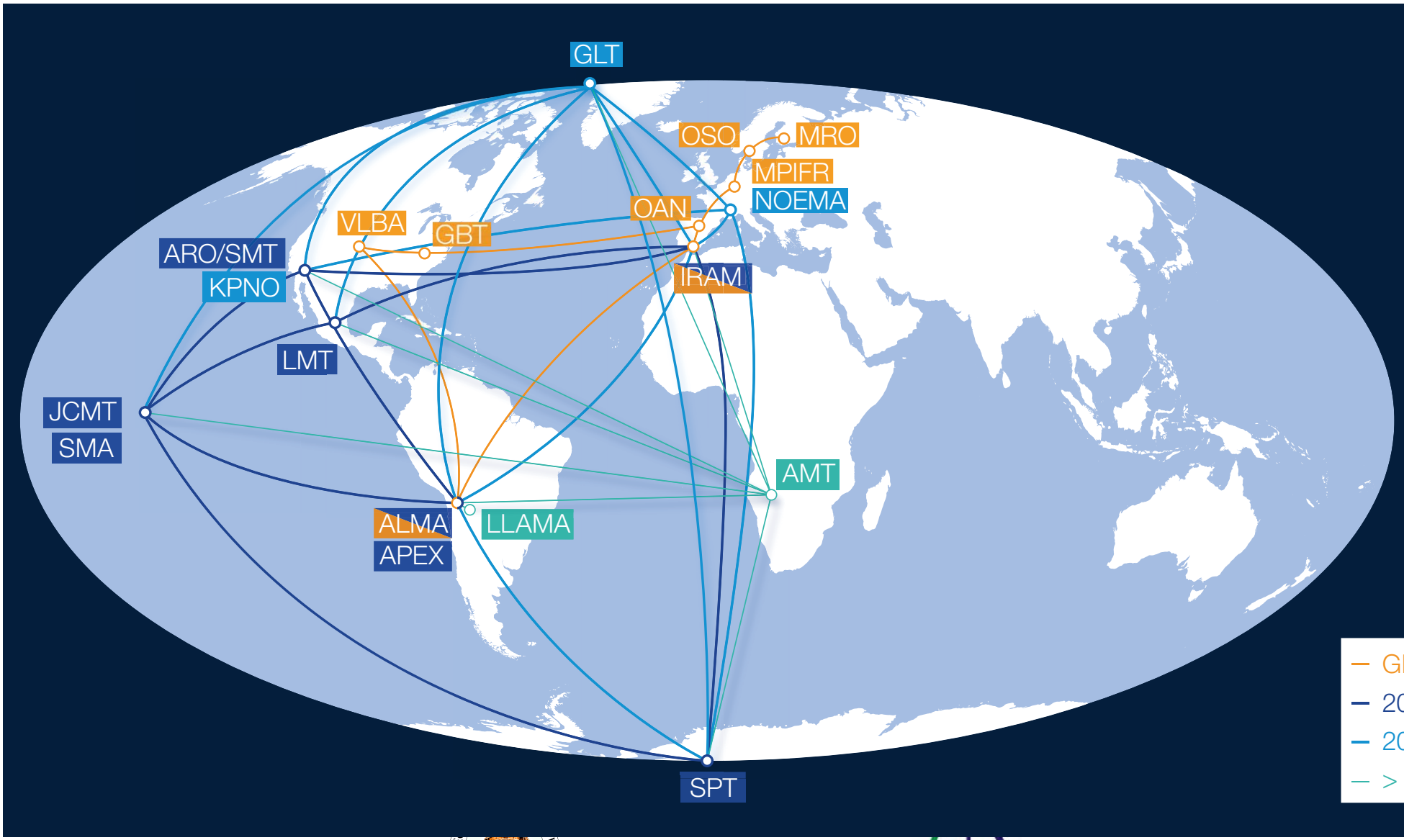
GLT
OSO
MRO
MPIFR
NOEMA
OAN
VLBA
GBT
ARO/SMT
KPNO
IRAM
LMT
JCMT
SMA
AMT
ALMA
APEX
LLAMA
SPT

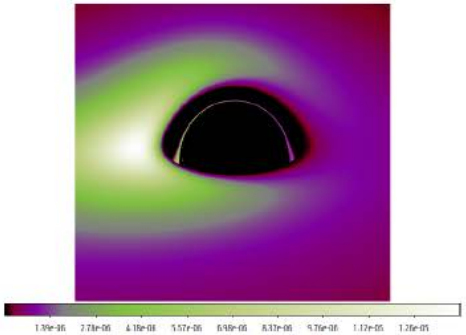

(a)$a = 0.10, \theta = 0.39\pi$

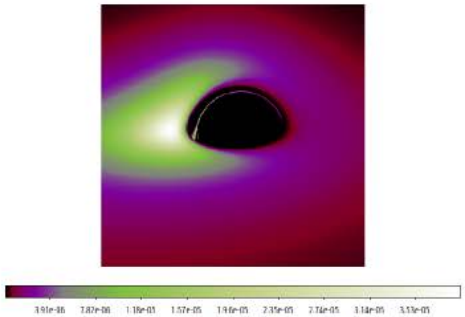

(b)$a = 0.50, \theta = 0.39\pi$

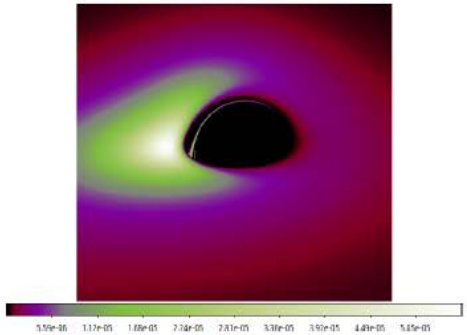

(c)$a = 0.60, \theta = 0.39\pi$

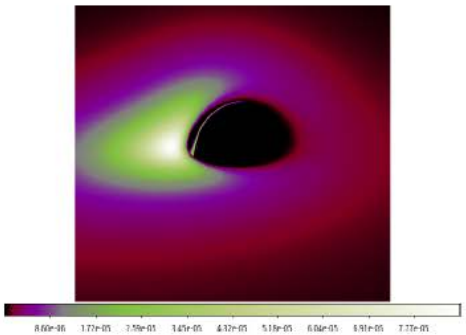

(d)$a = 0.70, \theta = 0.39\pi$

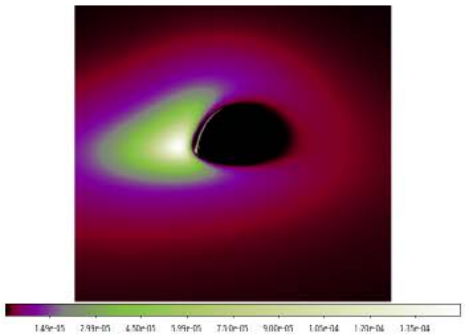

(e)$a = 0.80, \theta = 0.39\pi$

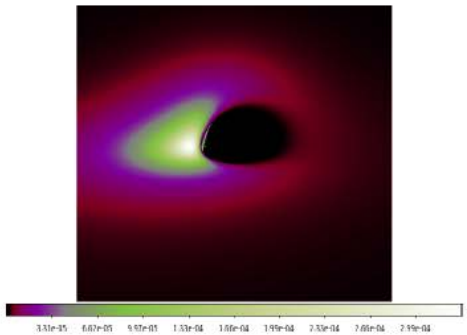

(f)$a = 0.90, \theta = 0.39\pi$

11

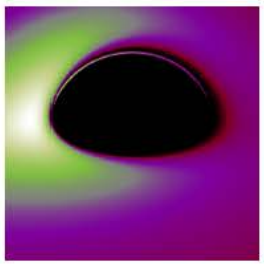

(a)$a = 0.01, \delta = 2, \theta = 0.39\pi$

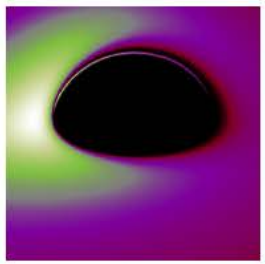

(b)$a = 0.10, \delta = 2, \theta = 0.39\pi$

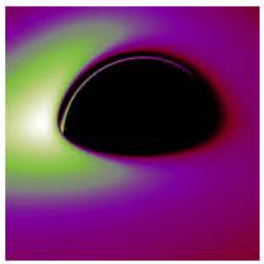

(c)$a = 0.50, \delta = 2, \theta = 0.39\pi$

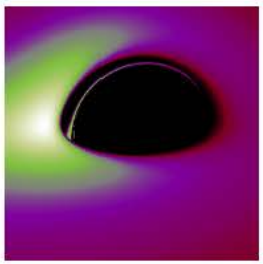

(d)$a = 0.70, \delta = 2, \theta = 0.39\pi$

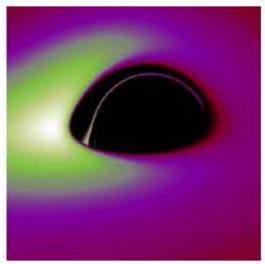

(e)$a = 0.90, \delta = 2, \theta = 0.39\pi$

FIG. 15. The geometrically thin infinite accretion disk in the δ-Kerr space-time for different values of black hole spin a when

Gravitational collapse of the magnetized star

Due to conservation of magnetic flux during collapse

$$BR^2 = const \Rightarrow B = B_0 \left(R_0/R\right)^2$$

in the nonrelativistic limit magnetic moment $\mu \sim BR^3$ decays as

$$\mu = \mu_0 \left(R/R_0\right) \Rightarrow \lim_{R\to 0} \mu = 0 \ .$$

In GR during collapse magnetic moment decays as

$$\mu(t) = \mu_0 \left(4M^2/3R_0 ct\right) \ ,$$

and exterior magnetic field should decay with t^{-1} (Ginzburg & Ozernoy 1964, Anderson & Cohen 1970, Zeldovich & Novikov 1971).
The correct decay rate at late times of an initially static dipole electromagnetic radiation field outside a black hole is $t^{-(2l+2)}$ (Price 1972, Thorne 1971).

BHs in MF

- Wald (1971) – exact analytical solution for BH immersed in asymptotically uniform MF.
- Expulsion of magnetic flux/Meissner-like effects for extreme BH – King, Lasota & Kundt (1975), Bicak & Janis (1985)
- Membrane paradigm – MacDonald & Thorne (1982), Thorne et al. (1986)

The strength of MF in the vicinity of stellar mass and supermassive black holes is
$B \approx 10^8 \mathrm{Gauss}, \quad \text{for} \quad M \approx 10 M_\odot$; $B \approx 10^4 \mathrm{Gauss}, \quad \text{for} \quad M \approx 10^9 M_\odot$

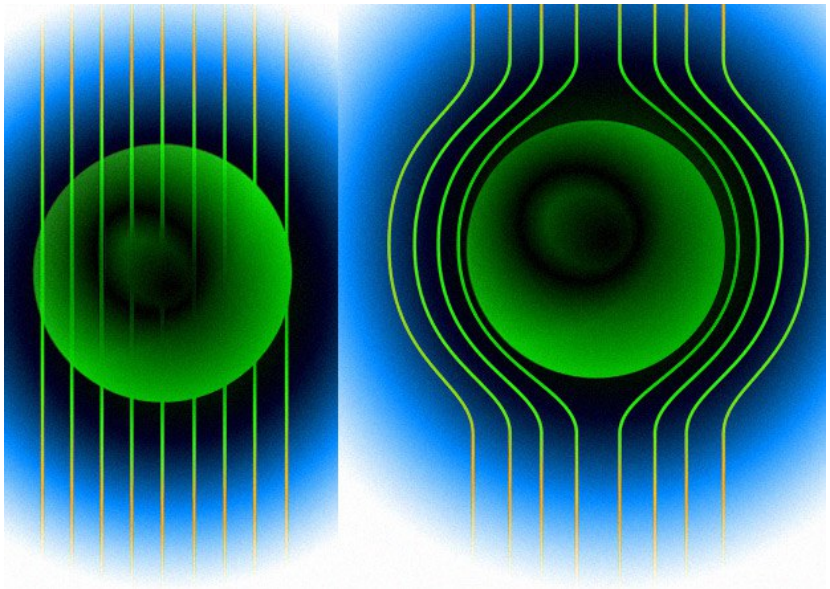

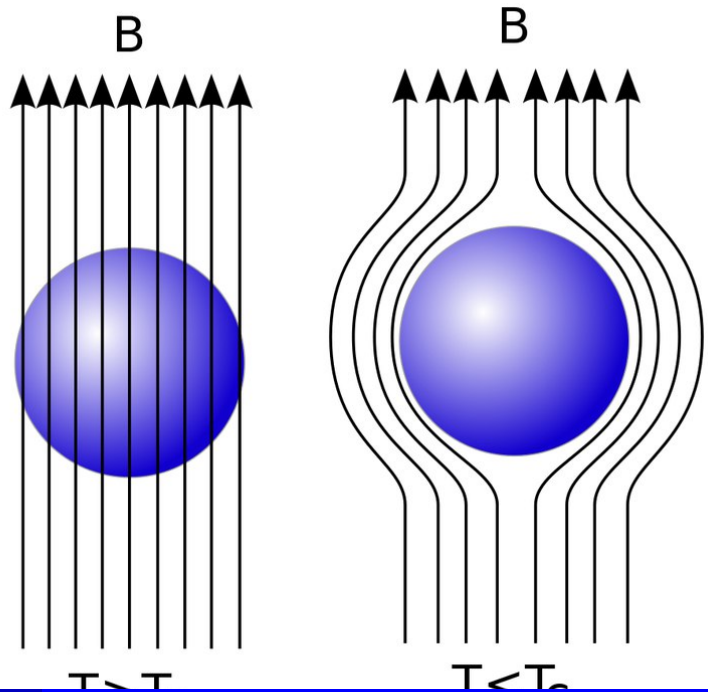

Effect of MF on charged particles: Cyclotron vs Keplerian frequency

$$\Omega_c = \frac{|qB|}{mc}\,, \quad \Omega_K = \frac{r_g^{1/2} c}{r^{3/2}\sqrt{2}}\,.$$

For electron in 10 $M_\odot$ BH environment ratio between two frequencies at $r_{\rm ISCO}$ becomes ~ 1 for milliGauss MF

$$\frac{\Omega_c}{\Omega_K} = \beta \equiv \frac{qBMG_N}{mc^4}\,.$$

Black holes are weakly magnetized

- Dynamics of surrounding plasma or accretion disk of BH
- Magnetic field of the companion or collapsed progenitor star

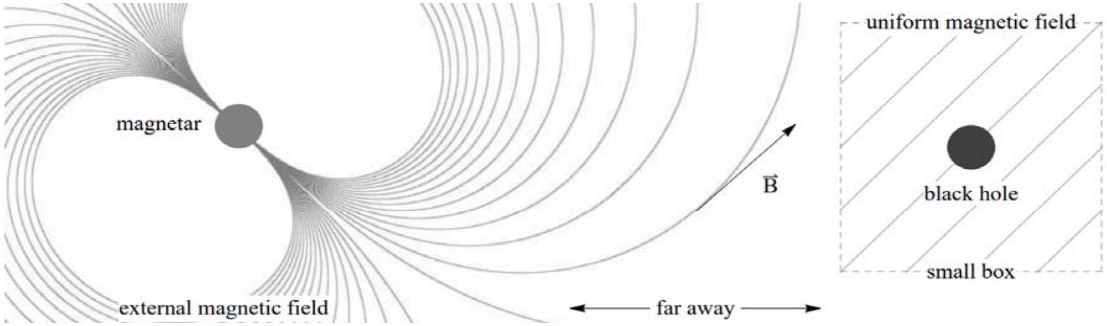

e.g. Magnetar with 10^{14} G has been found at 0.3 light years from Galactic Center by Effelsberg

- MF of **SgrA* ~ 10G**. Characteristic MF for $10^9 M_\odot$ is 10^4G; for $10 M_\odot$ up to 10^8G.
- MF is weak – it does not modify the spacetime geometry

$$B \ll \frac{c^4}{G^{3/2} M_\odot} \left(\frac{M_\odot}{M}\right) \sim 10^{19} \frac{M_\odot}{M} \, \mathrm{G}$$

- Cannot neglect **MF effects** on the charged matter

$$\frac{F_{\mathrm{lorentz}}}{F_{\mathrm{grav.}}} = \frac{eBGM}{m_p c^4} \approx 10^{11} \left(\frac{B}{10^4 \mathrm{G}}\right) \left(\frac{M}{10^9 M_\odot}\right)$$

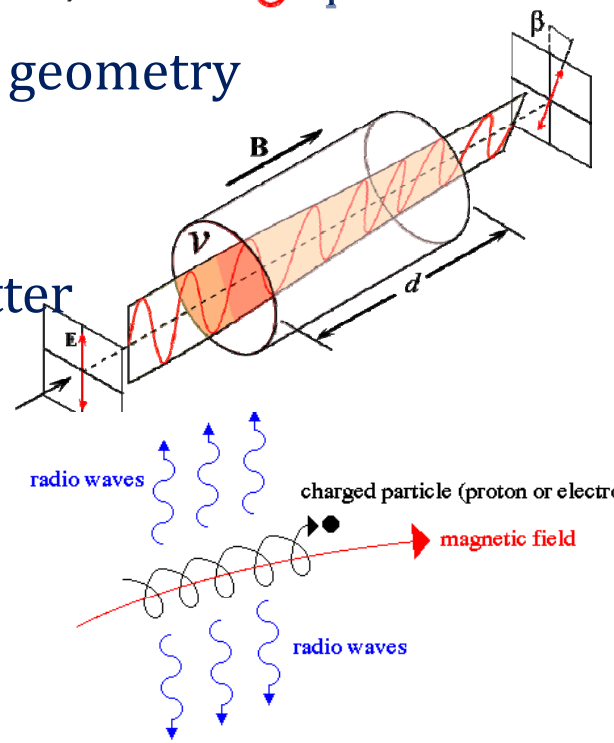

- This ratio for **SgrA* ~ 10^6**
- Measurements: Faraday rotation and synchrotron radiation

Black holes are weakly charged

Black hole + Magnetic field

- BH is characterized by M and a and Q *(usually set to zero)*
- BHs are not located in vacuum – Sgr A* is in hot plasma and threaded by MF $$A^\alpha = C_1 \xi^\alpha_{(t)} + C_2 \xi^\alpha_{(\phi)},$$
- External EM vector potential
- BH rotation generates electric field – magnetic field twist!

Process	Limit	Notes
Mass difference between p and e	$Q_{\rm eq} = 3.1 \times 10^8 \left(\frac{M_\bullet}{4\times10^6\, M_\odot}\right)$ C	stable charge
Accretion of protons	$Q^+_{\rm max} = 6.16 \times 10^8 \left(\frac{M_\bullet}{4\times10^6\, M_\odot}\right)$ C	unstable charge
Accretion of electrons	$Q^-_{\rm max} = 3.36 \times 10^5 \left(\frac{M_\bullet}{4\times10^6\, M_\odot}\right)$ C	unstable charge
Magnetic field & SMBH rotation	$Q^{\rm max}_{\bullet\rm ind} \lesssim 10^{15} \left(\frac{M_\bullet}{4\times10^6 M_\odot}\right)^2 \left(\frac{B_{\rm ext}}{10\rm G}\right)$ C	stable charge
Extremal SMBH	$Q_{\rm max} = 6.86 \times 10^{26} \left(\frac{M_\bullet}{4\times10^6\, M_\odot}\right) \sqrt{1-\tilde{a}^2_\bullet}$ C	uppermost limit

Zajacek, Tursunov, Eckart, Britzen, MNRAS (2018)

Influence of black holes charge on ISCO

One of the important characteristics of black holes in accretion theory playing crucial role in observational constraints of black hole spin is the location of the innermost stable circular orbit (ISCO).

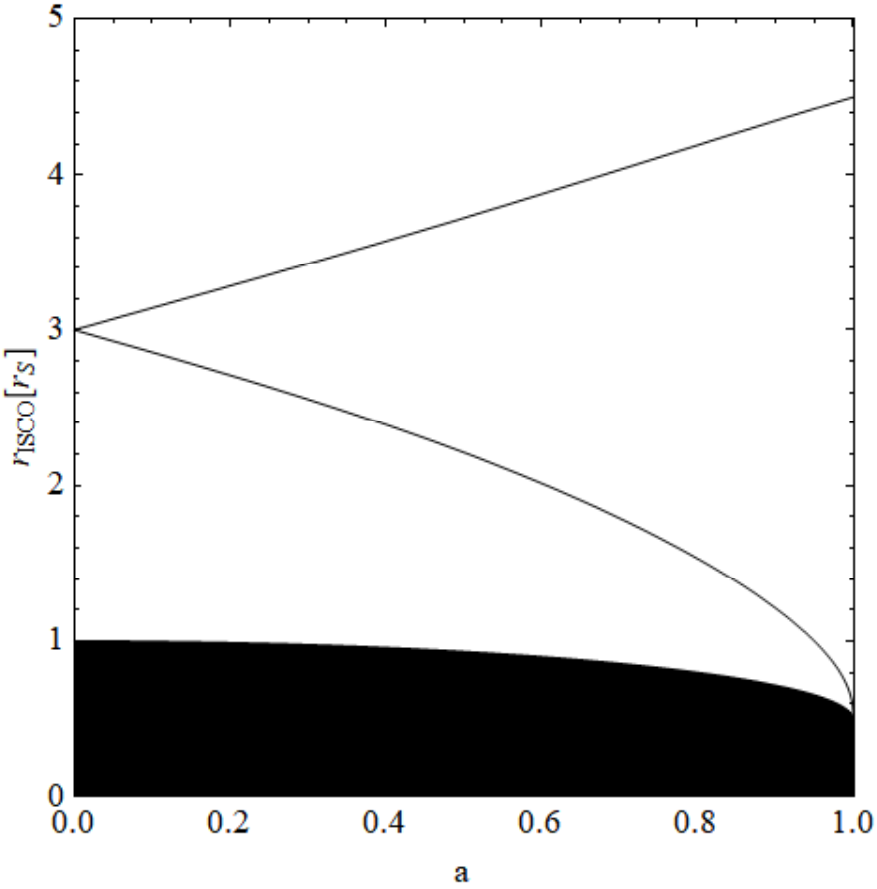

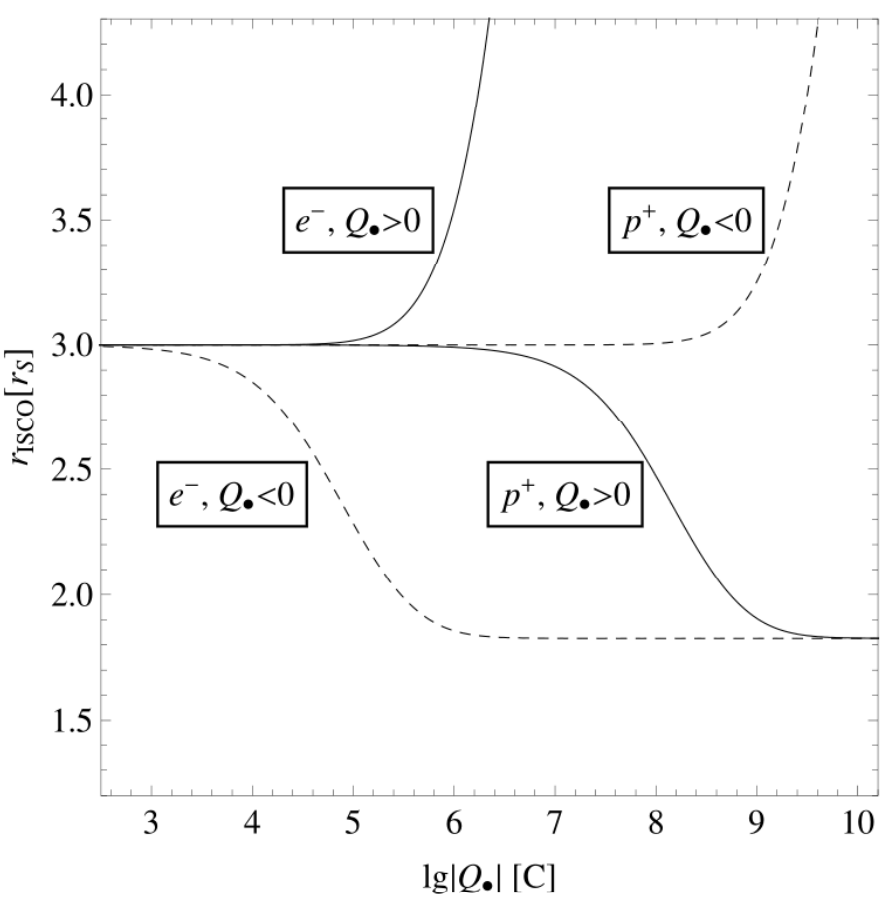

Induced charge can mimic the black hole spin of 0.6. – MNRAS,

Hot-spot orbiting SgrA*

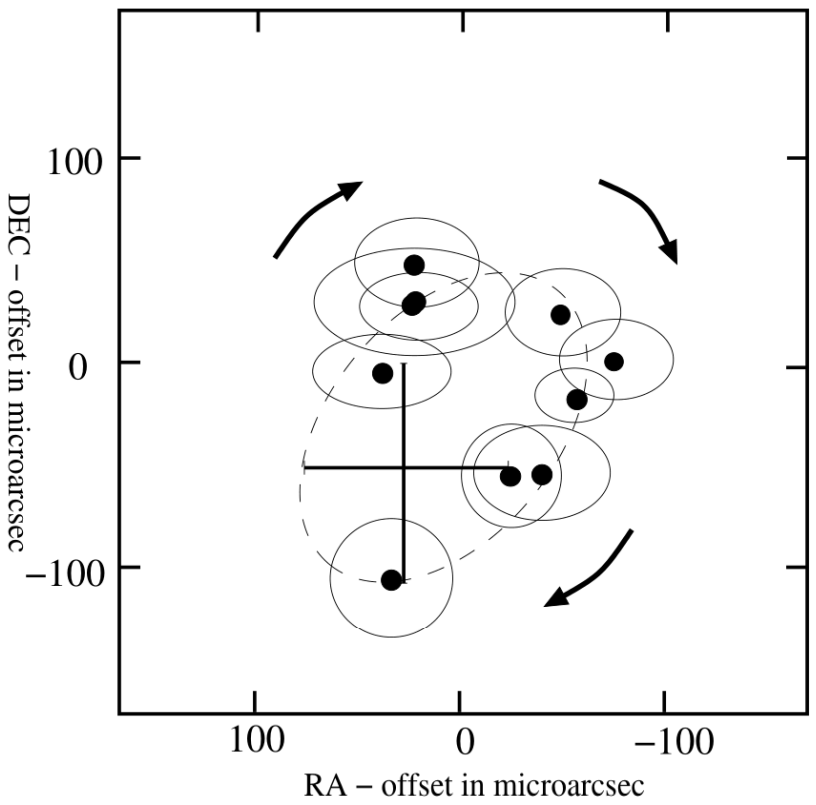

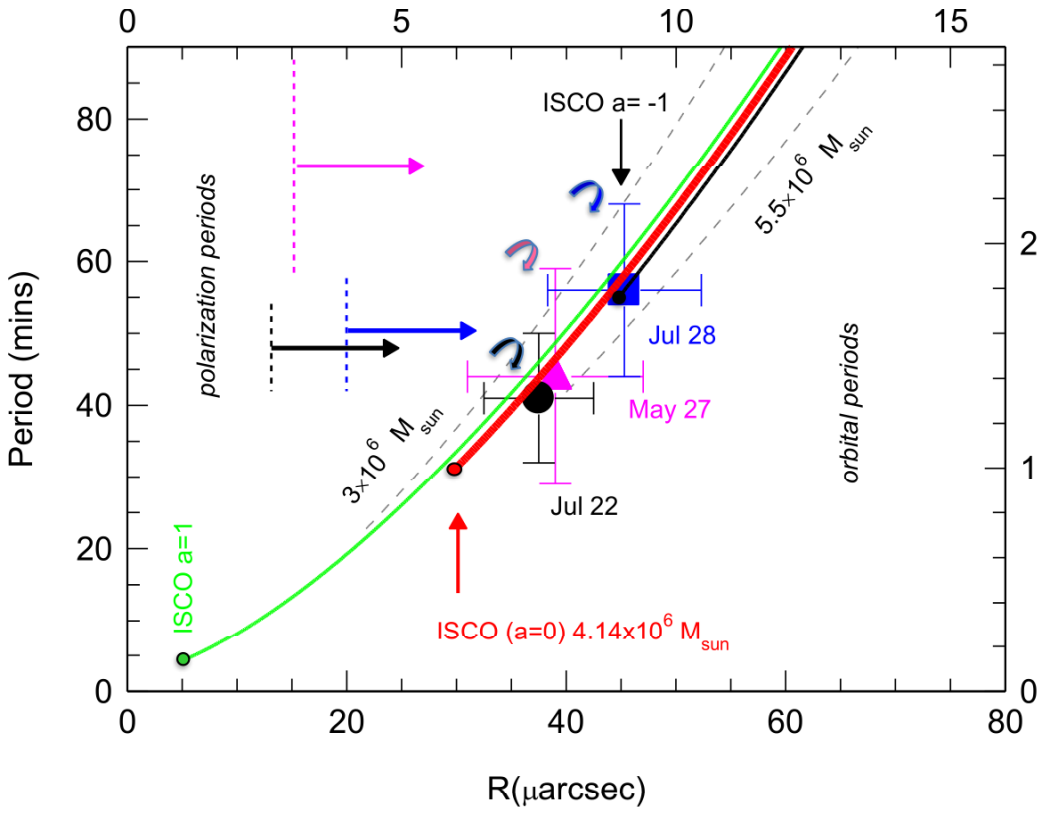

Left: Sky projected orbit of the flare emitting source component.

Right: The dependence of the orbital period on the orbital radial distance for three flare events in which orbital motion was detected.

- GRAVITY Collaboration (A&A 618, 2018) **NIR**

Presence of charge can mimic the black hole spin up to $a = 0.6$

Content

BZ versus MPP

Blandford-Znajek mechanism:

- Rapidly rotating black hole
- Negative energy inflow
- Discharge of electric field produced from twisting of magnetic field lines.
- **Charged matter**
- **Magnetic field of $> 10^4$ Gauss**

Magnetic Penrose Process:

- Rapidly rotating black hole
- Negative energy inflow
- Discharge of electric field produced from twisting of magnetic field lines.
- **Charged or neutral matter**

MPP works in three regimes:

1. Low: Penrose limit **$< 20\%$** **(neutral matter)**
2. Middle: same as BZ **$< 300\%$** **(charged matter)**
3. High: must be tested **$> 10^9\%$** **(both charged of neutral matter)**

MNRAS Letters, 478, L89 (2018)

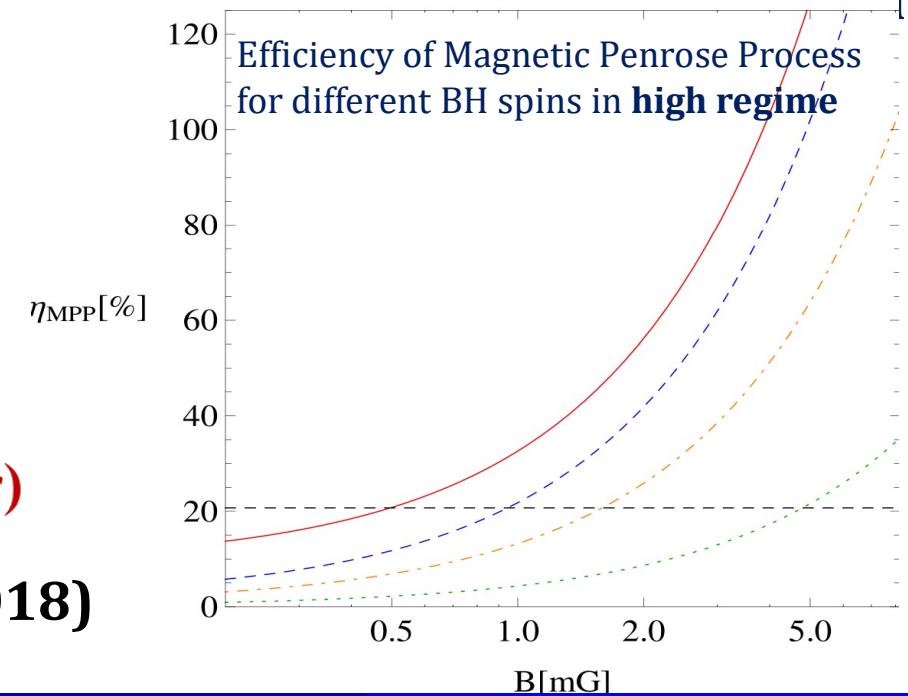

Beta-decay in ergosphere

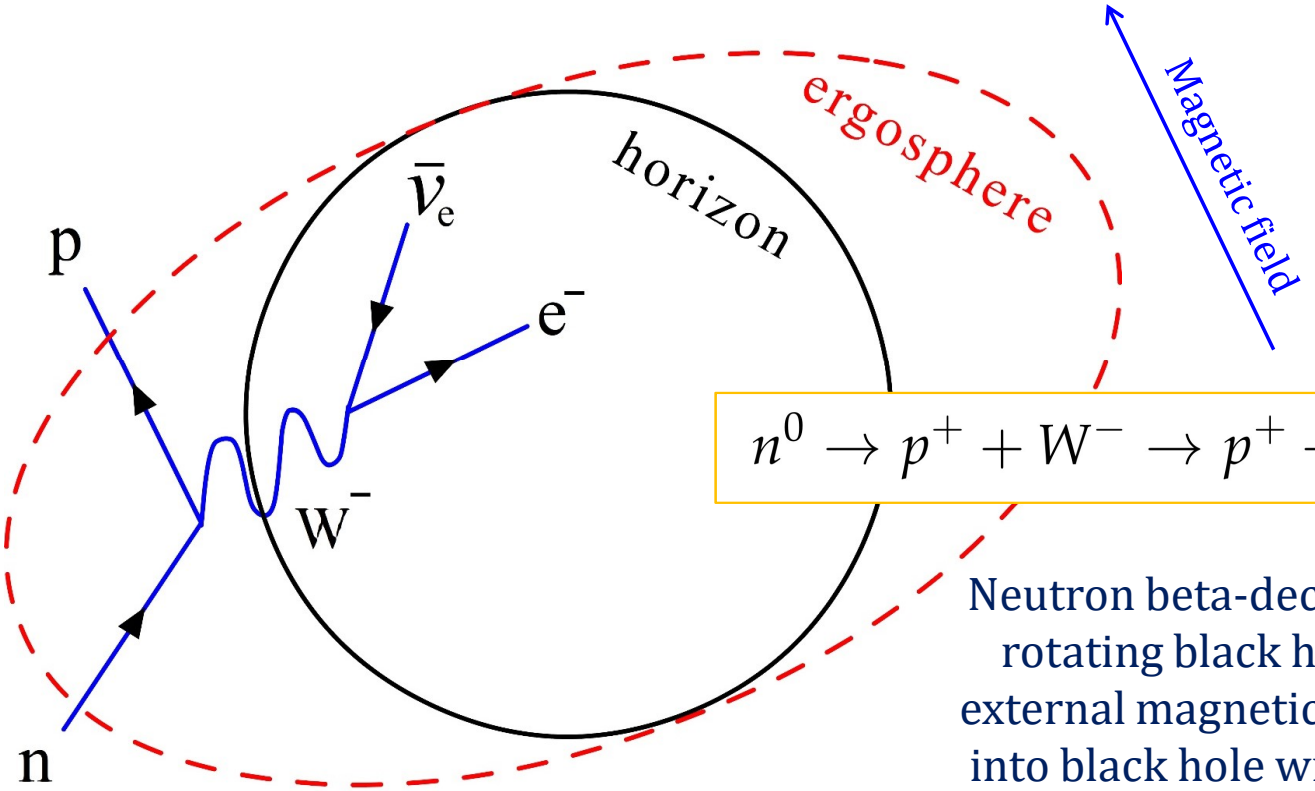

$$n^0 \to p^+ + W^- \to p^+ + e^- + \bar{\nu}_e,$$

Neutron beta-decay in the ergosphere of rotating black hole in the presence of external magnetic field. The electron falls into black hole with the negative energy.

In the hot and dense torus, with temperature of $\sim 10^{11}$ K and density $>10^{10}$ g·cm^{-3}, neutrinos are efficiently produced. The main reactions that lead to their emission are the electron/positron capture on nucleons, as well as the neutron decay. Their nuclear equilibrium is described by the following reactions:

$$p + e^- \to n + \nu_e$$
$$p + \bar{\nu}_e \to n + e^+$$
$$p + e^- + \bar{\nu}_e \to n$$

A. Janiuk et al, Galaxies 5, 15 (2017

Energy of proton driven away from BH

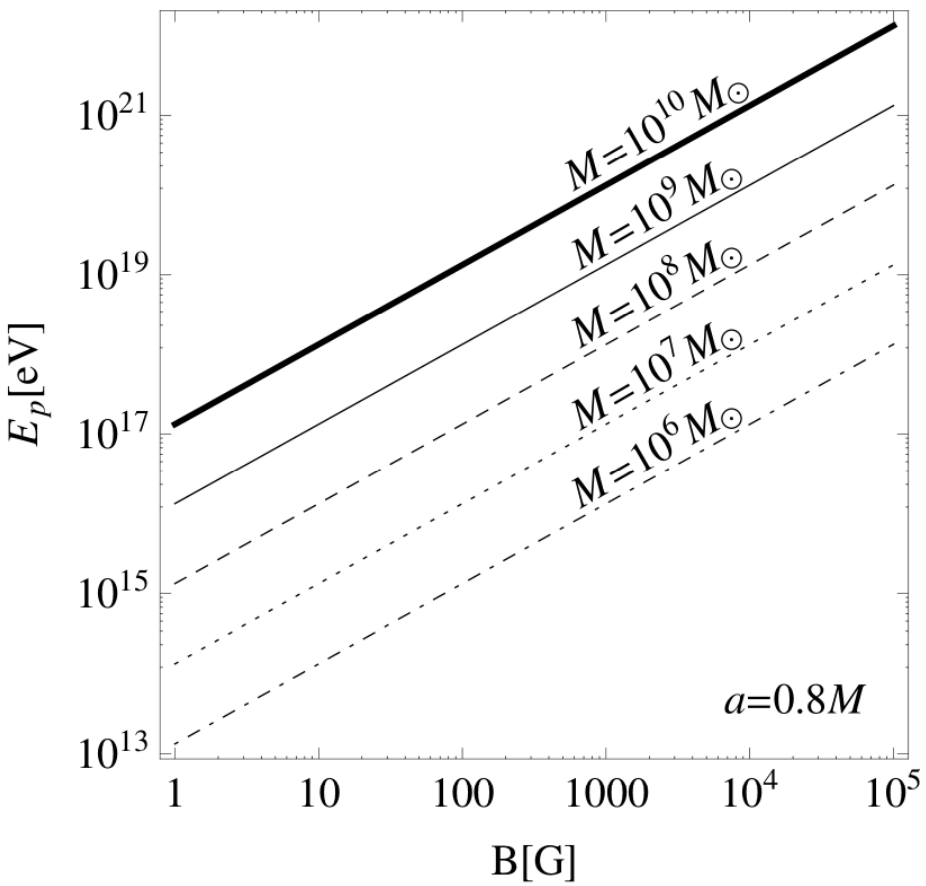

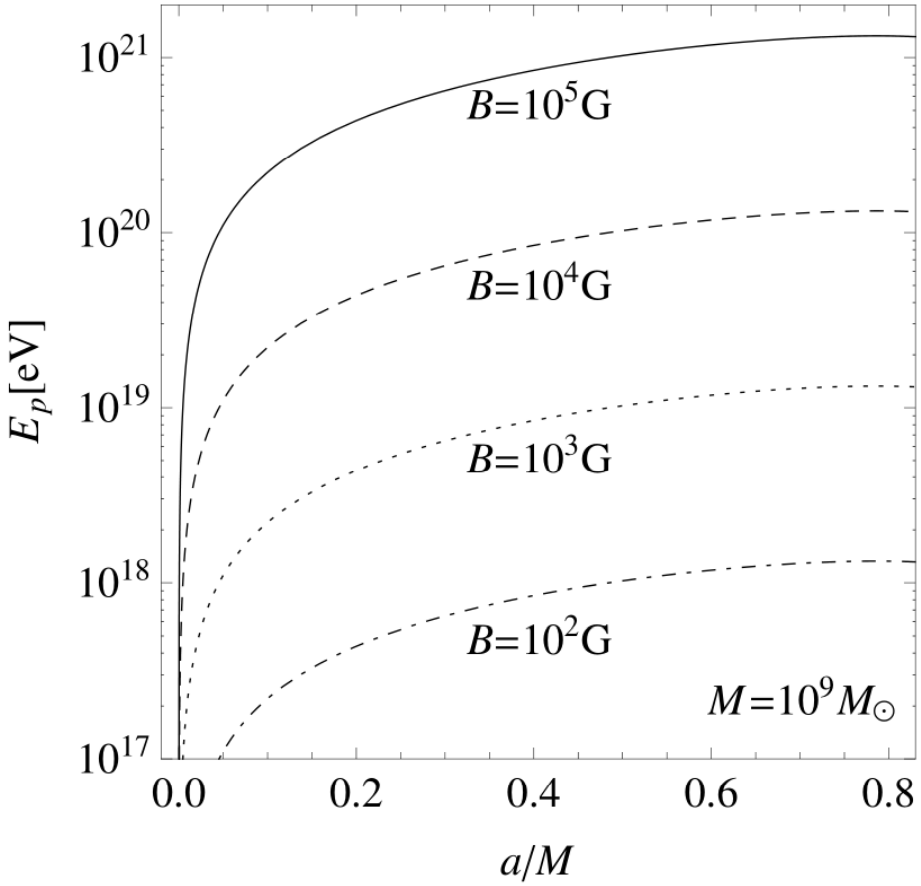

The energy of free neutron is ~ 0.94 × 10^9eV

$$E_{p^+} = 1.33\times10^{20}\mathrm{eV}\left(\frac{q}{e}\right)\left(\frac{m}{m_{p^+}}\right)^{-1}\left(\frac{B}{10^4\mathrm{G}}\right)\left(\frac{M}{10^9 M_\odot}\right).$$

Constraints on parameters

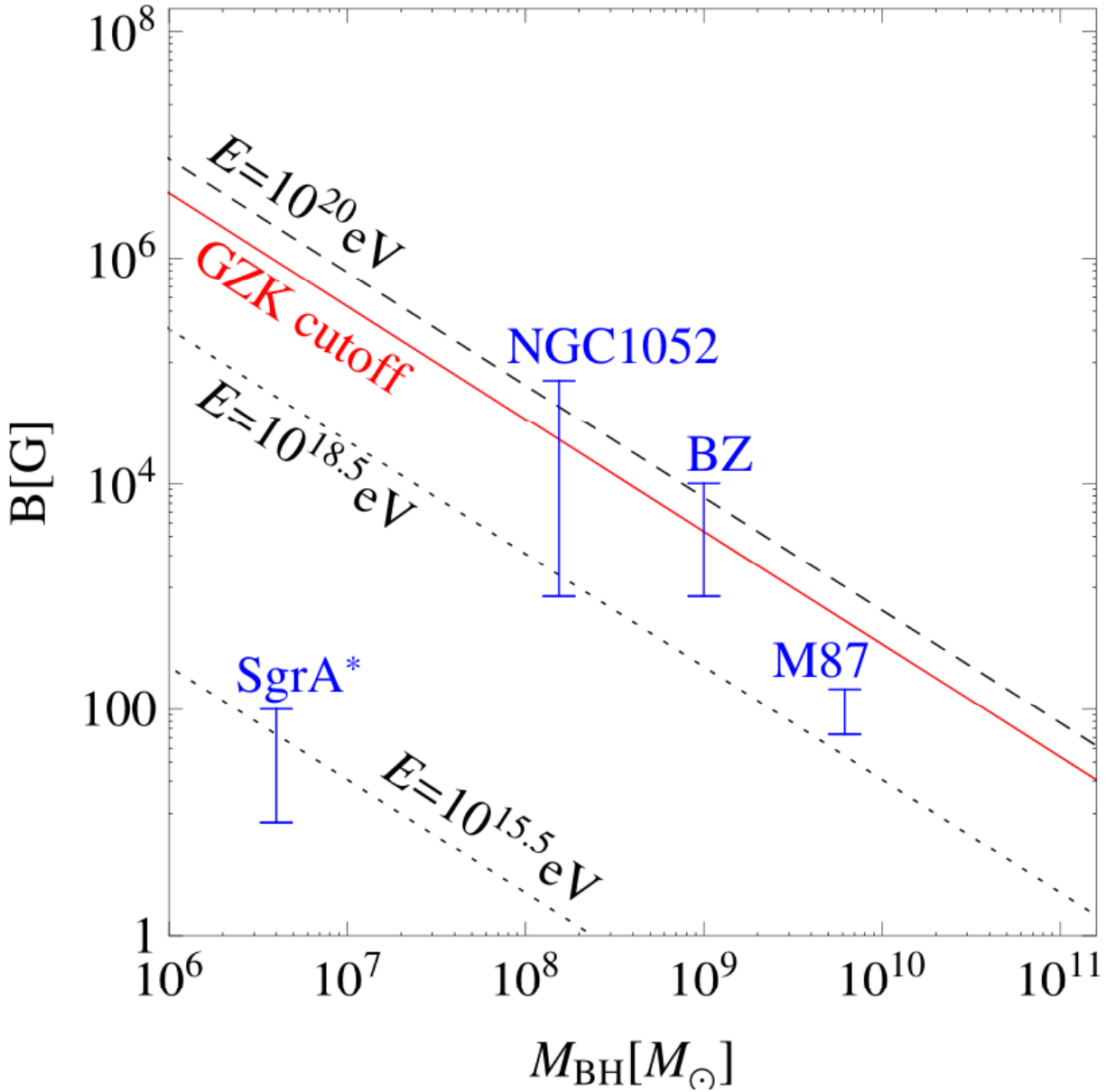

IceCube and multimessenger observations

RESEARCH ARTICLE

NEUTRINO ASTROPHYSICS

Neutrino emission from the direction of the blazar TXS 0506+056 prior to the IceCube-170922A alert

IceCube Collaboration*†

Science 361, 147 (2018)

RESEARCH ARTICLE SUMMARY

NEUTRINO ASTROPHYSICS

Multimessenger observations of a flaring blazar coincident with high-energy neutrino IceCube-170922A

The IceCube Collaboration, *Fermi*-LAT, MAGIC, *AGILE*, ASAS-SN, HAWC, H.E.S.S, *INTEGRAL*, Kanata, Kiso, Kapteyn, Liverpool Telescope, Subaru, *Swift/NuSTAR*, VERITAS, and VLA/17B-403 teams*†

Science 361, 146 (2018)

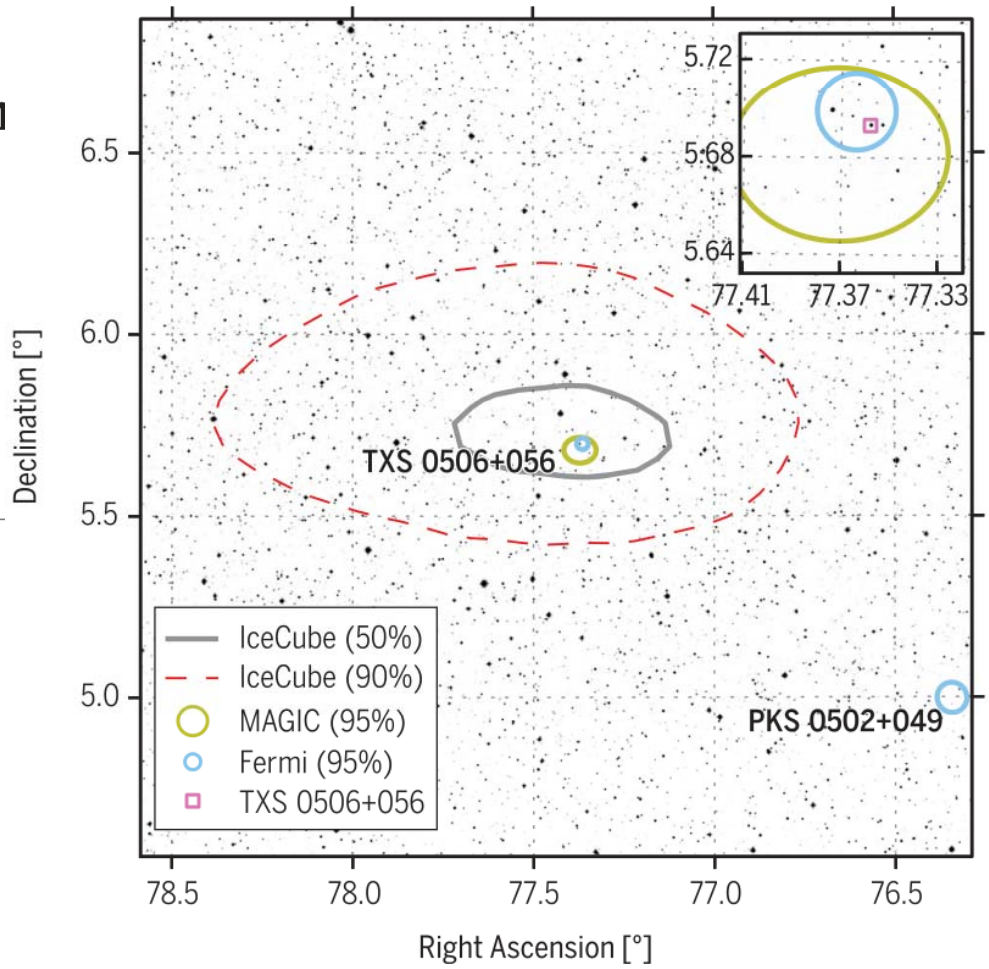

Multimessenger observations of blazar TXS 0506+056.

Content

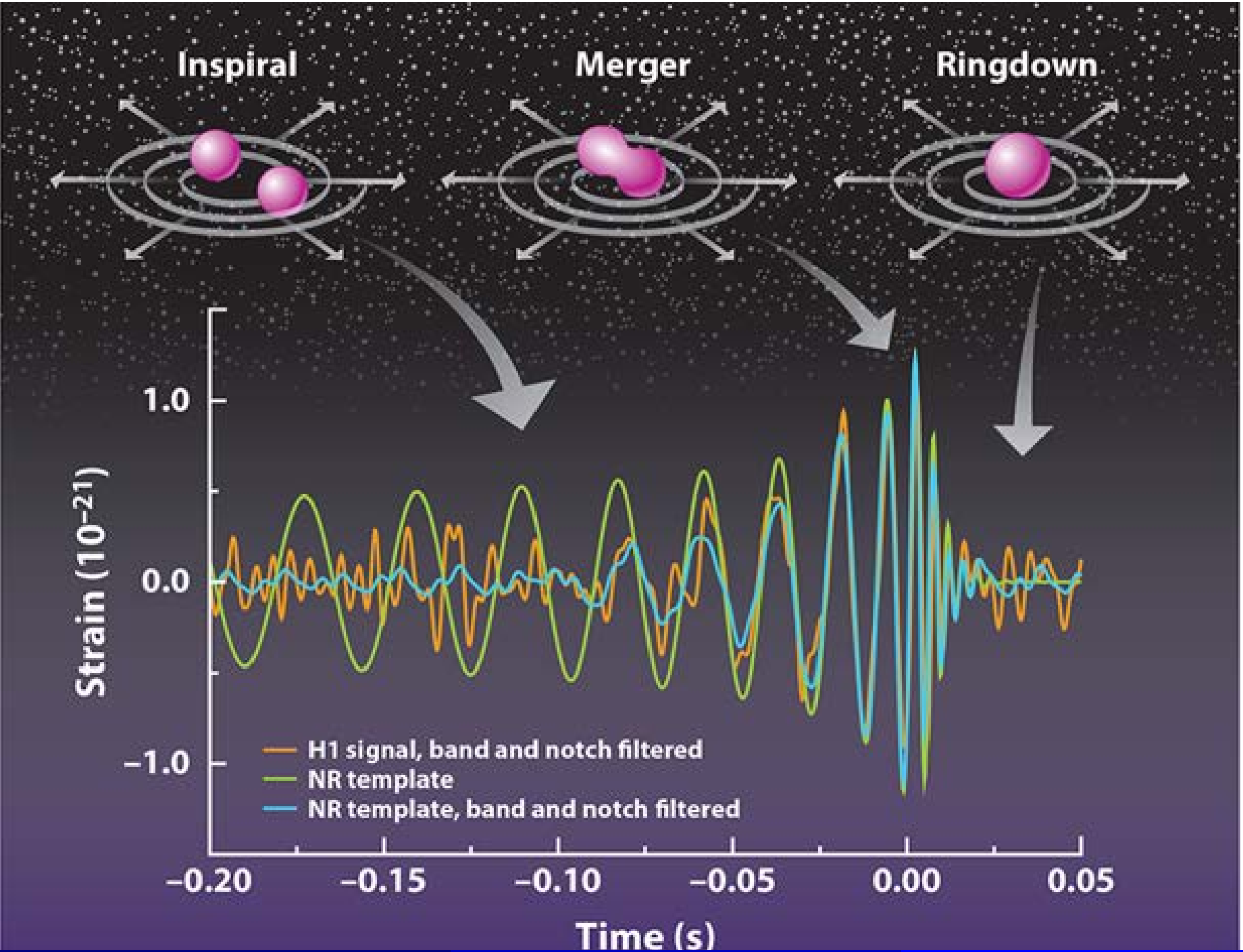
Inspiral
Merger
Ringdown
1.0
0.0
−1.0
Strain (10−21)
H1 signal, band and notch filtered
NR template
NR template, band and notch filtered
−0.20
−0.15
−0.10
−0.05
0.00
0.05
Time (s)

QNMs of test fields around regular BHs, Toshmatov, Abdujabbarov, Stuchlik, AB, PRD 91, 083008 (2015)

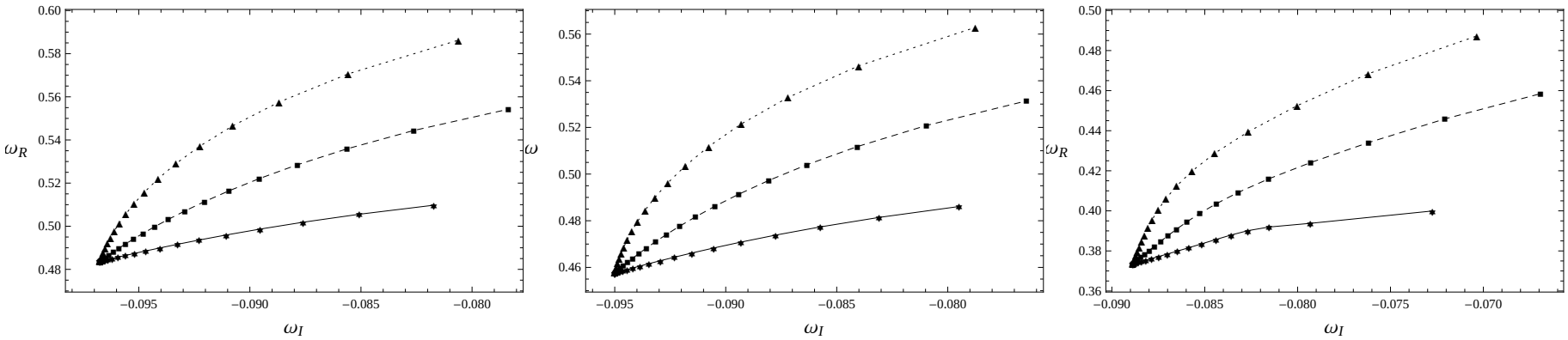

From left to right: QNMs of the scalar, electromagnetic and gravitational perturbative fields in the Hayward (solid $*$), Bardeen (dashed ■) and Ayón-Beato-García (dotted ▲) BH spacetimes.

QNMs of BH in braneworld, Toshmatov, Stuchlik, Schee, AB, PRD 93, 124017 (2016)

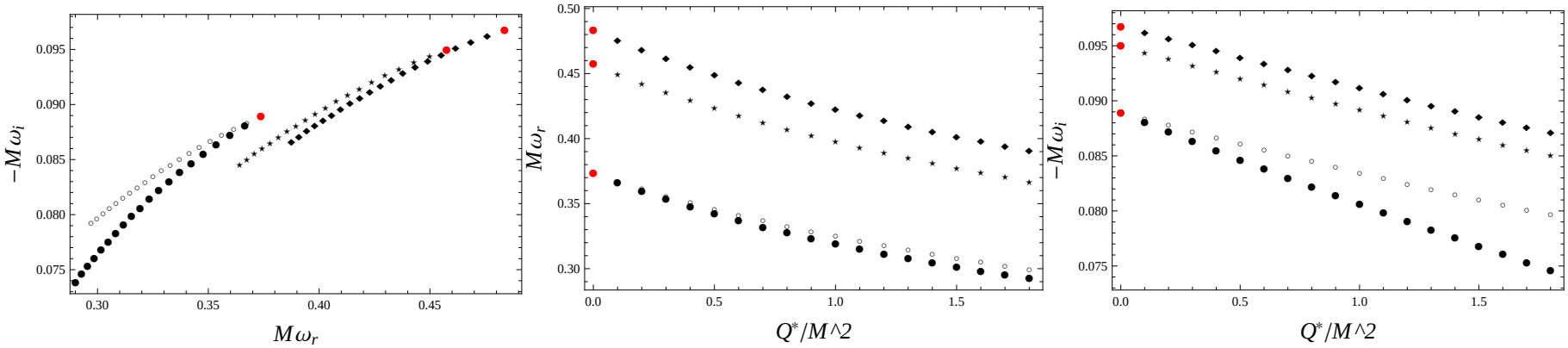

$l = 2$, $n = 0$ QNMs of the scalar (■), electromagnetic (★), axial (○) and polar (●) gravitational perturbations of the BH on the brane with the change of the tidal charge parameter Q^*/M^2. Where red spot corresponds to the ones of the Schwarzschild BHs.

EM perturbations of BHs in GR coupled to NED, Toshmatov, Stuchlik, Schee, AB, PRD 97, 084058 (2018)

General formalism of the EM perturbations of BHs in GR+NED is derived for the both electrically and magnetically charged BHs.

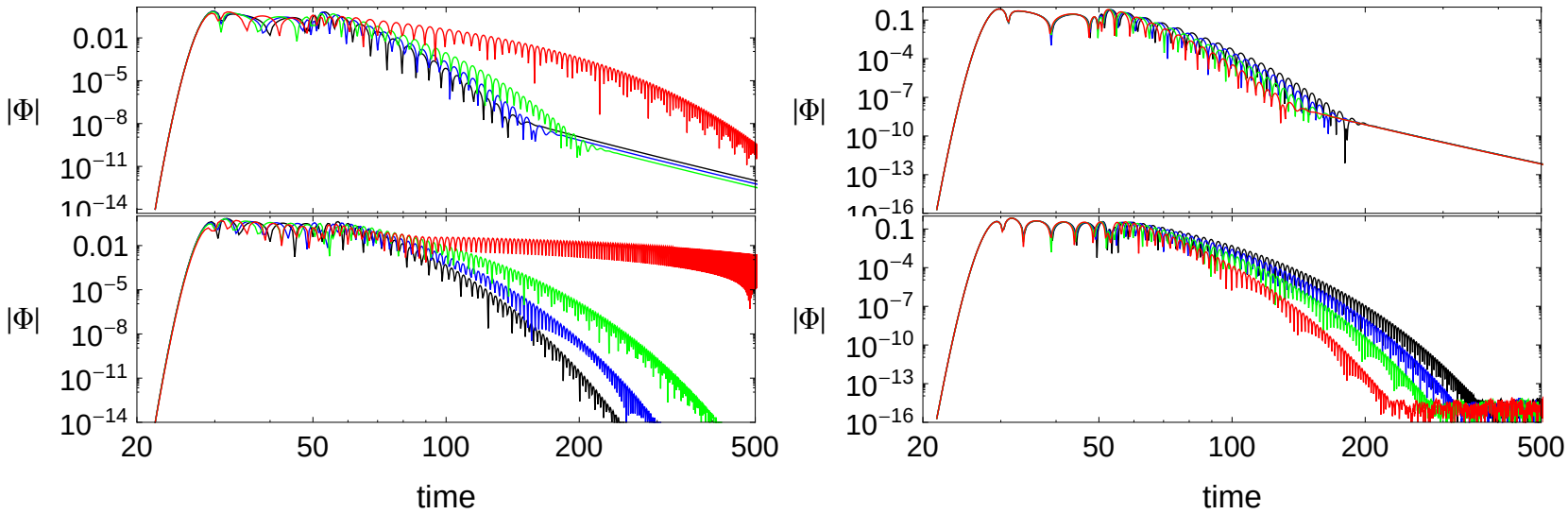

Temporal evolution of $\ell = 2$ (top panel) and $\ell = 4$ (bottom panel) fundamental modes of the EM perturbations of the Maxwellian regular (left panel) and the RN (right panel) BHs for the values $Q = 0.2$ (black), $Q = 0.6$ (blue), $Q = 0.8$ (green), and $Q = 0.998$ (red).

PRD 97, 084058 (2018)

Cardoso et al (2009): for the large multipole numbers QNMs are determined as

$$\omega = \Omega_c \ell - i\left(n + \frac{1}{2}\right)|\lambda|$$

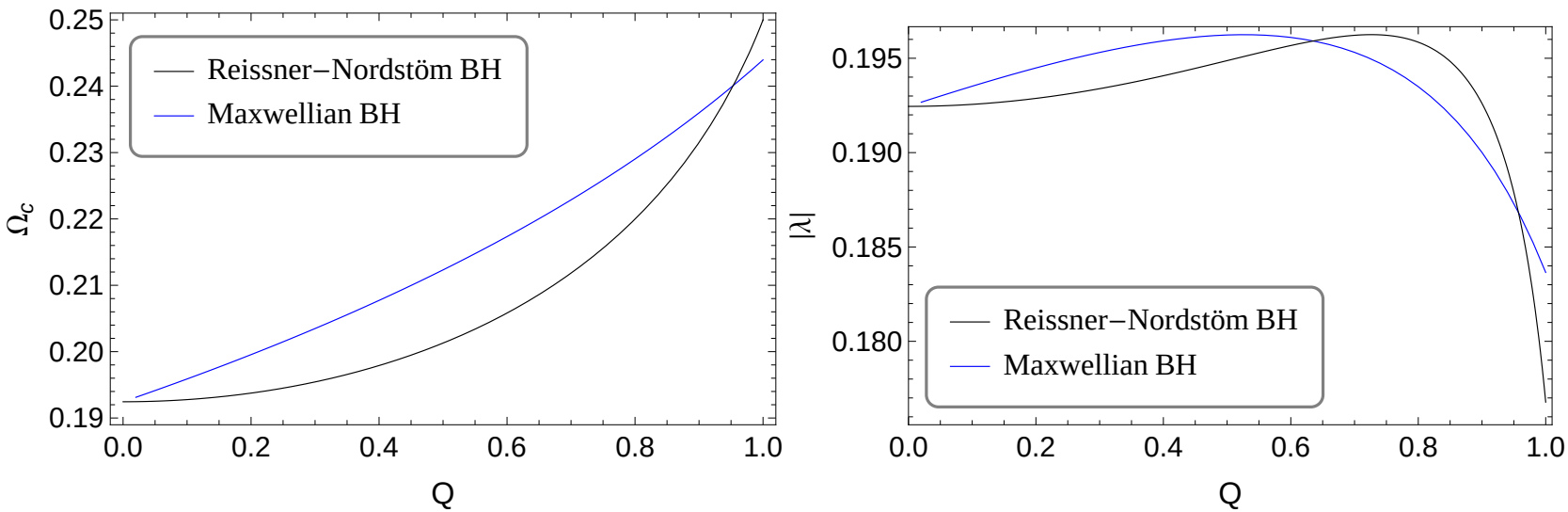

Dependence of angular velocity (Ω_c) and lyapunov exponent (λ) of circular unstable null geodesics on the normalized charge parameter of RN (black) and Maxwellian regular (blue) BHs.

Content

ENERGETICS

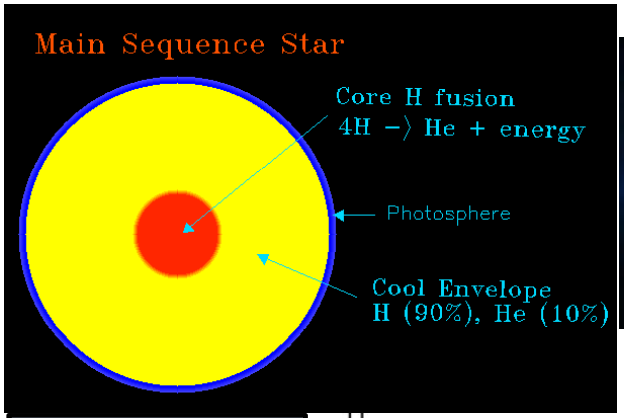

a few 10^{33} erg/s

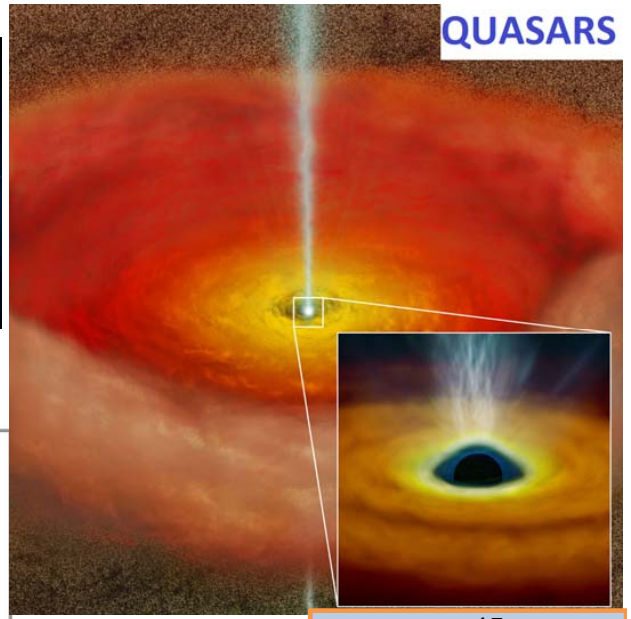

a few 10^{45} erg/s

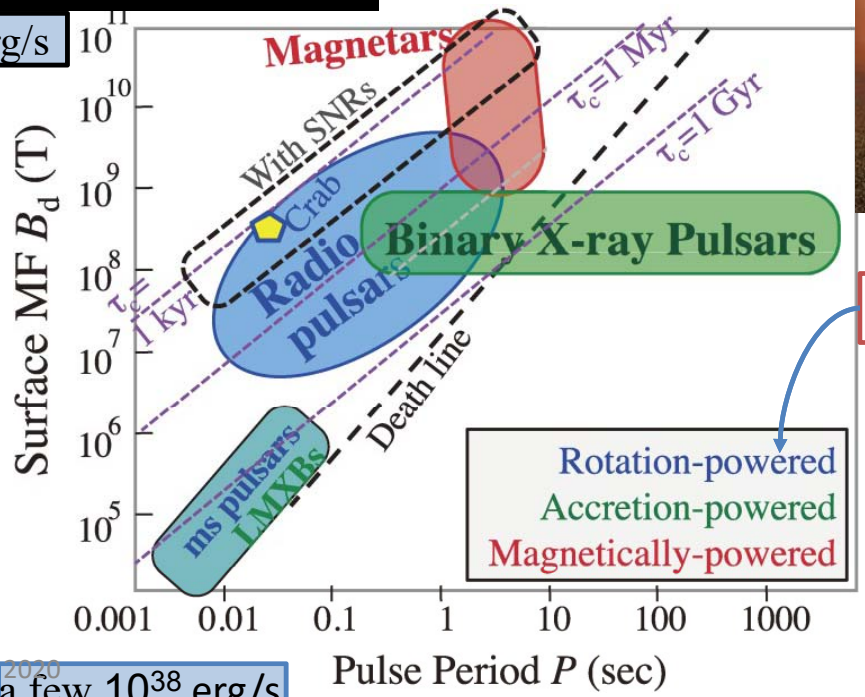

a few 10^{38} erg/s

T.Gold,Nature,1968

Moreover, oscillating-powered pulsars/magnetars model has also been suggested and shown how oscillating kinetic energy transforms to EM radiation energy.

NS Magnetosphere

EF on the Star Surface:

$$E \propto \frac{\Omega R}{c} B \propto \frac{\Omega \xi}{c} B \propto 10^{10} \mathrm{V} \cdot \mathrm{cm}^{-1}$$

Goldreich & Julian, 1969, Astrophys.J, 157, 869
Cascade generation of electron-positron plasma leads to formation of MS with plasma screening longitudinal EF.
Plasma is corotating with the neutron star.
Charges along open field lines create plasma modes.

Plasma magnetosphere of NS

Goldreich & Julian 1969

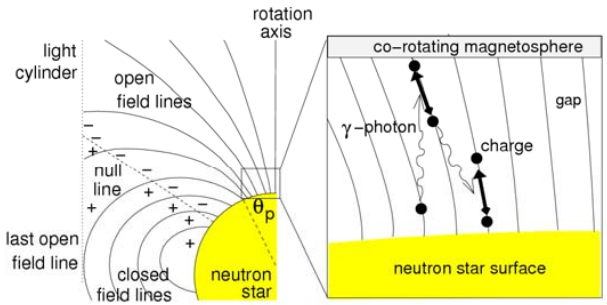

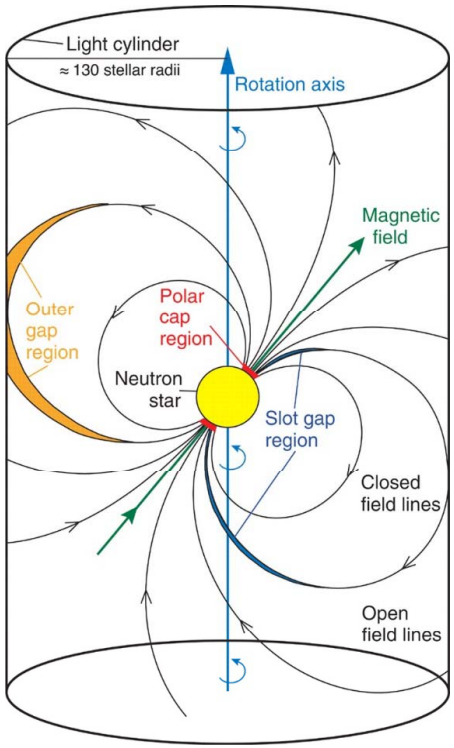

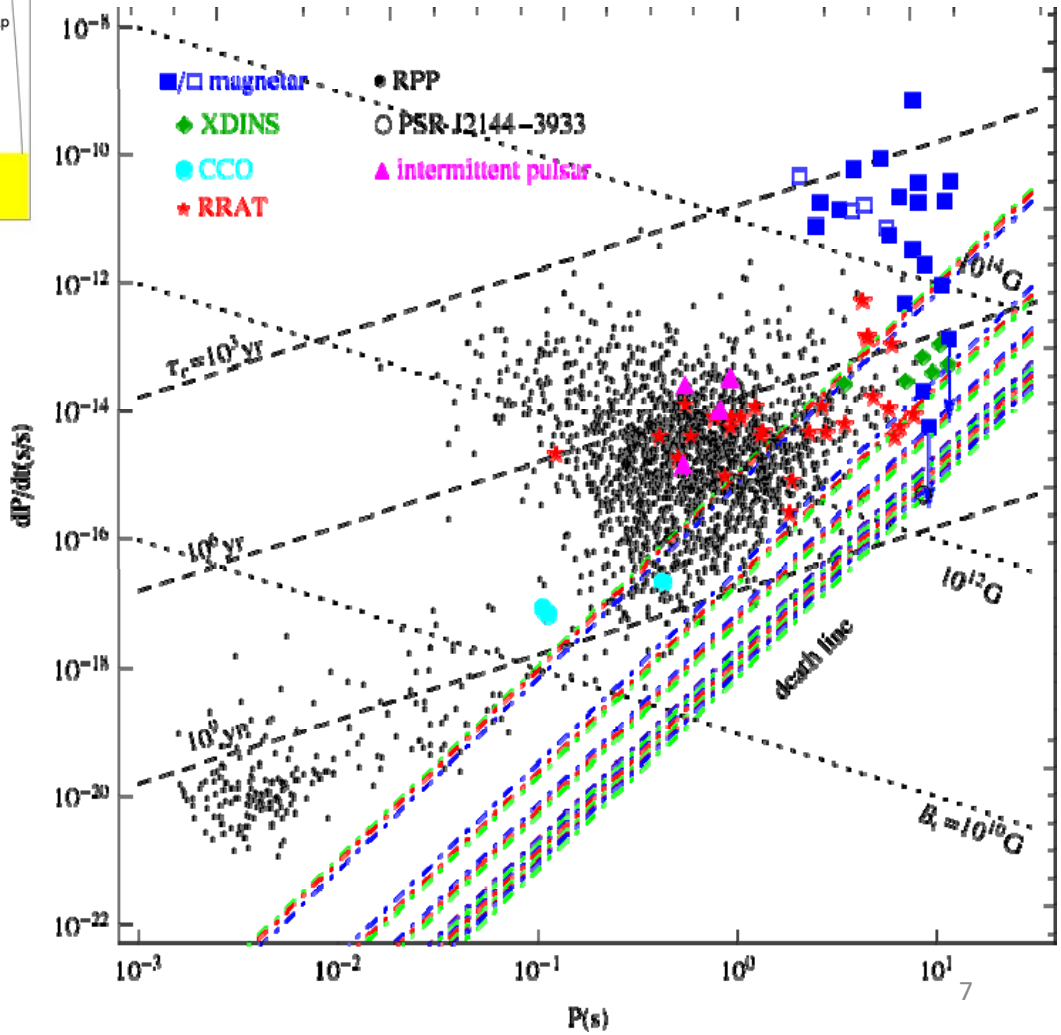

Content

Ratio $\delta\rho_{\mathrm{GJ}\ l'm'}/\rho_{\mathrm{GJ},0}$ for the mode $(1,0)$ (left-hand top panel), $(1,1)$ (left-hand bottom panel), $(2,0)$ (right-hand top panel) and $(2,1)$ (right-hand bottom panel). NS parameters $\kappa = 0.15$, $\varepsilon = 1/3$, $K = 0.01$, $\Theta_0 = 0.008$, $\Omega = 1\mathrm{rad\ s}^{-1}$.

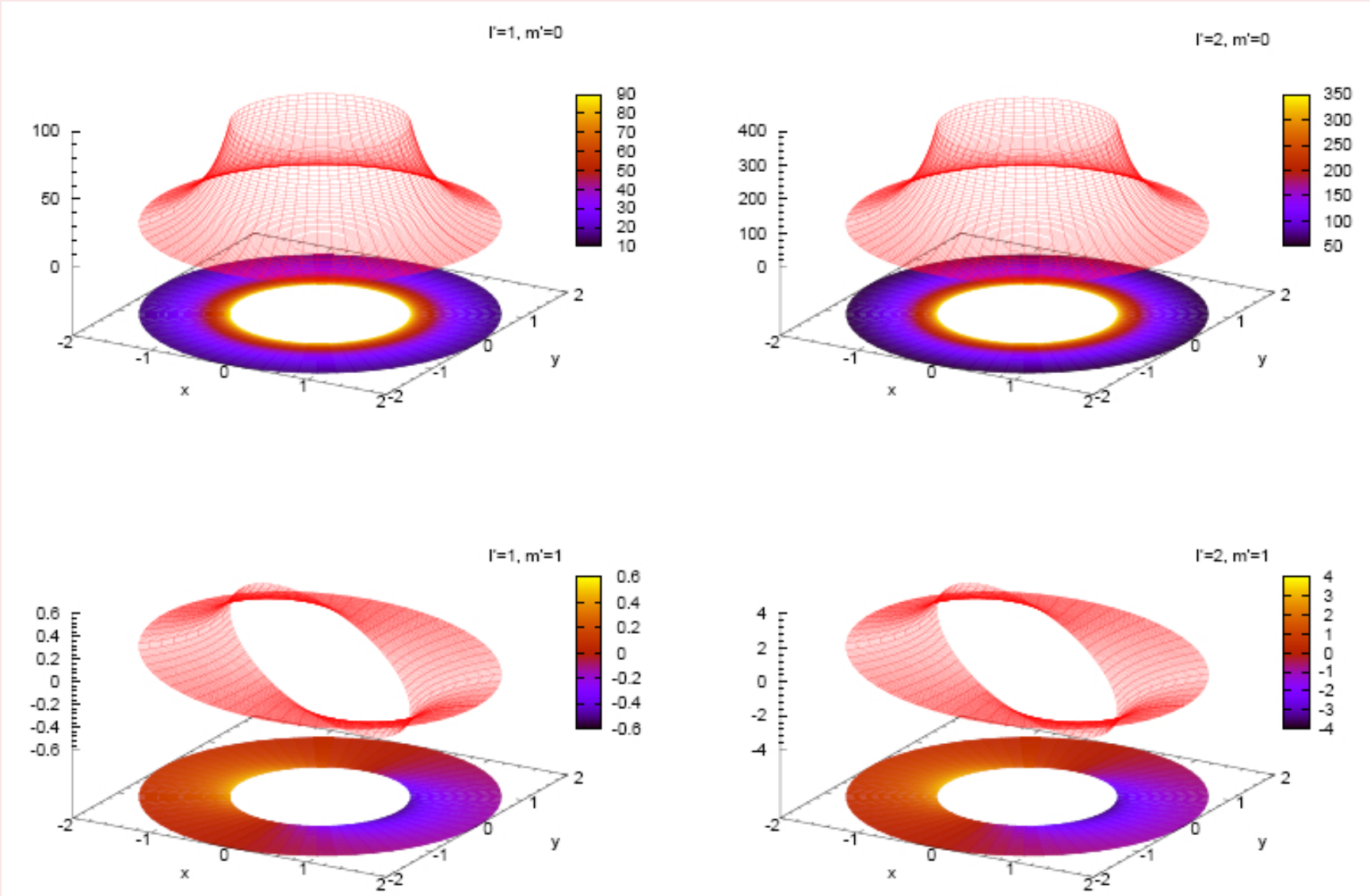

Ratio of longitudinal component of EF to E_0 for the mode $(1,0)$ (left-hand top panel), $(1,1)$ (left-hand top panel), $(2,0)$ (right-hand top panel) and $(2,1)$ (right-hand bottom panel).

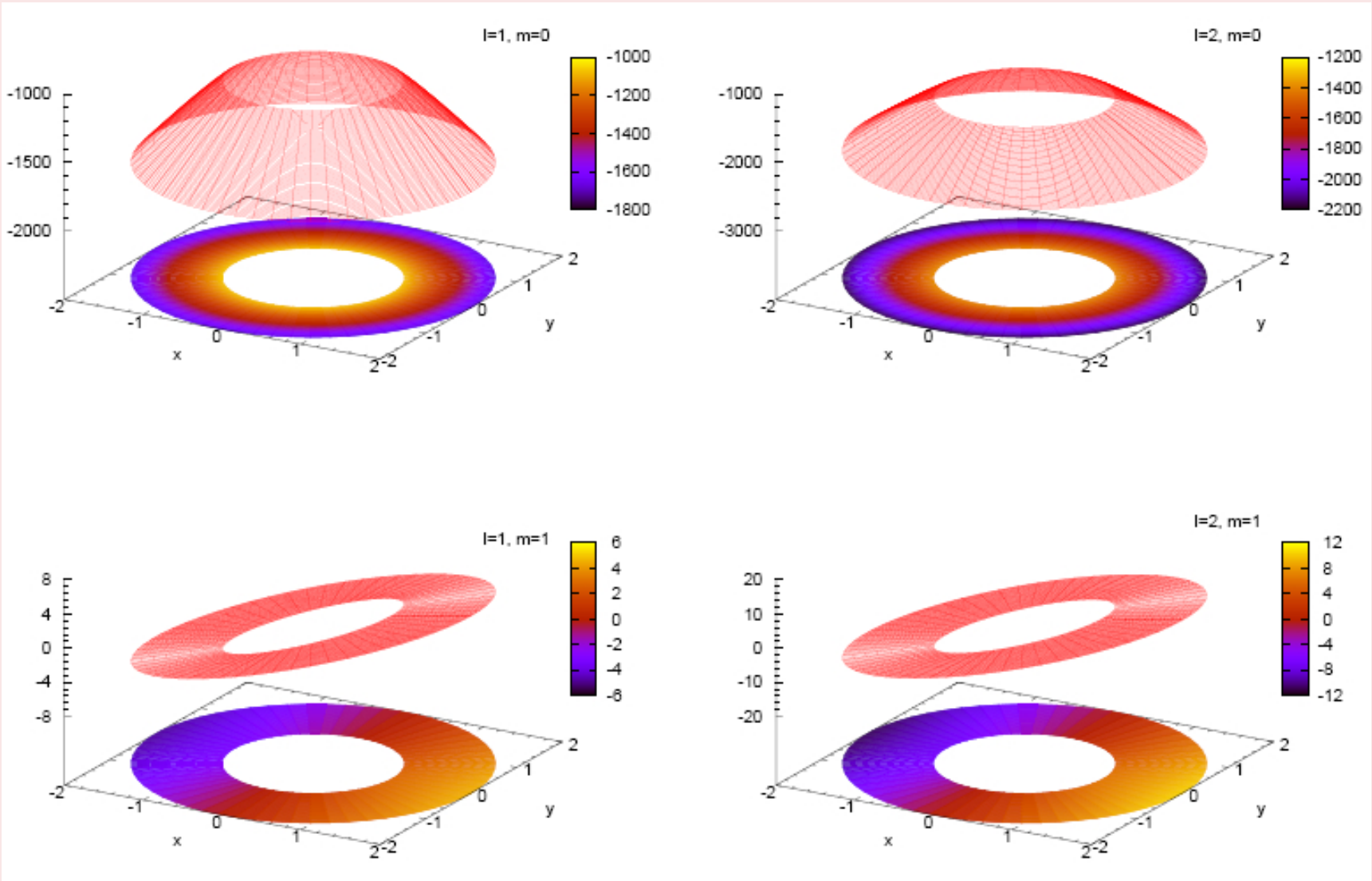

The ratio L_m/L_{rot} as a function of parameter $K = \tilde{\eta}(1)/\Omega R$ for modes $(1,1)$ (continuous red line) and $(2,1)$ (dotted blue line).

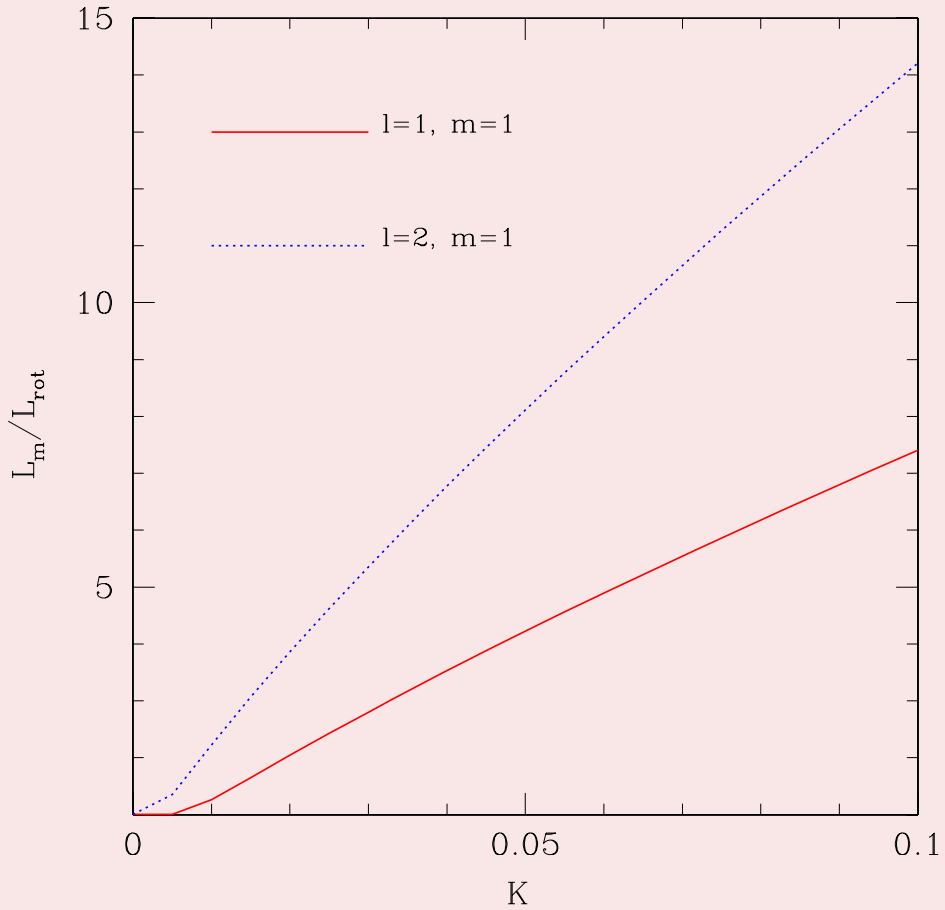

Constrains on parameters of Einstein-Aether gravity

Radio-load isolated NSs

P. A. Caraveo, Annual Review of Astronomy and Astrophysics, (2014)

Neutron star	Period, P millisecond	$\frac{dP}{dt} \times 10^{-15}\ s/s$	c_{13}, (c_{14}=0) ICS	c_{14}, (c_{13}=0) ICS	c_{13}, (c_{14}=0) CR	c_{14}, (c_{13}=0) CR
PSR J1057 – 52269	197.114	5.83	0.952158	-39.8041	0.98342	-42.3326
PSR J1509 – 5850	88.925	9.17	0.951734	-39.4366	0.98658	-41.6524
PSR J1952 + 3252	39.534	5.83	0.951968	-39.9528	0.98698	-42.1368
PSR J2030 + 3641	200.129	6.51	0.952169	-39.8139	0.97986	-43.0021
PSR J2043 + 2740	96.131	1.23	0.952085	-39.7405	0.97963	-43.0124

Radio-quite isolated NSs

S.Mereghetti, Astrophysics and Space Science 2011

Neutron star	Period, P millisecond	$\frac{dP}{dt} \times 10^{-15}$ s/s	c_{13}, (c_{14}=0) ICS	c_{14}, (c_{13}=0) ICS	c_{13}, (c_{14}=0) CR	c_{14}, (c_{13}=0) CR
PSR J1746 – 3239	199.541	6.56	0.952171	-39.8153	0.98465	-42.6547
PSR J0106 + 4855	83.157	0.428	0.951896	-39.3827	0.98015	-43.0154
PSR J1836 + 5925	173.264	1.5	0.951938	-39.3482	0.98652	-43.65812
PSR J2028 + 3332	176.707	4.86	0.952156	-39.8026	0.9845	-42.6895
PSR J2139 + 4716	282.849	1.8	0.951767	-39.4654	0.98432	-43.0098
PSR J2030 + 4415	227.070	6.49	0.952144	-39.7917	0.98654	-42.3651
PSR J1957 + 5033	374.806	6.83	0.952022	-39.6858	0.97986	-42.3651
PSR J2055 + 2539	319.561	4.11	0.95196	-39.6324	0.9814	-41.9856

Content

Part time (Intermittent) pulsars (PSR 1931+24)

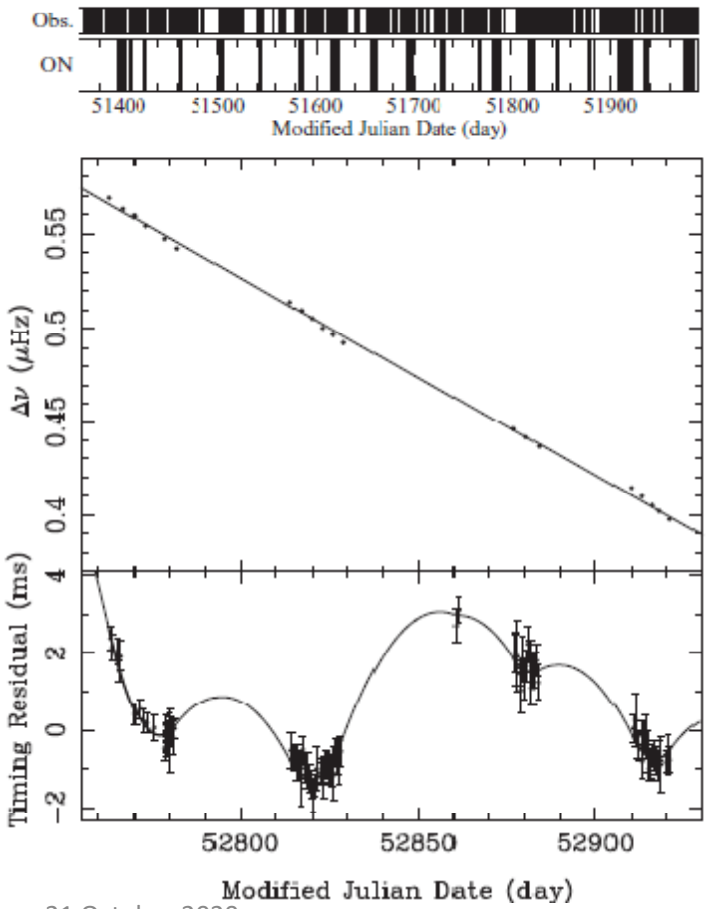

Kramer et.al, Nature, 2006

- Only visible for 20 % of time
- ON period 5-10 days
- OFF period 25-35 days
- Spin period 813ms
- Distance 4,6 kpc

$$\dot{\nu}_{ON} = -16.3 \times 10^{-15} Hz/s$$

$$\dot{\nu}_{OFF} = -10.8 \times 10^{-15} Hz/s$$

Bing Zhang et.al MNRAS 2006

REACTIVATED DEAD PULSAR

Damping times of toroidal modes for a neutron star

Mode	ν (kHz) (1)	$E_{\rm T}$(erg) (2)	$L_{\rm em}^{\rm Newt}$(erg s^{-1}) (3)	$L_{\rm em}^{\rm GR}$(erg s^{-1}) (4)	$\tau_{\rm gw}(s)$ (5)	$\tau_{\rm em}^{\rm Newt}(s)$ (6)	$\tau_{\rm em}^{\rm GR}(s)$ (7)	$\tau_{\rm gw}/\tau_{\rm em}^{\rm GR}$ (8)	$\tau_{\rm em}^{\rm Newt}/\tau_{\rm em}^{\rm GR}$ (9)
${}_1t_1$	17.9	1.09×10^{49}	1.77×10^{43}	1.57×10^{44}	...	1.23×10^{6}	1.39×10^{5}	...	8.85
${}_1t_2$	30	6.40×10^{48}	1.44×10^{44}	1.28×10^{45}	...	8.88×10^{4}	1.00×10^{4}	...	8.88
${}_1t_3$	43	1.59×10^{48}	5.98×10^{44}	5.30×10^{45}	...	5.32×10^{3}	6.00×10^{2}	...	8.87
${}_1t_4$	52.7	2.72×10^{47}	1.33×10^{45}	1.18×10^{46}	...	4.08×10^{2}	4.60×10^{1}	...	8.87
${}_2t_0$	0.36	3.31×10^{47}	6.86×10^{32}	3.45×10^{33}	6.62×10^{11}	9.65×10^{14}	1.92×10^{14}	3.45×10^{-3}	5.03
${}_2t_1$	17.9	3.26×10^{49}	9.32×10^{42}	4.96×10^{43}	7.60×10^{5}	7.00×10^{6}	1.31×10^{6}	0.58	5.34
${}_2t_2$	30	1.92×10^{49}	2.17×10^{44}	1.15×10^{45}	2.33×10^{5}	1.77×10^{5}	3.33×10^{4}	70	5.32
${}_2t_3$	43	4.76×10^{48}	1.83×10^{45}	9.72×10^{45}	1.51×10^{4}	5.21×10^{3}	9.79×10^{2}	15.43	5.32
${}_2t_4$	52	8.15×10^{47}	6.10×10^{45}	3.24×10^{46}	4.68×10^{3}	2.67×10^{2}	5.03×10^{1}	93.04	5.31

Damping times of spheroidal modes for a neutron star

Mode	ν (kHz) (1)	$E_{\rm T}$(erg) (2)	$L_{\rm em}^{\rm Newt}$(erg s^{-1}) (3)	$L_{\rm em}^{\rm GR}$(erg s^{-1}) (4)	$\tau_{\rm gw}(s)$ (5)	$\tau_{\rm em}^{\rm Newt}(s)$ (6)	$\tau_{\rm em}^{\rm GR}(s)$ (7)	$\tau_{\rm gw}(s)/\tau_{\rm em}^{\rm GR}(s)$ (8)	$\tau_{\rm em}^{\rm Newt}/$ (9)
${}_2p_2$	104.72	1.55×10^{50}	9.04×10^{44}	4.56×10^{45}	0.23×10^{-3}	3.43×10^{5}	6.79×10^{4}	0.34×10^{-6}	4.4
${}_2f$	28.56	1.59×10^{52}	2.38×10^{43}	7.41×10^{44}	7.50×10^{-3}	1.34×10^{9}	4.29×10^{7}	1.75×10^{-10}	31.24
${}_2s_2$	14.61	2.53×10^{53}	4.46×10^{43}	1.03×10^{45}	1×10^{4}	1.13×10^{10}	4.90×10^{8}	0.2×10^{-4}	23.06
${}_2s_1$	8.6	1.32×10^{54}	5.13×10^{43}	1.12×10^{45}	4.32×10^{4}	5.15×10^{10}	2.36×10^{9}	1.83×10^{-5}	21.82
${}_2i_2$	0.63	4.08×10^{47}	5.49×10^{43}	1.16×10^{45}	5.04×10^{9}	1.48×10^{4}	7.01×10^{2}	0.72×10^{7}	21.11
${}_2i_1$	0.35	1.63×10^{53}	5.49×10^{43}	1.16×10^{45}	8.64×10^{5}	5.93×10^{9}	2.80×10^{8}	3.1×10^{-3}	21.18
${}_2g_2^s$	0.12	5.49×10^{43}	5.49×10^{43}	1.16×10^{45}	7.57×10^{16}	5.24×10^{-3}	2.47×10^{-4}	3.1×10^{20}	21.21
${}_2g_3^s$	0.1	1.96×10^{40}	5.49×10^{43}	1.16×10^{45}	1.17×10^{17}	0.71×10^{-3}	0.34×10^{-4}	3.4×10^{21}	20.88

Alternative idea for the explanation of part time pulsars phenomena

- During the ON state pulsar is oscillating: stellar oscillations create relativistic wind of charged particles by virtue of additional accelerating electric field
- In a period of about 10 days the stellar oscillations are damped and the OFF period starts
- Quasi-periodic stellar glitches excite oscillations again, thus, being responsible for the emergence of new ON states with a certain periodicity

Scheme for part-time pulsar model

Deathline for radio pulsars shifts up due to negative deformation, and limited by lower limit for the deformation parameter.

Schematic view for to explain the nature of part-time pulsars by time dependence of their deformation

$$L(t) = f(\epsilon(t)) \rightarrow \epsilon(t) = f^*(L(t))$$

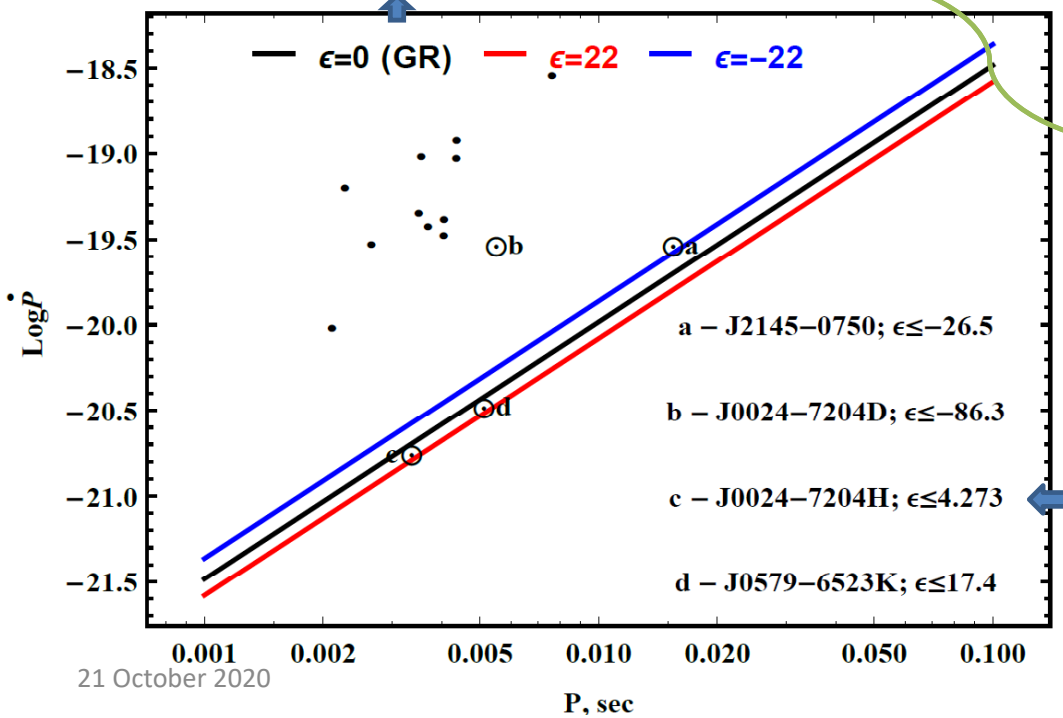

from observational data for ON and OFF states

Fitting function for deformation parameter taking account the lower limit.

Content

Death-lines for the aligned magnetar for different values of the parameter κ. The dashed line indicates the position of the Newtonian death-line. Crosses and squares indicate the position of SGRs and AXPs, respectively. AXPs from which the radio emission has been registered are marked with ticks, radio-loud soft gamma-ray repeater is enclosed in circle.

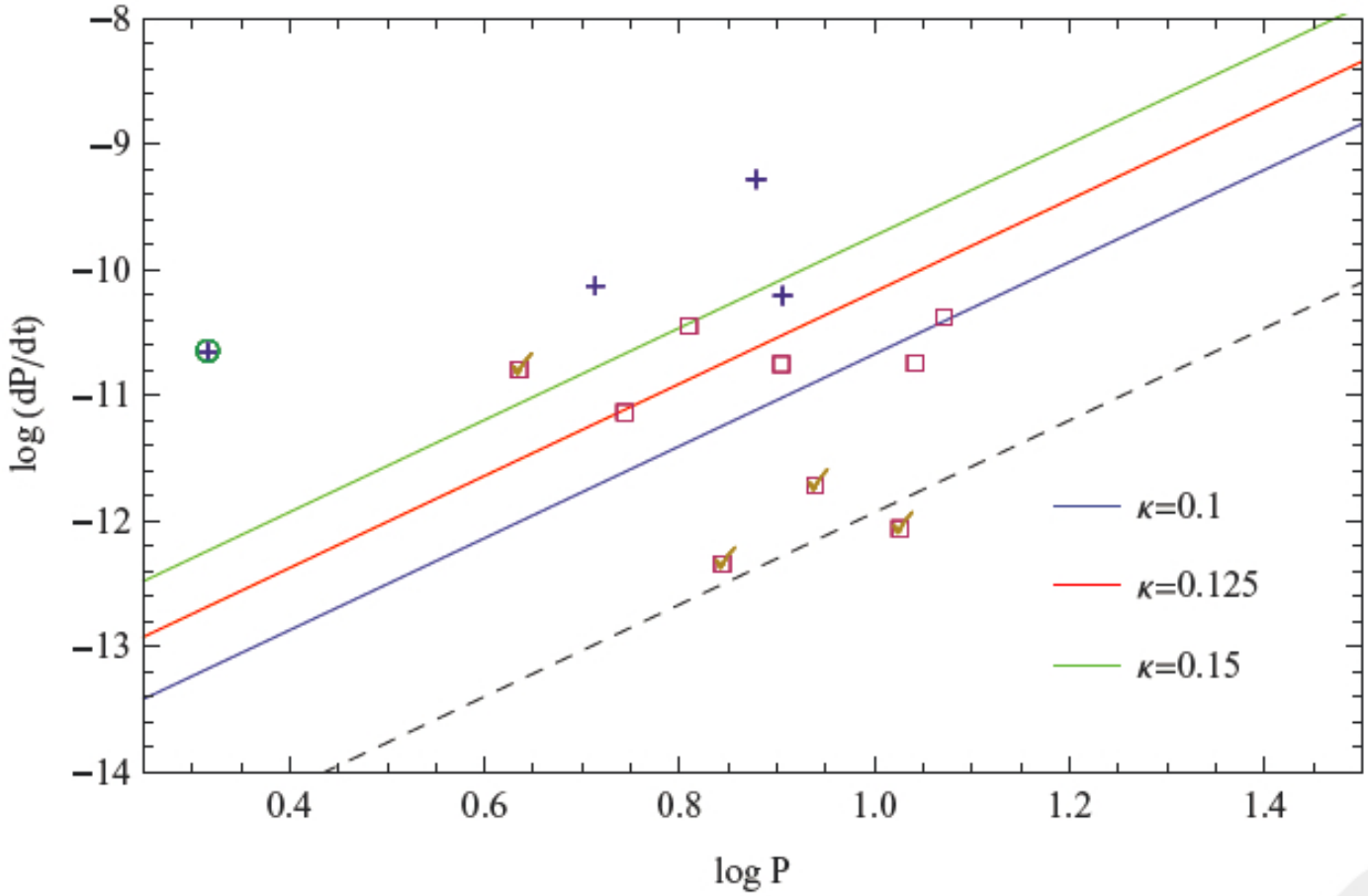

Death-lines for the misaligned magnetar for different values of the inclination angle χ. The value of κ is taken to be 0.1. The dashed line indicates the position of the Newtonian death-line. Crosses and squares indicate the position of SGRs and AXPs, respectively. Anomalous X-ray pulsars from which the radio emission has been registered are marked with ticks, radio-loud soft gamma-ray repeater is enclosed in circle.

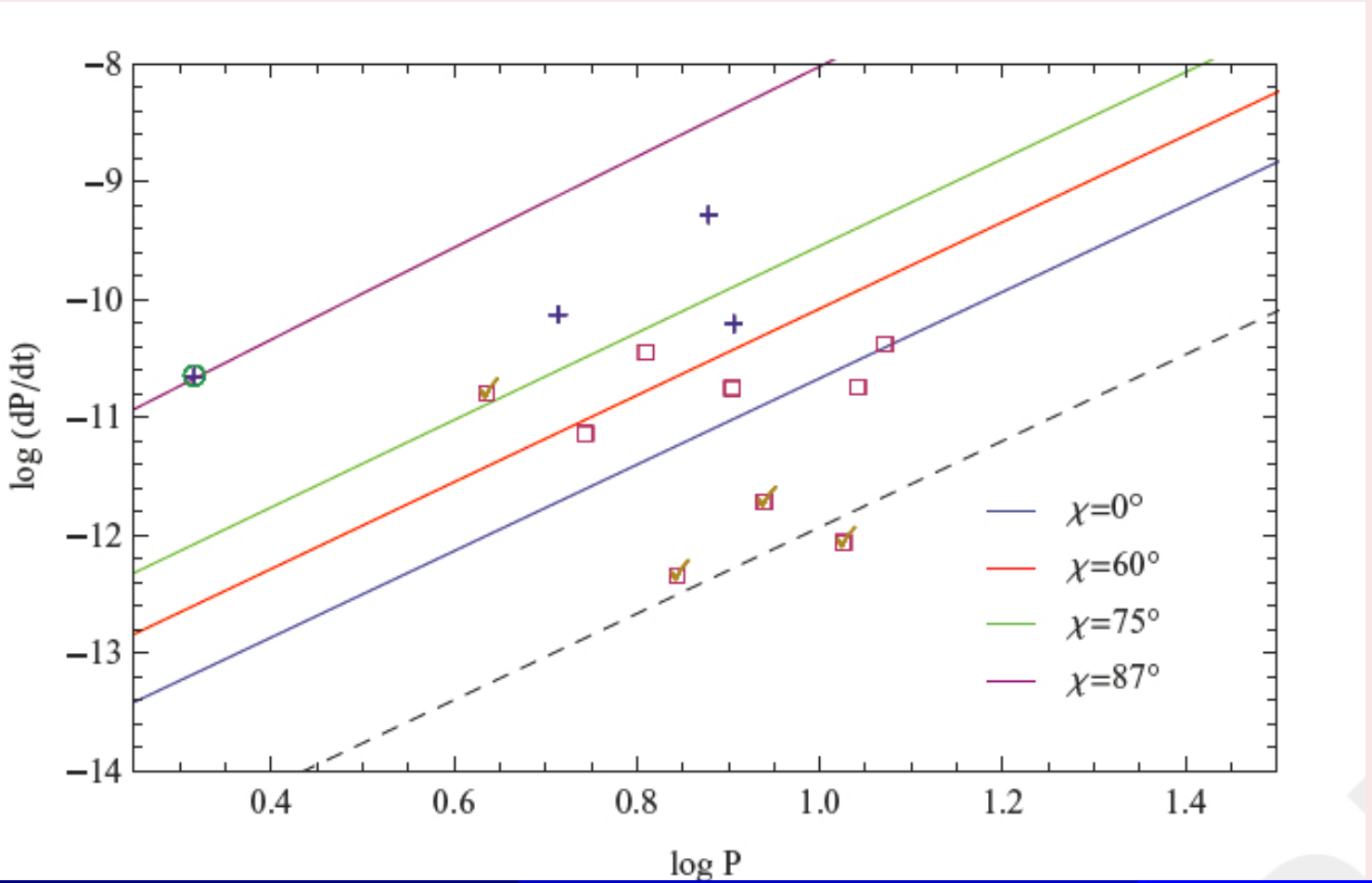

Content

Dependence of death-lines from parameter K

The amplitude of the oscillation is now parametrized in terms of the small number $K = \tilde{\eta}(1)/\Omega R$, giving the ratio between the velocity of oscillations and the linear rotational velocity of magnetar. The death-lines for rotating as well as oscillating magnetars for two modes of oscillations and different values of the parameter K are provided.

Death-lines for rotating and oscillating magnetars in the $P - \dot{P}$ diagram. The left panel corresponds to the mode $(1, 1)$ and values of $K = 0\ , 0.01\ , 0.02\ , 0.03$. The right panel corresponds to the mode $(2, 1)$ and values of $K = 0\ , 0.01\ , 0.02\ , 0.03$. Other parameters are taken to be $R_s = 10\text{km}$, $M = 2M_\odot$ and $\kappa = 0.15$. Crosses and squares indicate the position of SGRs and AXPs, respectively. AXPs from which the radio emission has been registered are marked with ticks, radio-loud soft gamma-ray repeater is enclosed in circle.

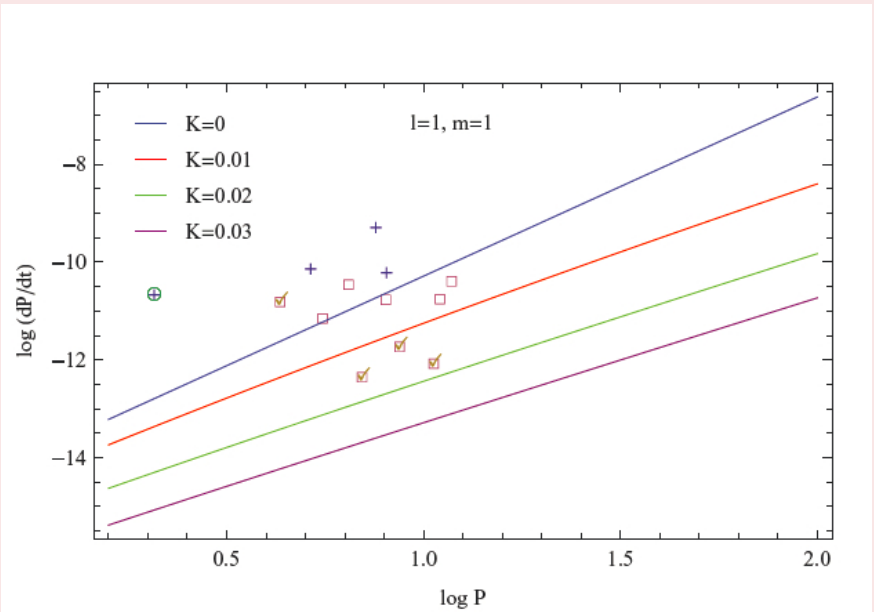

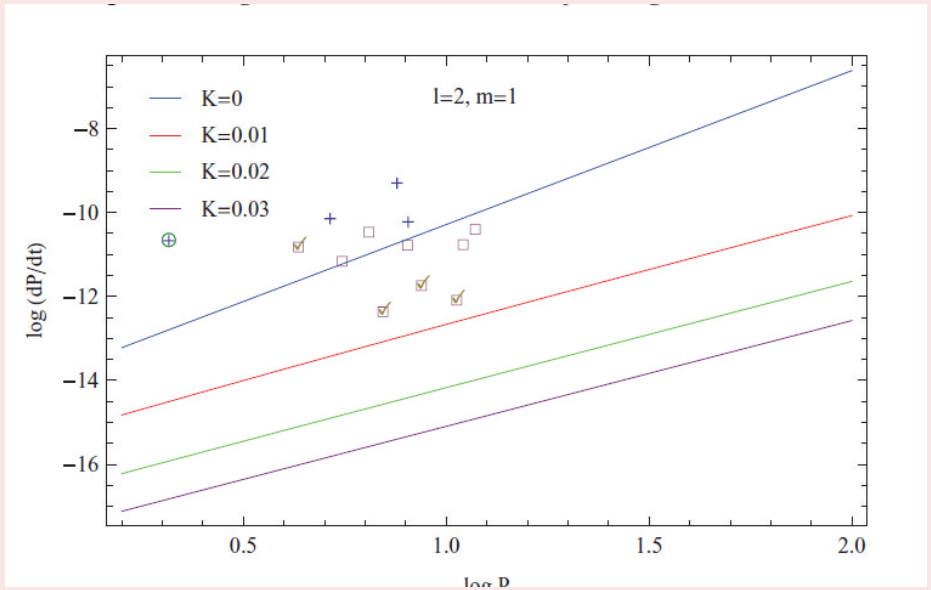

Fast Radio Bursts (FRBs)

D.Lorimer, D. Narkevic
Nature 2007

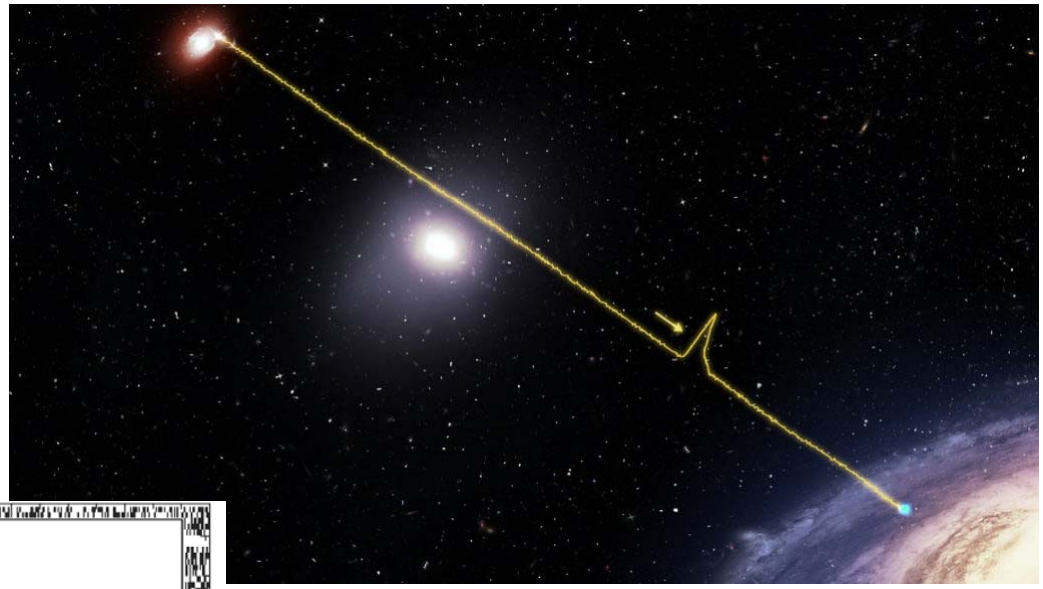

"Lorimer" bursts

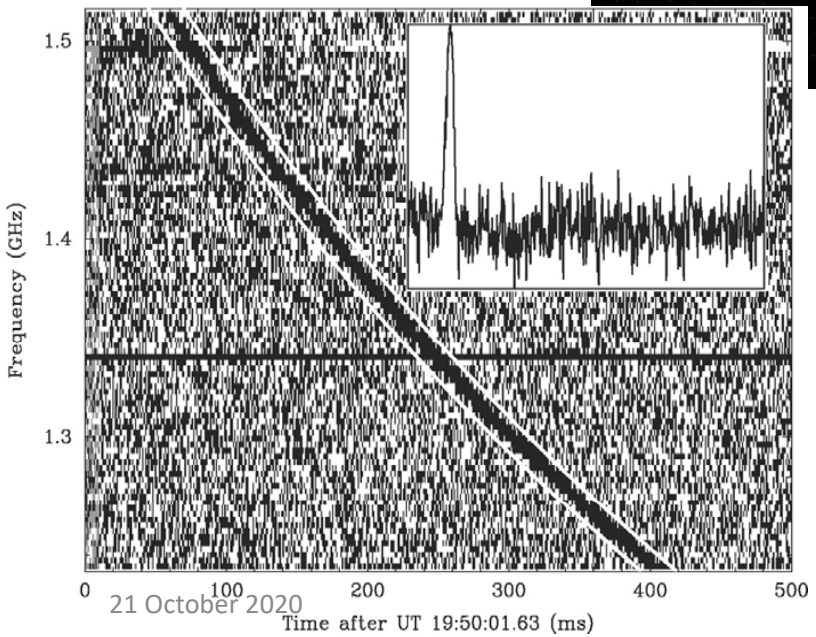

Quasi-periodically Repeating FRBs

K M Raj wade et.al **Possible periodic activity in the repeating FRB 121102, MNRAS 2020**
(P= 10-150 days) 600MHz-8GHz (4÷50 cm)

Periodic activity from a fast radio burst source
(The CHIME/FRB Collaboration*) *Nature* 2020
(P=16.35 ± 0.15 days) 400-800MHz (40÷75cm)

Radiation luminosity

Plasma magnetospheric radiations

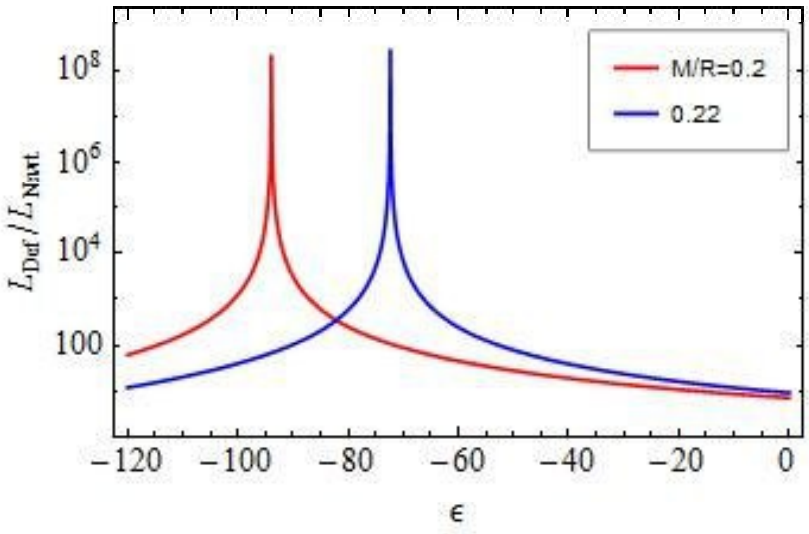

$$L_{Newt} \cong 10^{38} erg/sec$$
$$L_{max} \cong 10^{47} erg/sec$$

Magnetodipolar radiations

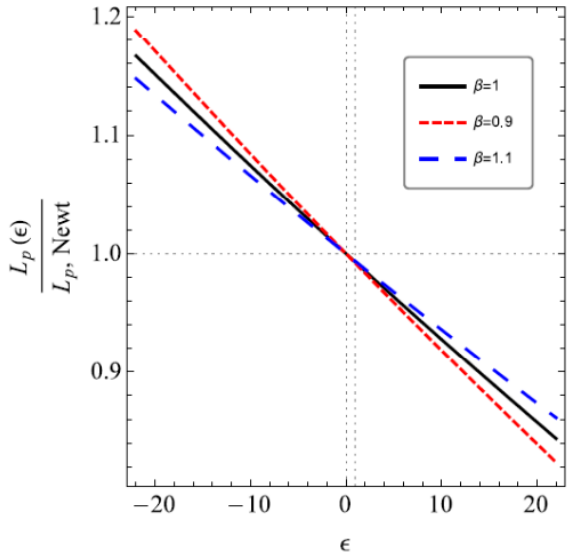

Wenbin & Kumar, MNRAS Letters, 483,1 (2019)

$$L_{max} \cong 2 \times 10^{47} erg/sec$$

one may fit the time dependence of the source NS deformation using recorded data of appearance of a repeating FRB

Content

Dependence of the Lorentz factor on the ratio $j/\bar{j}_*$ for a neutron star with $M = 1.4M_\odot$, $R = 10$ km, $P = 0.1s$, $\chi = 30°$, $B_0 = 1.0 \times 10^{12}$G, $\theta_* = 0°$, $\Theta_0 = 2°$, $\gamma_* = 1.01$.

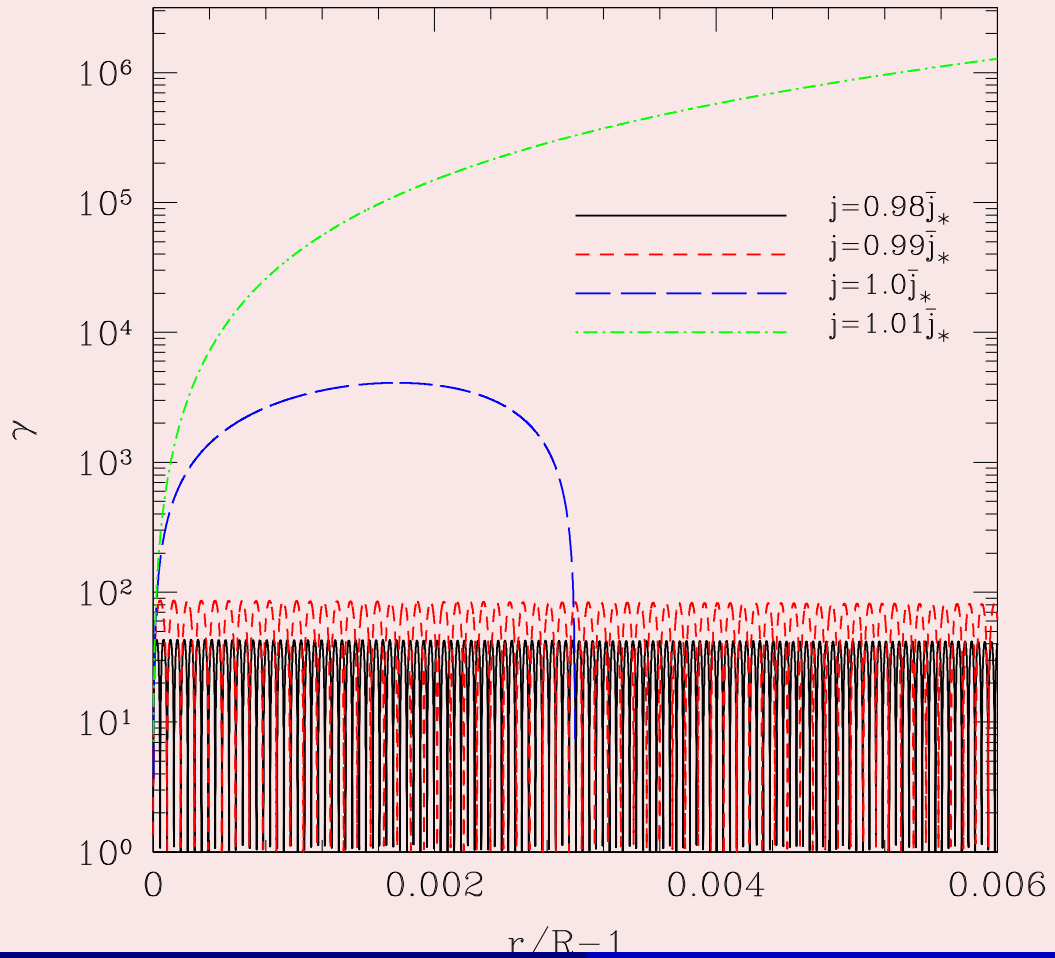

Lorentz factor dependence on the intensity of the magnetic field for a neutron star with $M = 1.4M_\odot$, $R = 10$ km, $P = 0.1s$, $\chi = 30^\circ$, $\theta_* = 0^\circ$, $\Theta_0 = 2^\circ$, $\gamma_* = 1.01$. Top panel: $j = 0.98\bar{j}_*$. Bottom panel: $j = 1.01\bar{j}_*$.

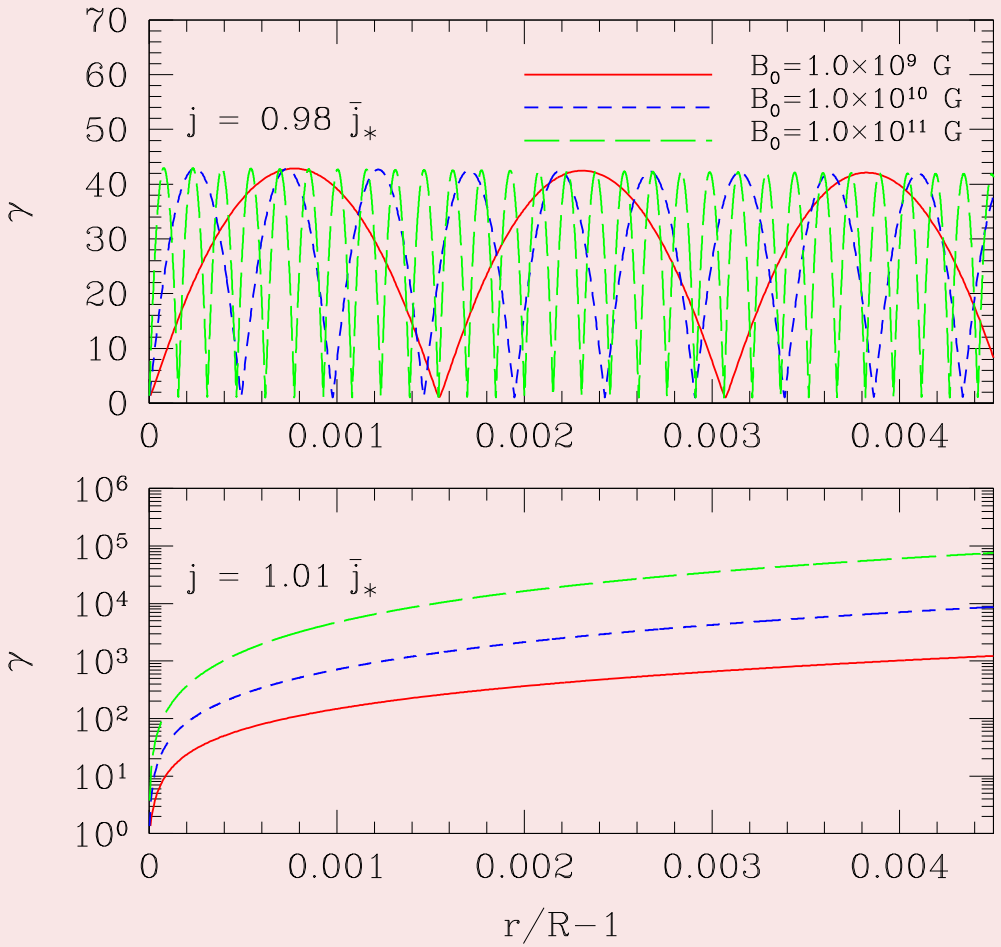

Lorentz factor dependence on the inclination angle χ for a neutron star with $M = 1.4M_\odot$, $R = 10$ km, and $P = 0.1s$, $j = 1.01\bar{j}_*$, $\theta_* = 0°$, $\Theta_0 = 2°$, $\gamma_* = 1.01$, $B_0 = 1.0 \times 10^{12}$G. The Lorentz factor decreases for larger inclination angles.

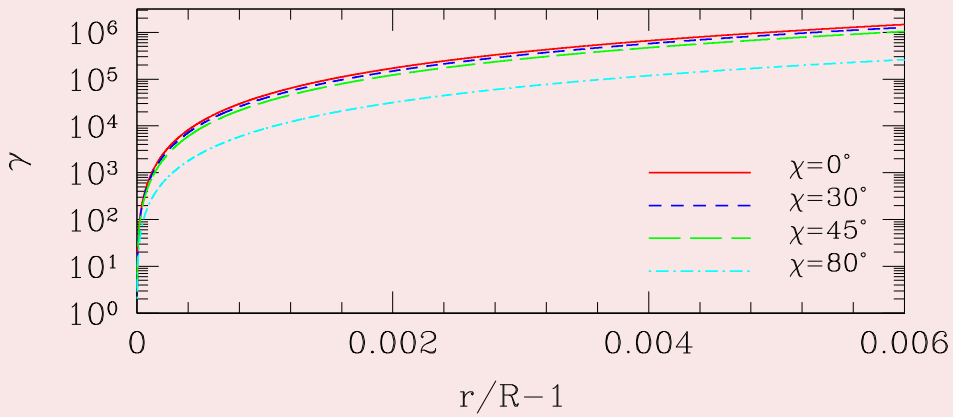

Lorentz factor dependence on the normalized amplitude of the stellar oscillations K for the mode of oscillations $(l, m) = (1, 1)$ with $\theta_* = 2°$, $\Theta_0 = 3°$,$\gamma_* = 1.015$, $B_0 = 1.0 \times 10^{12}$G for the case $j = 0.98\bar{j}_*$. The left panels show the solution for $\phi = 0$, the right panels for $\phi = \pi$.

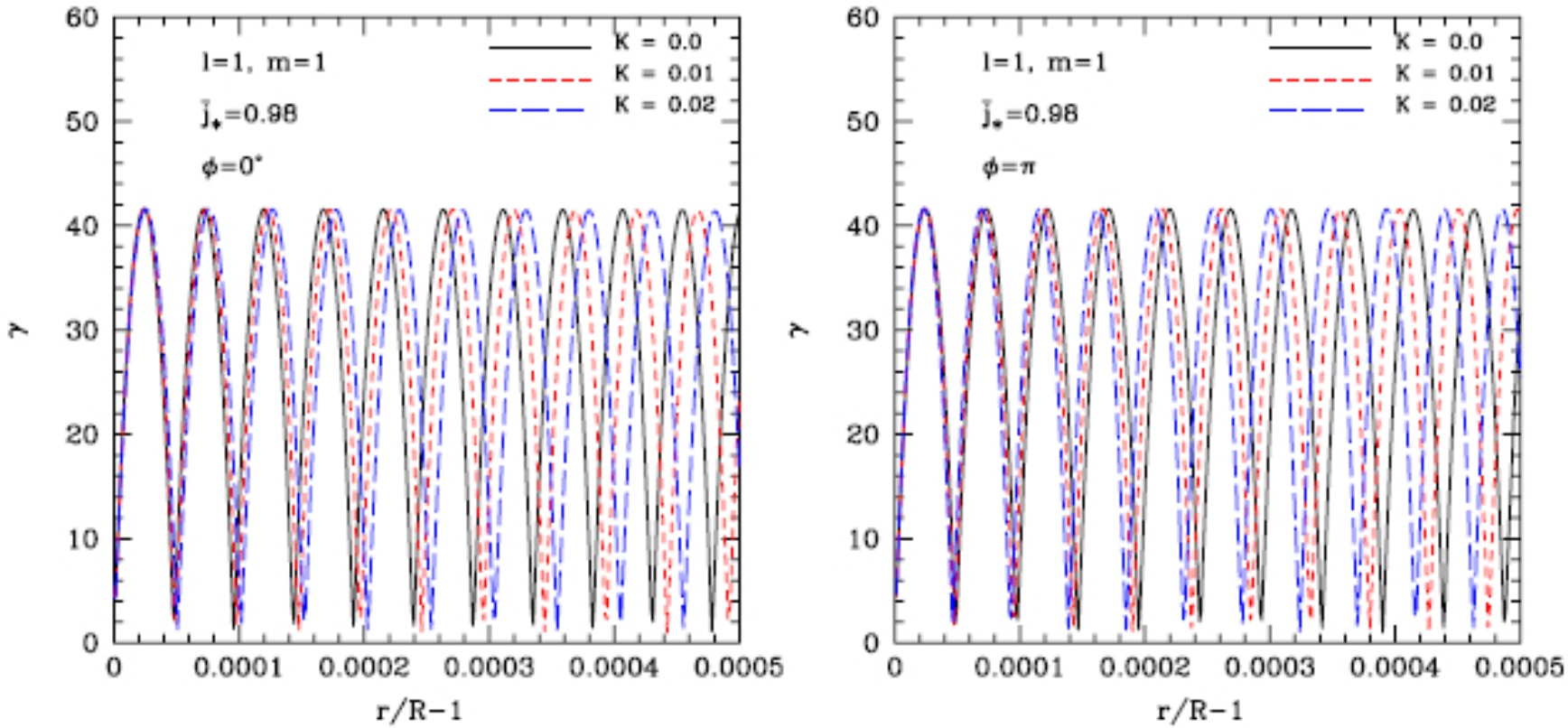

Lorentz factor dependence on the normalized amplitude of the stellar oscillations K for the mode of oscillations $(l, m) = (1, 1)$ with $\theta_* = 2°$, $\Theta_0 = 3°$,$\gamma_* = 1.015$, $B_0 = 1.0 \times 10^{12}$G for the case $j = 1.001\bar{j}_*$. The left panels show the solution for $\phi = 0$, the right panels for $\phi = \pi$.

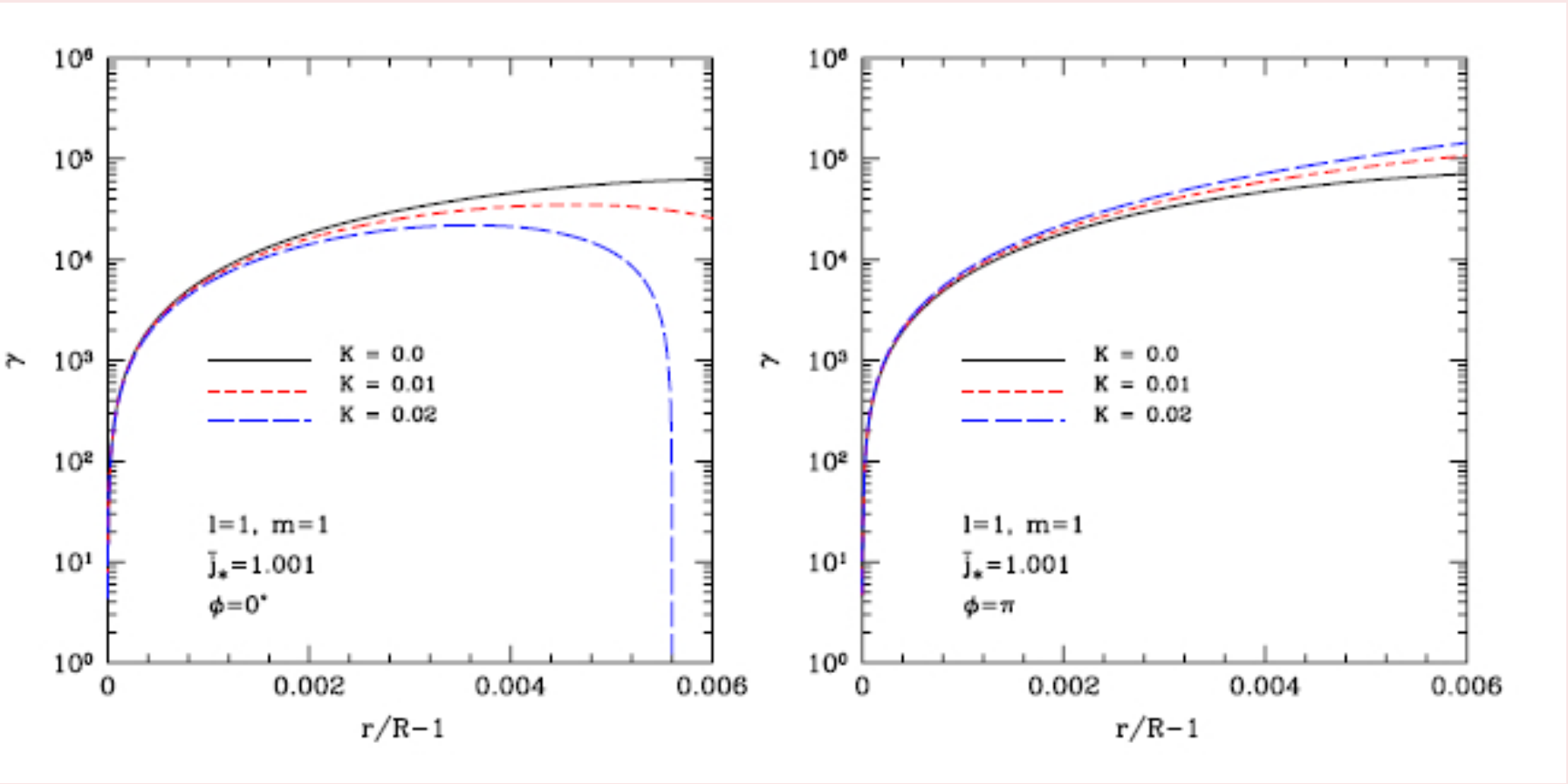

Lorentz factor dependence on the normalized amplitude of the stellar oscillations K for the mode of oscillations $(l, m) = (2, 1)$ with $\theta_* = 2°$, $\Theta_0 = 3°$,$\gamma_* = 1.015$, $B_0 = 1.0 \times 10^{12}$G. The two panels correspond to the case $j = 1.001\bar{j}_*$. The left panel shows the solution for $\phi = 0$, the right panel for $\phi = \pi$

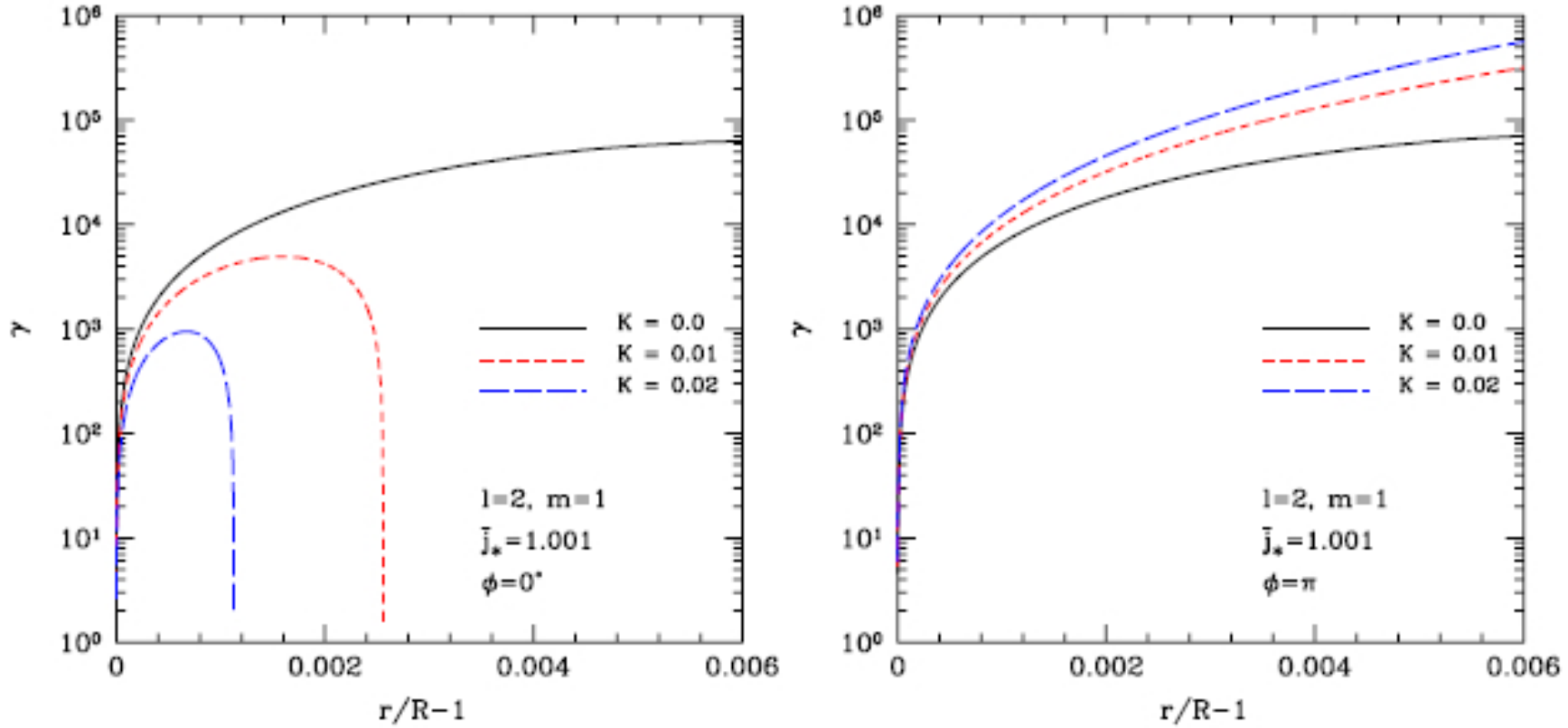

Lorentz factor as a function of radial distance and azimuthal angle ϕ for a model with stellar oscillations $K = 0.02$, $(l, m) = (1, 1)$, $\theta_* = 2°$, $\Theta_0 = 3°$, $\gamma_* = 1.015$, $B_0 = 1.0 \times 10^{12}$G. Left panel: $j = 1.001\bar{j}_*$. Right panel: $j = 1.01\bar{j}_*$.

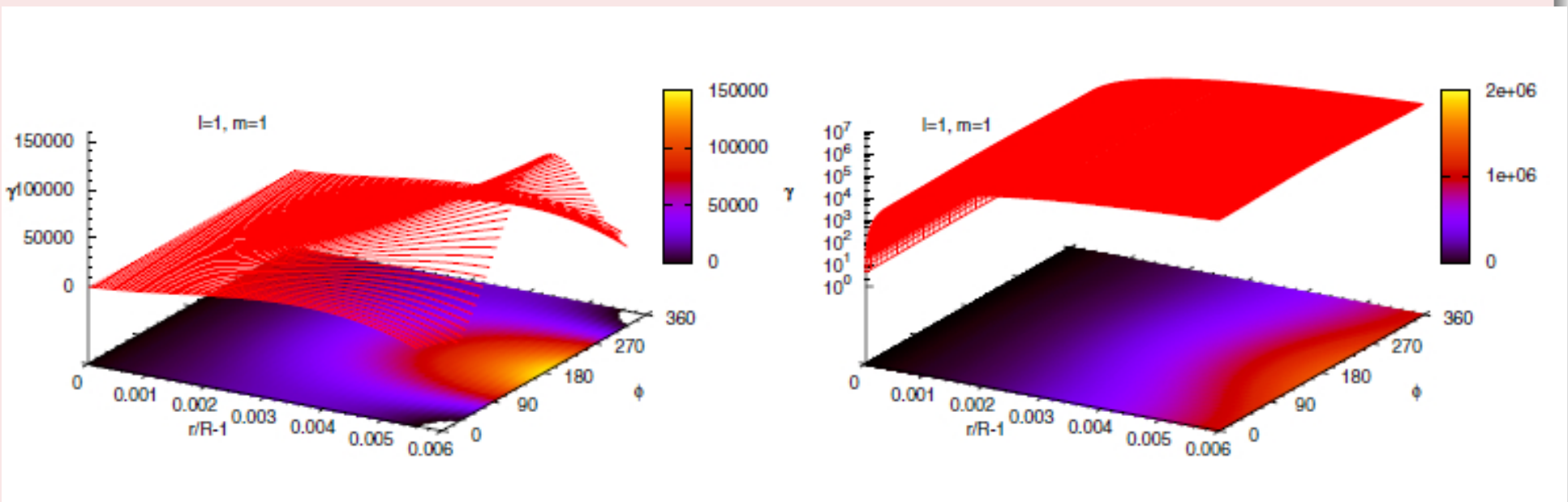

Content

Drifting Subpulses as a Tool for Studies of Pulsar Magnetosphere

- Phenomena of drifting subpulses
- Existing models for the drifting subpulses
- Our results in frame of the space charge limited flow model

V.S. Morozova, Ahmedov B.J., O. Zanotti, Explaining the subpulse drift velocity of pulsar magnetosphere within the space-charge limited flow model, **MNRAS**, 2014, V. 444, 1144

Drifting subpulses

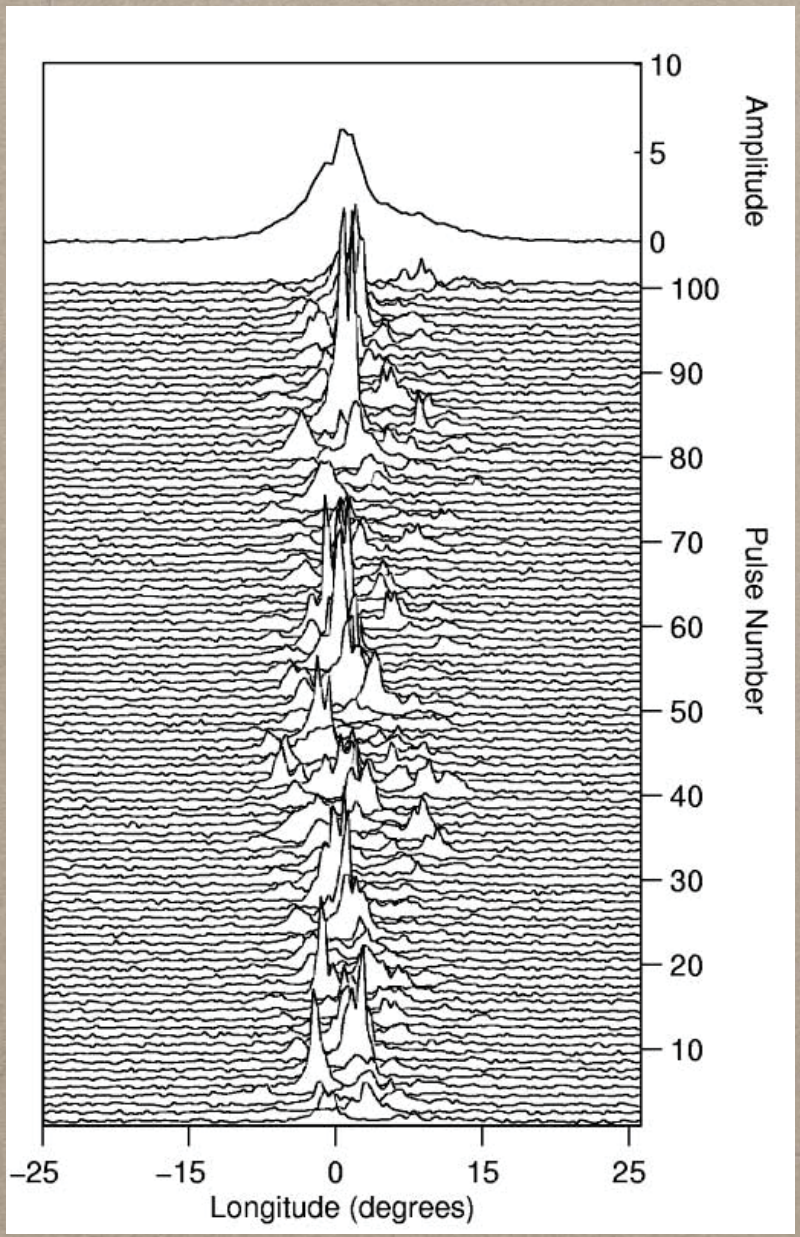

- *Average pulse profile is very stable and represents a unique "fingerprint" of a given pulsar*
- *Subsequent pulses plotted on top of each other show rich microstructure*

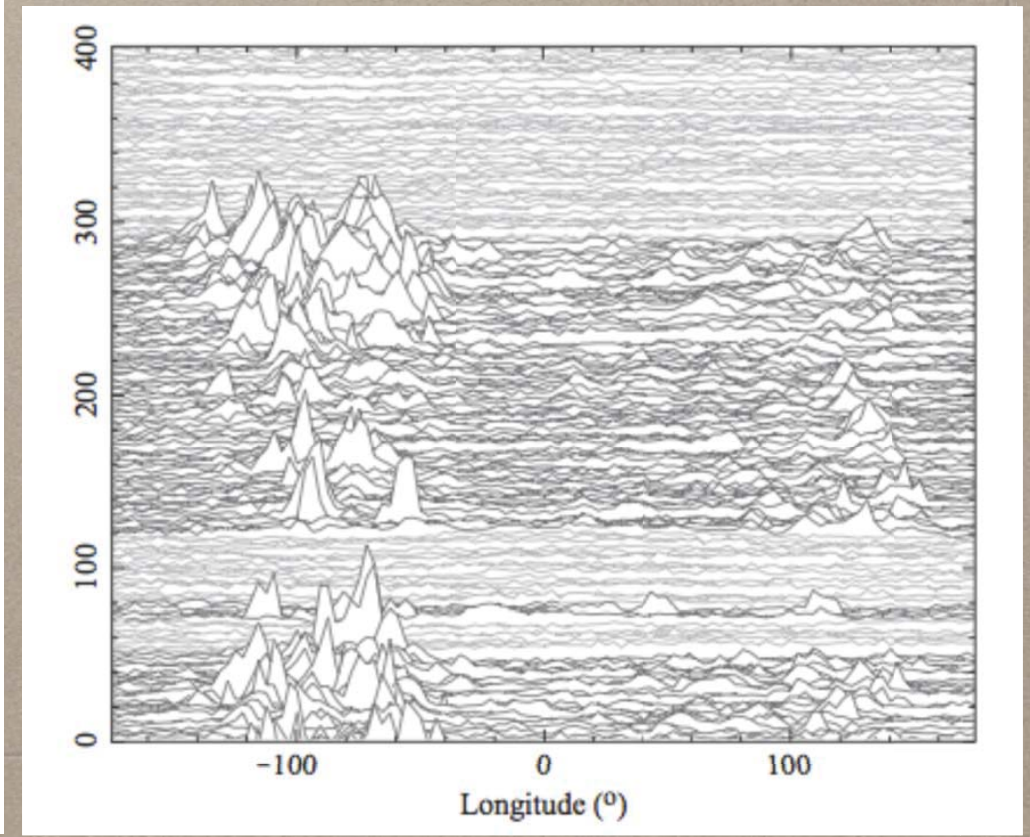

Drifting subpulses

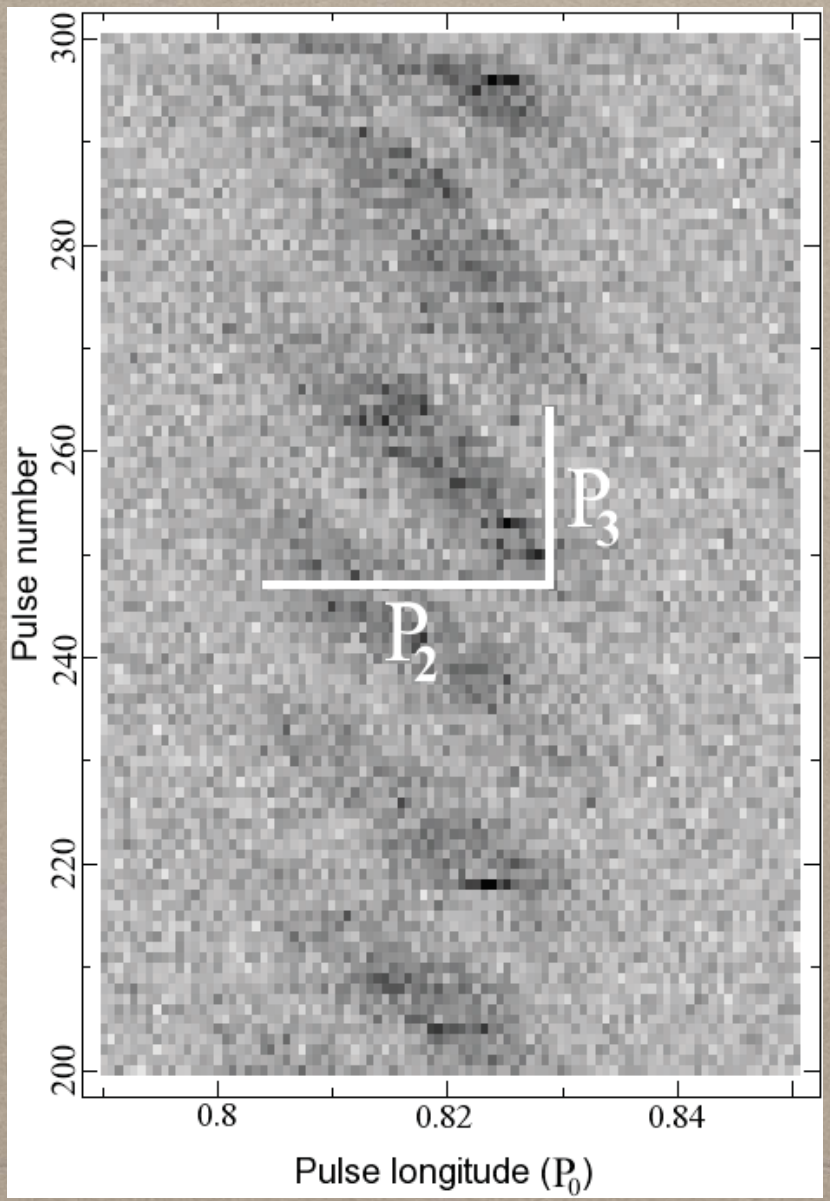

Subpulse drift velocity

$$\omega_D = \frac{P_2}{P_3}$$

Various subpulse behavior

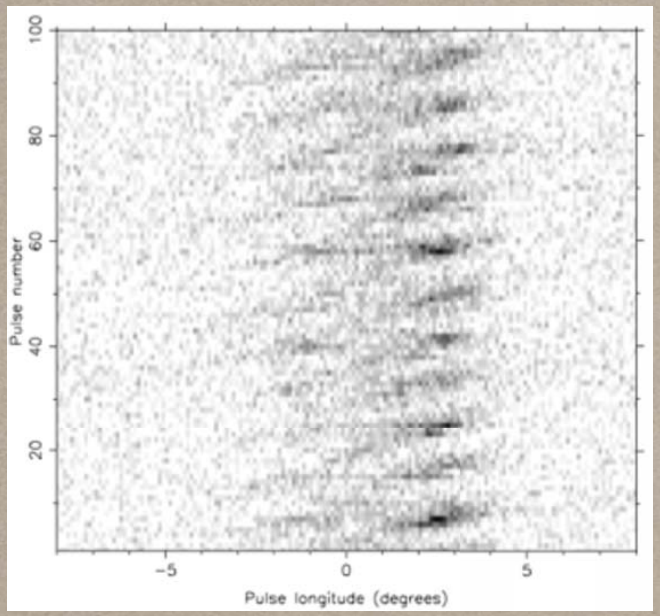

PSR B0320+39 from R. T. Edwards et al. (2003)

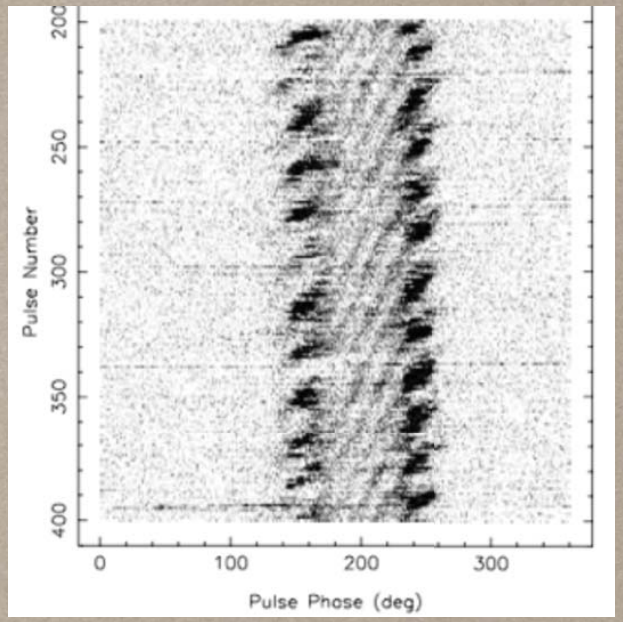

PSR B0818–41 from B. Bhattacharyya et al. (2007)

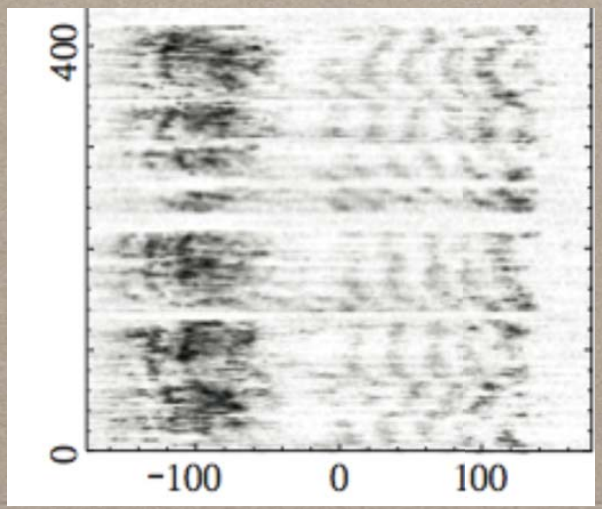

PSR B0826-34 from van Leeuwen & Timokhin (2012)

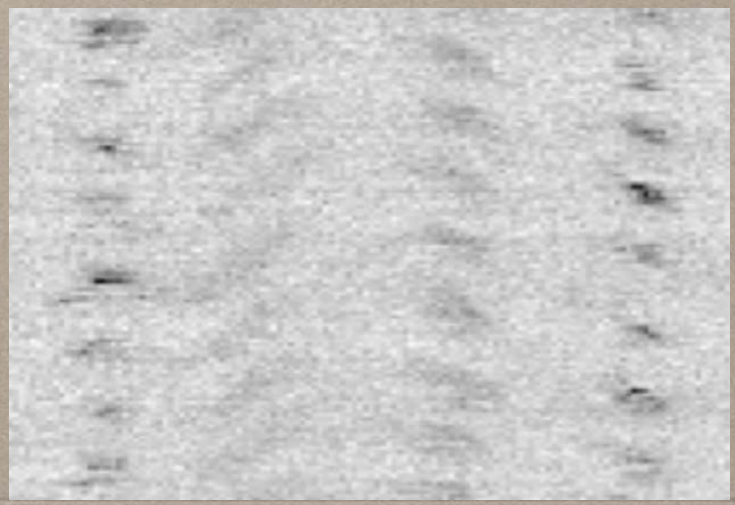

PSR J0815-09 from Qiao et al. (2004)

Angular dependence of the drift velocity can account for the curved subpulse drift bands of B0818-41

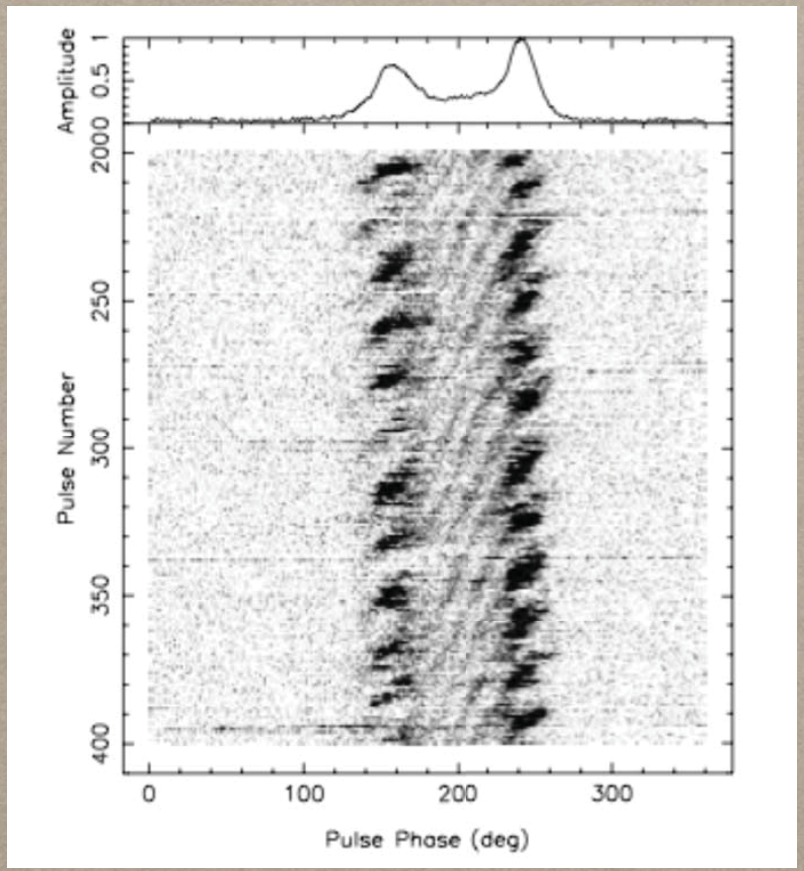

from Bhattacharyya et al. (2009)

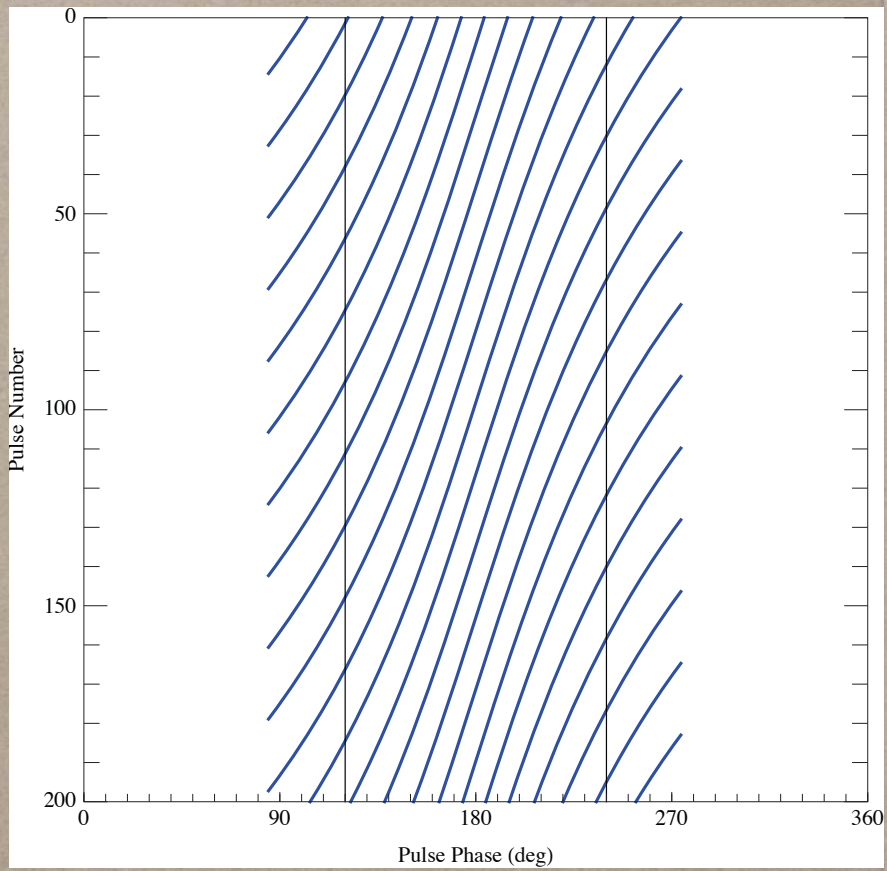

obtained with our model

Thank You